UNIVERSITY OF SÃO PAULO
SÃO CARLOS SCHOOL OF ENGINEERING

Luis Eduardo Jaramillo Bustamante

Numerical evaluation of a damage detection method for composite plates using Lamb wave response with piezoelectric transducers

São Carlos
2019

Luis Eduardo Jaramillo Bustamante

Numerical evaluation of a damage detection method for composite plates using Lamb wave response with piezoelectric transducers

Thesis presented to the São Carlos School of Engineering, University of São Paulo, in fulfillment of the requirements for the Master of Science degree in Mechanical Engineering.

Concentration area: Aircraft

Supervisor: Prof. Dr. Marcelo Leite Ribeiro

REVISED VERSION

São Carlos

2019

Catalog card prepared by Patron Service at
"Prof. Dr. Sergio Rodrigues Fontes Library" at EESC/USP

J37n

Jaramillo Bustamante, Luis Eduardo
Numerical evaluation of a damage detection method for composite plates using Lamb wave acoustic response sensed with piezoelecric transducers / Luis Eduardo Jaramillo Bustamante; supervisor Marcelo Leite Ribeiro. -- São Carlos, 2019.

Master (Thesis)--(Graduate Program in Mechanical Engineering and Research area in Aircraft) -- São Carlos School of Engineering of the University of São Paulo, 2019.

1. Structural health monitoring. 2. Damage detection. 3. Laminated carbon fiber reinforced composites. 4. Hilbert-Huang transform. 5. Lamb waves. I. Title.

Prepared by Flávia Helena Cassin - CRB-8/5812

Luis Eduardo Jaramillo Bustamante

Avaliação numérica de um método para detecção de dano em placas de compósito usando a resposta de ondas Lamb com transdutores piezoelétricos

Dissertação apresentada à Escola de Engenharia de São Carlos da Universidade de São Paulo, para obtenção do título de Mestre em Ciências - Programa de Pós-Graduação em Engenharia Mecânica.

Área de concentração: Aeronaves

Orientador: Prof. Dr. Marcelo Leite Ribeiro

VERSÃO CORRIGIDA

São Carlos
2019

Ficha catalográfica elaborada pela Biblioteca Prof. Dr. Sérgio Rodrigues Fontes da EESC/USP com os dados inseridos pelo(a) autor(a).

Jaramillo Bustamante, Luis Eduardo
J37a Avaliação numérica de um método para detecção de dano em placas de compósito usando a resposta acústica de ondas Lamb medidas com transdutores piezoeléctricos / Luis Eduardo Jaramillo Bustamante; orientador Marcelo Leite Ribeiro. São Carlos, .

Dissertação (Mestrado) - Programa de Pós-Graduação em Engenharia Mecânica e Área de Concentração em Aeronáutica -- Escola de Engenharia de São Carlos da Universidade de São Paulo, .

1. Monitoramento da Saúde Estrutural. 2. Detecção de Dano. 3. Laminados de compósito. 4. Transformada de Hilbert-Huang. 5. Ondas Lamb. I. Título.

Eduardo Graziosi Silva - CRB - 8/8907

FOLHA DE JULGAMENTO

Candidato: Engenheiro **LUIS EDUARDO JARAMILLO BUSTAMANTE.**

Título da dissertação: "Avaliação numérica de um método para detecção de dano em placas de compósito usando a resposta acústica de ondas Lamb medidas com transdutores piezoeléctricos".

Data da defesa: 06/06/2019.

Comissão Julgadora:	**Resultado:**
Prof. Dr. **Marcelo Leite Ribeiro** **(Orientador)** (Escola de Engenharia de São Carlos/EESC)	Aprovado
Prof. Dr. **Ricardo de Medeiros** (Universidade do Estado de Santa Catarina/UDESC)	Aprovado
Prof. Dr. **Eurípedes Guilherme de Oliveira Nobrega** (Universidade Estadual de Campinas/UNICAMP)	Aprovado

Coordenador do Programa de Pós-Graduação em Engenharia Mecânica:
Prof. Associado **Carlos De Marqui Junior**

Presidente da Comissão de Pós-Graduação:
Prof. Titular **Murilo Araujo Romero**

Este trabajo se lo dedico a mi madre, Aura Elena, a mi abuela, Aura, y a Dios, a quienes les debo todo lo que hoy soy.

ACKNOWLEDGEMENTS

This work was long and hard, and there are a lot of people to which I must thank for helping me in achieving this goal. I wish to extend my gratitude to them.

To my mother, Aura Elena, who taught me the value of hard work as she fought, since I was a child and while being a single mother, to overcome any economic barrier to the progress of our household, while filling my heart with love.

To my grandmother, Aura Alvarado, who took care of me while my mother worked and I was young and vulnerable. Also, who took me through the moments that defined my love for music, culture, folklore, and Caribbean traditions.

To Prof. Marcelo Leite for the opportunity, guidance, and the freedom he gave me to try any kind of new ideas. Also, to all the staff that made my experience possible, from Prof. Volnei Tita to Iara and Ana Paula, who were also advisers and friends. I'm still feeling sorry for Ana Paula's too early departure.

Special thanks to Elizabeth Maria Alvis Alexandre, who offered me much more than a room to rent and to whom I will be forever grateful.

To my father, Luis Jaramillo Sr., my brother, Luigi, my grandmother, Maria Elena, and my aunt Lucy for all the motivational and economical support. This is also their victory.

To my friends in the GEA research group: David, Matheus, Fernando, Gregorio, Bruno, Rafael, Eduardo, Denys, José, and Humberto for all the experiences inside and outside the lab. To Nicoly, Victor, Pedro, Yuleidis, Miguel, Arnol, Paola, and many others who made my experience worth full. To my "Republica" partners: Alysson, João, Douglass, Edimilson, Mário, Renato, Victor, Caique, Kevin and André, for the great moments.

To my closest friends in Cartagena and Barranquilla: Gustavo, Carlos, Luis Alberto, Hector, and Roberto, Maria Camila, Eder, Jaime, Maria Alexandra, Orlando Barros, Sheryl, Andres Aldana, Maria José, Karen, Melizza, Brillith and many others for always keeping in touch and encouraging me to keep moving forward.

This study was financed in part by the Coordenação de Aperfeiçoamento de Pessoal de Nível Superior - Brasil (CAPES) - Finance Code 001, through a Scholarship for which I will be forever grateful to the Brazilian People represented by the CAPES, the São Carlos School of Engineering, and the city of São Carlos, which has been my home during these three years of work.

Last but not least, I would like to thank God for guiding my way and putting the right people around me.

AGRADECIMENTOS

Este trabalho foi duro e comprido, e há muitas pessoas para quem devo agradecer por terem me ajudado em atingir este objetivo. Desejo estender minha gratidão para eles.

Para a minha mãe, Aura Elena, quem me ensino o valor de trabalhar duro enquanto ela lutava, desde que eu era uma criança e sendo mãe solteira, para vencer quaisquer barreiras econômicas para o progresso do nosso lar, enquanto enchia meu coração com amor.

Para minha avó, Aura Alvarado, quem me cuidou enquanto minha mãe trabalhava e eu era jovem e vulnerável. Também, quem me levou através dos momentos que definiram meu amor pela música, a cultura, e as tradições do Caribe.

Para o Prof. Marcelo Leite pela oportunidade, orientação, e liberdade que me deu para tentar quaisquer novas ideias. Também, para os funcionários que fizeram toda minha experiencia possível, desde o Prof. Volnei Tita até Iara e Ana Paula, quem também foram conselheiras e amigas. Ainda sinto muita pena pela partida tão ceda da Ana Paula.

Agradecimentos especiais para Elizabeth Maria Alvis Alexandre, quem me ofereceu muito mais do que um quarto para alugar e para quem estarei por sempre agradecido.

Para meu pai, Luis Jaramillo, meu irmão, Luigi, minha avó, Maria Elena, e minha tia Lucy pela motivação emocional e econômica. Essa também é vitória deles

Para meus amigos do grupo de pesquisa GEA: David, Matheus, Fernando, Gregório, Bruno, Rafael, Eduardo, Denys, José, e Humberto pelas experiencias dentro e fora do laboratório. Para Nicoly, Victor, Pedro, Yuleidis, Miguel, Arnol, Paola, e muitos outros que fizeram da minha experiencia valiosa. Para meus amigos de Republica: Alysson, João, Douglass, Edimilson, Mário, Renato, Victor, Caique, Kevin, e André, pelos bons momentos.

Para meus amigos mais próximos em Cartagena e Barranquilla; Gustavo, Carlos, Luis Alberto, Hector e Roberto, Maria Camila, Eder, Jaime, Maria Alexandra, Orlando Barros, Sheryl, Andres Aldana, Maria José, Karen, Melizza, Brillith y outros por sempre estar em contato e me animar para continuar sempre indo para frente.

Este estudo foi financiado em parte pela CAPES, código 001, através de uma bolsa de estudos pela qual estarei eternamente agradecido com o Povo Brasileiro representado pela CAPES, a EESC, e a cidade de São Carlos, a qual tem sido meu lar pelos últimos três anos.

Finalmente, quero agradecer a Deus por guiar meu caminho e colocar as pessoas corretas ao meu redor.

AGRADECIMIENTOS

Este trabajo fue duro y extenso, y hay muchas personas a las que debo agradecer por haberme ayudado en alcanzar esta meta. Deseo extender mi gratitud a ellos.

A mi madre, Aura Elena, quien me enseñó el valor de trabajar duro mientras ella luchaba, desde que era un niño y siendo madre soltera, para vencer todas las barreras económicas para el progreso de nuestro hogar, mientras llenaba mi corazón con amor.

A mi abuela, Aura Alvarado, quien cuido de mi mientras mi madre trabajaba y yo era joven y vulnerable. También, quien me llevó a través de los momentos que definieron mi amor por la música, la cultura, el folclor y las tradiciones del Caribe.

Al Prof. Marcelo Leite por la oportunidad, la orientación y la libertad que me dio para probar todo tipo de nuevas ideas. También, a todos los funcionarios que hicieron mi experiencia posible, desde el Prof. Volnei Tita hasta Iara y Ana Paula, quienes también fueron consejeras y amigas. Aún siento mucha pena por la partida tan pronta de Ana Paula.

Gracias especiales a Elizabeth María Alvis Alexandre, quien me ofreció mucho más que un cuarto par alquilar y a quien le estaré eternamente agradecido.

A mi padre, Luis Jaramillo, mi hermano, Luigi, mi Abuela, María Elena, y mi tía Lucy por todo el apoyo emocional y económico. Esta es también su victoria.

A mis amigos del grupo de investigación GEA: David, Matheus, Fernando, Gregorio, Bruno, Rafael, Eduado, Denys, José, y Humberto por todas las experiencias dentro y fuera del laboratorio. A Nicoly, Víctor, Pedro, Yuleidis, Miguel, Arnol, Paola, y muchas otras por haber hecho mi experiencia valiosa. A mis amigos de "República": Alysson, João, Douglass, Edimilson, Mário, Renato, Victor, Caique, Kevin, y André, por los buenos momentos.

A mis amigos más cercanos en Cartagena y Barranquilla: Gustavo, Carlos, Luis Alberto, Héctor, y Roberto, María Camila, Eder, Jaime, María Alexandra, Orlando Barros, Sheryl, Andrés Aldana, María José, Karen, Melizza, Brillith y muchos otros por siempre mantener el contacto y motivarme en seguir hacia adelante.

Este estudio fue financiado en parte por la CAPES, código 001, a través de una beca de estudios por la cual estaré eternamente agradecido al Pueblo Brasileño representado por la CAPES, la EESC y la ciudad de Sao Carlos, la cual ha sido mi hogar estos últimos tres años.

Finalmente, quiero agradecer a Dios por guiar mi camino y colocar las personas correctas a mi alrededor.

"Los seres humanos no nacen para siempre el día en que sus madres los alumbran,
sino que la vida los obliga a parirse a sí mismos una y otra vez"
Gabriel García Márquez

RESUMO

JARAMILLO BUSTAMANTE, L. E. **Avaliação numérica de um método para detecção de dano em placas de compósito usando a resposta de ondas Lamb com transdutores piezoelétricos**. 2019. 146p. Dissertação (Mestrado) - Escola de Engenharia de São Carlos, Universidade de São Paulo, São Carlos, 2019.

Quando comparados com os metais, os materiais compósitos exibem uma performance estrutural superior devido à sua razão de rigidez sobre peso e sua resistência à corrosão, virando atrativos para sua aplicação em estruturas do setor aeroespacial. Embora, o impacto econômico da rigorosa manutenção preventiva, requerida devido aos mecanismos complexos de dano que possuem, impede um uso mais extensivo desses materiais; um de esses modos de falha é a delaminação. Nesta ordem, o uso da resposta ativa de ondas Lamb mediante o emprego de transdutores piezoeléctricos para detecção de anomalias tem sido uma área de pesquisa de muita atividade nos recentes anos. Neste trabalho, um modelo para a detecção acústica de delaminação ao longo de uma linha de transdutores piezo é proposta. A metodologia utiliza técnicas de processamento de sinais no domínio do tempo e é avaliada numericamente para placas de fibra de carbono bidirecional com diferentes delaminações. O modelo proposto detecta a existência de descontinuidades de rigidez, as quais são atribuídas ao dano, processando sinais mediante a Transformada de Hilbert-Huang e as quantifica usando a magnitude e tempos de voo do modo de propagação Antissimétrico das ondas Lamb extraídas dos dados de resposta de voltagem. Nos estudos numéricos, o modelo atinge uma detecção de dano confiável e resulta numa precisão razoável enquanto o localiza e quantifica sua extensão com estimativas conservadoras, portanto, estimulando a continuidade do modelo para trabalhos futuros.

Palavras-chave: Monitoramento da Saúde Estrutural. Detecção de Dano. Laminados de compósito. Transformada de Hilbert-Huang. Ondas Lamb.

ABSTRACT

JARAMILLO BUSTAMANTE, L. E. **Numerical evaluation of a damage detection method for composite plates using Lamb wave response with piezoelectric transducers**. 2019. 146p. Dissertação (Mestrado) - Escola de Engenharia de São Carlos, Universidade de São Paulo, São Carlos, 2019.

When compared to metals, composite materials exhibit superior structural performance due to their higher Stiffness-to-weight ratio and corrosion resistance, becoming attractive for their application in aerospace structures. However, the economic impact of their rigorous preventive maintenance, required due to their complex damage mechanics, hinders a more extensive use of these materials; one of such failure modes is delamination. In this regard, the use of Lamb wave active response through the employment of piezoelectric transducers for feature detection in composites is a hot research topic nowadays. In this work, a model for the acoustic detection of delamination along a line of piezo transducers is proposed. The methodology utilizes time-domain processing techniques and is numerically assessed for a set of bidirectional laminated composites with different delaminations. The model proposed detects the existence of stiffness discontinuities, which can be attributed to damage, by processing signals through the Hilbert-Huang Transform and then it quantifies it by using the magnitude and times of flight of the Antisymmetric Lamb wave propagation mode extracted from the voltage response data. In the numerical studies, the model achieves reliable damage detection and gives reasonable accuracy as localizes it and quantifies its extension with conservative estimations, thus encouraging its extension for future works.

Keywords: Structural Health Monitoring. Damage Detection. Laminated Carbon Fiber Reinforced composites. Hilbert-Huang Transform. Lamb waves.

LIST OF FIGURES

LIST OF ABBREVIATIONS AND ACRONYMS

CFL	Courant-Friedrichs-Lewy criterion
CFRP	Carbon-Fiber Reinforced Polymer
DOF	Degree(s) of Freedom
EMD	Empirical Mode Decomposition
EMD-EDI	Empirical Mode Decomposition Energy Damage Index
EMD-PDI	Empirical Mode Decomposition Phase Damage Index
EESC	Escola de Engenharia de São Carlos
FE	Finite Element
FEM	Finite Element Method
FT	Fourier Transform
FFT	Fast Fourier Transform
GEA	Grupo de Estruturas Aeronáuticas
GW	Guided wave(s)
GLR	Global-Low Resolution
HHT	Hilbert-Huang Transform
HT	Hilbert Transform
IMF	Intrinsic Mode Function(s)
IEEE	Institute of Electrical and Electronic Engineers
LAMSS	Laboratory for Active Materials and Smart Structures
LHR	Local-High Resolution
MP-FEM	Multi-Physic Finite Element Method
NASA	National Aeronautics and Space Administration
NDT	Non-Destructive Test
USP	Universidade de São Paulo

SHM	Structural Health Monitoring
P	P-, longitudinal wave(s)
RLE	Residual Life Estimation
SH	SH-, shear horizontal wave(s)
SV	SV-, shear vertical wave(s)
STFT	Short-Time Fourier Transform
UF	Unified Formulations
VBM	Vibration Based Methods
WT	Wavelet Transform

LIST OF SYMBOLS

α	Rayleigh damping constant
β	Rayleigh damping constant
δ_{ij}	Kronecker's Delta
ϵ_{kl}	Strain tensor
η	Material Structural damping
θ	Phase Angle
Θ	Relative Phase Angle
λ	Lamé's Lambda parameter
Λ_{min}	Minimum wavelength
μ	Lamé's Mu parameter
ν	Poisson's coefficient
ρ	Density
σ_{kl}	Stress tensor
τ	Generic integration variable
ϕ	Generic harmonic disturbance
Φ	Generic basis/shape function
ψ	Wavelet basis function
ω	Angular Frequency
A	Amplitude
A_0	Fundamental Antisymmetric mode
C	Generic Stiffness Tensor
C_P	Stiffness Tensor in Non-Damaged state
C_D	Stiffness Tensor in Damaged state
c_k	k-th Intrinsic Mode Function

D	Dielectric constants matrix
d	Piezoelectric coupling matrix, d-form
E	Wave energy
E^p	Electric field vector
e	Piezoelectric coupling matrix, e-form
G	Shear Modulus
g	Piezoelectric coupling matrix, g-form
k	Wavenumber
K	Acoustic impedance ratio
L_e	Maximum edge length for numerical model
q	Electric Displacement vector
r_n	Residue function after n modes extracted
S	Compliance matrix
S_0	Fundamental Symmetric mode
u_I	Incident wave field
u_R	Reflected wave field
u_T	Transmitted wave field
V	Generic Voltage response
V^R	Reflected wave's voltage response
V^I	Incident wave's voltage response
v_g	Generic Group velocity
$v_{g,P}$	Group velocity through Non-Damaged medium
$v_{g,D}$	Group velocity through Damaged medium
v_p	Generic Phase velocity
$v_{p,P}$	Phase velocity, P-mode
$v_{p,S}$	Phase velocity, SH-,SV-mode

v_{slow}	Model's slowest linear velocity
Y	Young's Modulus
Z	Generic Acoustic Impedance
Z_I	Incident medium's Acoustic Impedance
Z_T	Transmitted medium's Acoustic Impedance

CONTENTS

Part I

Preliminaries

1 INTRODUCTION

To maintain the mechanical integrity of structures is not only a hard technical challenge, it is also a demanding economical one. In 2017, the Brazilian National Congress approved USD 1,8 billion for preventive and corrective maintenance of federal infrastructure valuated in about USD 167 billion, among roads and bridges. In 2014, for Brazilian air transport operators, the combined cost of aircraft maintenance and its depreciation was almost one third of all their costs (ASSIS et al., 2017). With the Brazilian aviation market estimated then close to 90 million domestic passengers (ASSIS et al., 2017) and rising USD 32,9 billion, a 1,4% of Brazil's GDP (MARAZZO; SCHERRE; FERNANDES, 2010), then a rough USD 7 billion were spent on structural integrity-keeping labors on aircrafts that year.

The allocation of resources to keep structural integrity usually impacts economy in micro and macro scales. For civil infrastructure, the money comes from tax pay, which affects citizens. For aircraft operation, it comes from seat price, which, if high, can discourage economical exchange, or even jeopardize the air transportation sector itself, which accounts for more than one million jobs only in Brazil (ASSIS et al., 2017).

Because of that, the area of Structural Health Monitoring —or SHM— of major engineering structures have gained relevance and it has been in intense developing for more than twenty years now. This area studies the technological means that allow moving from a preventive-based maintenance scheme, *i.e.* regular external inspection, to a condition-based one (BALAGEAS; FRITZEN; GÜEMES, 2010), *i.e.* autonomous internal inspection. If applied to reduce aircraft downtime due to scheduled maintenance, researchers such as Su, Ye and Lu (2006) have estimated a reduction of 30% in maintenance costs under such a scheme.

The economic and technological potentials are huge; but, today there is not a widespread solution available yet. The reason: **technological challenges had made difficult to develop a method with enough reliability to be applied, and with a solid know-how that would allow its application in a transverse range of structures**.

The present work is framed inside the SHM area and, in this first chapter, it will be introduced. The problem of interest, the specific objectives, the context in which the work was developed and the organization of the document itself will be presented.

1.1 THE PROBLEM OF INTEREST

The present work is interested in addressing the challenge of overcoming the complexities to achieve an SHM system using Active Acoustic Emission with piezoelectric transducers, by starting with the most simple and also most relevant structure in the aeronautical area: thin plates. More specifically, **it is of interest the study of damage detection on relevant aeronautical-**

grade laminated composites, as the case of Carbon-Fiber Reinforced Polymers (CFRP).

However, the scope is reduced into one particular, but common, case of damage for the aforementioned type of structure: **Delaminations in CFRP plates**. This type of damage can be caused by many operational reasons, and its detection is tricky because they could be present under a good-looking part in the exterior. Requiring, then, intense Non-Destructive Inspections, which result in aircraft downtime.

Due to this, the present work will study the integration of areas such as guided waves on thin plates, also called Lamb waves, the use of piezoelectric transducers for actuation and sensing, and signal processing under a single frame, or model, oriented to solve the delamination detection problem of predefined conditions.

The particular detection case, as it will be explained in the chapter concerning the damage detection model, is the detection in one dimension, *i.e.* a beam or plate with large (infinite) boundaries. The decisions regarding the selection of piezoelectric technology, as the decision of this detection scenario, will be explained in the chapter concerning Structural Health Monitoring (SHM).

1.2 INSTITUTIONAL CONTEXT

The present work was developed in the Aeronautical Structures Group (GEA in Portuguese), where works on SHM of composites have been carried out before, especially in the area of Vibration-Based Methods (VBM). However, **the present work is the group's first on the use of Lamb waves for SHM of composites; thus, most of the work, and also this document, was elaborated having in mind the beginning of know-how construction and the direction of future works on the area.**

1.3 OBJECTIVES

1.3.1 Main objective

To develop and numerically implement a delamination detection strategy for laminated composites using piezoelectric transducers in disk format, by the processing of Lamb wave signals and assess its effectiveness.

1.3.2 Specific objectives

- To do an exhaustive theoretical revision of all the physical phenomenons involved to exploit them for damage detection: Lamb wave propagation, piezoelectricity and signal processing.
- To configure a stable numerical model to simulate Lamb wave propagation on composite plates, with and without delamination.

- To configure a stable numerical model to simulate piezoelectric actuation and sensing.
- To successfully integrate models of the propagating medium and piezoelectric transducers into a single and stable multi-physics model.
- To develop a signal processing scheme that successfully extracts the information required by the detection model to be developed, and implement it in a commercial programming language.
- To study various delamination problems, and to assess the susceptibility of the strategy to the variation of parameters.
- To assess results and propose the steps to experimentally reproduce the simulations, by the GEA group, for the next phase of the project.

1.4 DOCUMENT ORGANIZATION

The document is organized, for its better comprehension, in five parts: Preliminaries, Theoretical Background, One Dimensional Damage Detection, Final Remarks, and Annexes, in that order.

- **Preliminaries:** The work is formally presented in this part. Its objective is to give full insight to the reader of its content.
  - **Introduction:** This chapter is intended to be a quick context giver to the reader. The problem of interest, work objectives, and text organization are described.
  - **Structural Health Monitoring of Aerospace Structures:** This chapter gives a more in-depth sight of how the SHM problem looks like when focusing only on aerospace. The reason for choosing the technologies studied in this work are also stated.
- **Theoretical Frame:** The relevant concepts and equations for every aspect of the study are presented.
  - **Lamb waves:** The basic concepts on Lamb waves involved in this work are thoughtfully explained to gain insight into the challenges facing methodology.
  - **Piezoelectricity:** The basic concepts of Piezoelectrical materials involved in the modeling of transducers are explained, including material characterization and numerical modeling.
  - **Signal Processing:** The traditional tools for the processing of time domain signals are presented, along with the Hilbert-Huang Transform, which is a relatively new tool.

- **Damage Detection in One Dimension:** This part will show the regarding state of the art revision, detection methodology, and its results.
  - **Damage Detection with Piezoelectric Transducers:** A revision of the state of the art on the technology is done along with the presentation of the proposed detection model.
  - **Methodology:** The way of assessment of the proposed model is exposed.
  - **Results:** The results after applying the model under the defined methodology are presented.
- **Final Remarks:** This part sums up the conclusions, future works, and annexes.
  - **Conclusions:** The conclusions obtained after all the revisions, methodology, and results are presented.
  - **Future Works:** The tasks to continue with the research are presented, along with recommendations.
- **Annexes:** Supplementary information is made available to the reader.

2 STRUCTURAL HEALTH MONITORING OF AEROSPACE STRUCTURES

Nowadays, Structural Health Monitoring is an active interdisciplinary area that concerns with improving the reliability and, at the end, to extend the service life of a given structure. These concerns rise, as explained in the last chapter, due to the high cost of maintenance or replacement of some of these structures, especially in the civil, automotive and aerospace sectors.

However, every sector has its own complexities. For the civil infrastructure sector, to efficiently monitor structures of large dimensions and with limited accessibility is an issue; for the aerospace sector, limited accessibility to components and to maximize the aircraft availability are issues, too.

In the particular case of the aerospace sector, many methods have been in intense developing to achieve autonomous structural health assessment. Such achievement has the potential to radically shape the economical availability of the aerospace sector.

Progress have been made. In 2017, researchers with the U.S. Army Research Laboratory and the U.S Army Aviation and Missile Research, Development and Engineering Center successfully developed and tested a network of Acoustic Emission sensors that detected airframe damage on a composite panel of a UH-60 Black Hawk rotorcraft (JAE, 2017). Nonetheless, work remains to be done to achieve a system that is also airworthiness compliance, which is another challenge of aerospace structures.

In this chapter, the Structural Health Monitoring area of study is presented with a particular interest in aerospace structures. Its motivations, and operational schemes described, and the technologies involved, including the ones used in this work, are explained.

2.1 WHY DO SOME STRUCTURES REQUIRE MONITORING?

In some structures, there are failure modes that could risk human lives or turn the structure unrecoverable once they occur. Such modes are denominated as catastrophic failures. Natural degradation of structures, with phenomenons like fatigue or corrosion, combined with in-service events, like sudden high loading or adverse weather conditions, increase the risk of catastrophic failures to happen. Also, materials and manufacturing techniques add uncertainties that could accelerate degradation, ranging from material quality to design test data used for dimensioning.

Uncertainties are accounted for with safety factors, in the design phase; and with inspection and maintenance, during the in-service phase of the life cycle. It should be noted that the inspection frequency has an inverse relation with structural robustness, which depends on the safety factors used to dimension them.

Theoretically, if one applies a sufficiently high safety factor that accounts for any event

during the structure's operational life, the structure tends to be inspection and maintenance free, *i.e.* has Infinite Life. However, to reduce the cost of the robustness of such approach, the Safe-Life design philosophy was proposed. The firsts commercial jetliners were designed with this philosophy, *i.e.* the DeHavilland Comet in 1949 (BRIGMAN, 2012). In Safe-Life, by knowing the load spectra and the fatigue properties of a material, a part can be designed for a specified lifetime by controlling stresses through geometric properties (thickness, cross-section, etc.), assuming no initial defects and not tolerating damage (BRIGMAN, 2012). However, to increase robustness also increases the structure's cost, risking the structure to be economically inviable. Aircraft depend on having a low weight to move more payload with the same amount of fuel for their operation to be profitable. Designing with excessive robustness risks the affordability of air transport operations.

To allow less robust, yet still safe designs, Damage Tolerance philosophy was developed in the 1970s. In this approach, initial cracks within the material are assumed to be present and, by studying crack growth in fatigue for a given material, the propagation rate can be predicted and inspections to detect and monitor these cracks while they grow can be specified, *i.e.* it "tolerates" and controls damage propagation.

The counterpart is that, now, contrary to Safe Life, **inspections are required to continuously monitor and assess a component's integrity and the state of damage propagation, if any**. In practice, many structures, due to its nature or operating environment, are hard to be inspected in their critical points. For instance, many of the structural components of an aircraft cannot be inspected without major disassembling, causing operational downtime.

2.2 DEFINITION

Structural Health Monitoring, or SHM, according to Farrar and Worden (2007), **is the process of implementing a damage identification strategy in civil, aerospace and mechanic infrastructure by means of embedded systems in the structure instead of the traditional approach without an external agent doing the inspection**.

A common example in literature is to compare SHM with the human central nervous system, as shown in Fig. 1. The human skin possesses pressure and temperature sensors that are continuously sending signals, through the nervous connections, to the brain about their "state". If some damage, like a burn, happens, the brain receives a differentiated signal, understood as pain or discomfort, from the sensors next to the damage location. By interpreting these signals, the brain can establish the existence of damage (pain), its type (burn), were it is located (left forearm), its severity (intense) and what the suggested action should be and its urgency (to take medicine, to make an appointment with the doctor or to go to emergency right away).

Likewise, the objective of an SHM is to achieve an autonomous central nervous system for structures that allows detecting damage (*i.e.* positive damage signal), characterize it (low

Figure 1 – SHM analogy with the human nervous system.

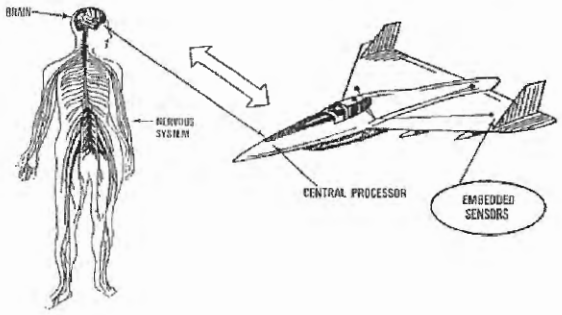

Source: Farrar and Worden (2007, p. 10).

velocity impact like), locate it (fifth panel of left-wing), quantify it (-5% rigidity loss, low severity), and estimate its urgency (part maintenance should be scheduled in maximum 200 flight hours).

In this way, Structural Health Monitoring switches maintenance operations practices from preventive to condition based. This will certainly act as a disruptive technology with the more efficient use of resources as the essence. The way in how the Structural Health Monitoring scheme would look like in the aviation field is explained next.

2.3 OPERATION SCHEME

2.3.1 Actual *vs.* Proposed Integrity Monitoring

A plot of component functionality versus time for a metallic Damage Tolerant component maintained preventively is presented in Fig. 2. The plot is divided by two horizontal lines: The Restoration limit (green) and the Failure limit (red). Above the Restoration limit, the component exhibits its intended performance with optimal reliability. In between the Restoration limit and the Failure limit, the component can still operate, but it is required to be repaired or replaced. Finally, below the Failure limit, the component operates with insufficient reliability and can fail at any moment.

The objective is to maintain the component's functionality (blue curve), which is in constant degradation, above the Restoration limit. This is achieved by performing scheduled inspections and overhauls in intervals, typically measured in flight cycles or hours. In Fig. 2, the component's functionality was inspected two times finding it acceptable. However, in the third inspection, its state is no longer acceptable, as it is below the green line. Once the component is restored (by repairing or replacing it), the curve is vertically displaced towards the optimal reliability region and the whole cycle is repeated. As already explained, the problem with this scheme is an economic one associated with its operation costs for operators and increased frequencies as the aircraft ages.

Figure 2 – Functionality *vs.* Time for a preventively maintained metallic component.

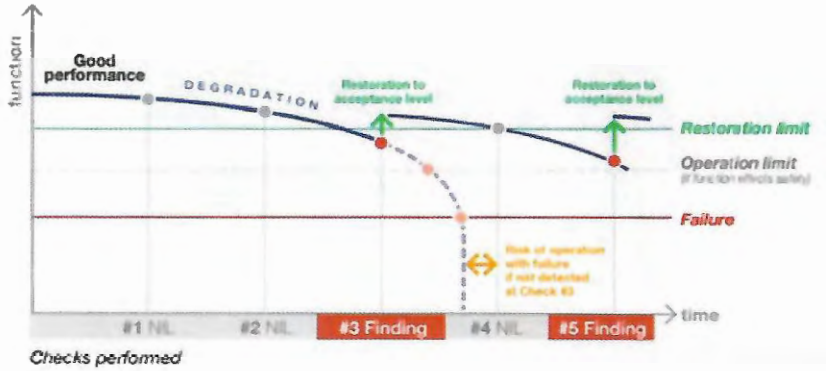

Source: Farrar and Worden (2007).

Figure 3 shows the case in which a condition based maintenance is implemented with the help of an SHM system. When the component suffers a degradation within the sensors' detection limit, the system begins to monitor it. When below the notification limit, the system gives a "maintenance needed" signal, so the time in between the notification and the operational limit is the maintenance window (orange horizontal gap). All the inspections done in the original scheme of Fig. 2, with their associated costs in downtime and repairs, are replaced by just one; only when it is really needed.

Figure 3 – Functionality *vs.* Time for a conditionally maintained metallic component.

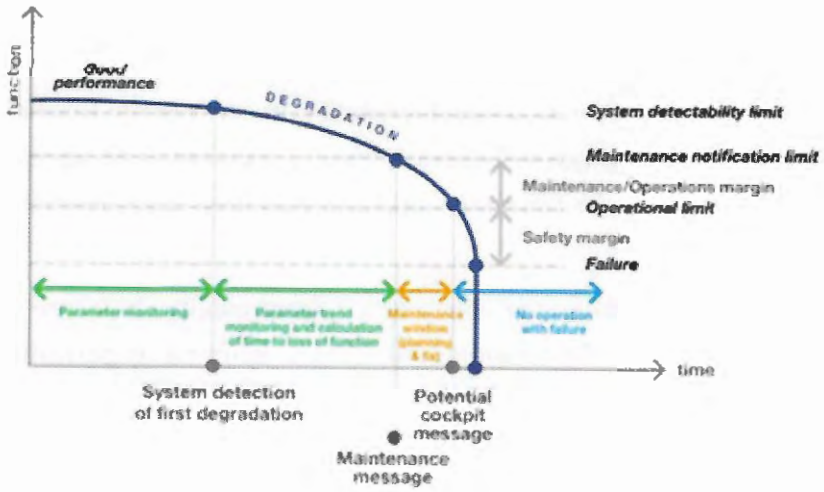

Source: Farrar and Worden (2007).

2.3.2 Market considerations

Nowadays, airline operations face intense market competition. The rise in seat demand added up with the high costs of new airplanes ranging on the millions of dollars, like USD 230 million for a Boeing 787-8 or USD 67 million for an Embraer E-190, encourage operators to squeeze every flight hour from their airplanes to obtain profit. As a result, aircraft are pushed to endure longer life spans before being replaced, thus increasing the average age steadily every year (BOLLER; STASZEWSKI, 2004). The tendency is expected to keep that track. For instance, according to 2017 Boeing's aircraft demand projection for the next 20 years, there were 24400 Boeing airplanes in operation and, in their projection to 2037, 18590 units will have to be replaced, leaving 5810 aged airplanes plus 24140 new ones (COMPANY, 2018).

About the age distribution, research done by Boller and Staszewski (2004) shown some insight of its state as beginning the 21^{st} century. In 1999, the total fleet of Boeing 727 airplanes operating all over the world was of 1831 units, for which the 75% had more than 15 years, 62% had more than 20 years and 38% had more of 25 years.

Due to these tendencies, SHM is key for the future growth of the aviation industry by developing the means of more efficient maintenance, in an operational point of view, for aging and new aircraft alike. This technology can also be seen as a value adding opportunity to the products of any aircraft manufacturer who could harness it and, do to the transversal range of solutions, to also add value in sectors such as civil infrastructure or marine and automobile transportation.

2.4 REVIEW ON SHM TECHNOLOGIES

The options for achieving an SHM system are wide in both working principles and applications. The initial idea behind many of them is to use already known Non-Destructive Tests (NDT) and to integrate them with structures.

These methods are usually classified as Local-High Resolution (LHR) or Global-Low Resolution (GLR) methods (THOMAS, 1995). GLR methods usually have a large area inspection capability and they can be used for quick inspections of large structures, but with low detection resolution due to the variety of factors, besides damages and defects, that can adversely affect inspection, such as complex geometries. In the other side, LHR methods are local in their application, but can better characterize defects (THOMAS, 1995). Some SHM working principles are presented next.

2.4.1 Ultrasonics

A principle already used for NDT, Ultrasonics-based inspection is a well-known LHR technology applied in a wide range of industries.

Low-frequency (typically between 1 and 50 MHz) and concentrated high energy acoustic

pulses are sent through a part and received by transducers. Damage causes a change in the reflected acoustic energy (KHAN et al., 2014). However, its implementation in structures with large surface area, like wings or fuselages, is expensive in both time and materials (DIAMANTI; SOUTIS, 2010).

2.4.2 Laser Doppler Vibrometry

A GLR method where the laser takes measures of vibration amplitude and frequency using the Doppler effect. The laser allows to do area measures, but a disadvantage is the amount of required access to the component to be monitored (BOLLER; MEYENDORF, 2008).

2.4.3 Eddy Current

Eddy Current, which is the most common NDT technique used in commercial aviation (BRIGMAN, 2012) for inspecting surface and near-surface cracks, corrosion, delaminations and other structural defects, in electrically conducting materials, by correlating the measured impedance with calibrated defect dimensions (DIAMANTI; SOUTIS, 2010). The main disadvantage of this method is the continuous demand for power supply; thus, requiring great amounts of power if a long-range inspection is desired.

2.4.4 Optical Fiber Bragg Grating

Optical fiber is a sensor that can achieve global inspection with a medium resolution. The sensor is able to monitor any kind of strain resulting from either mechanical loads, pressure, temperature, acoustic vibration or others. It works by identifying material changes based on variations in transmission intensities, phase, diffraction properties and interference fringe patterns (DIAMANTI; SOUTIS, 2010). A major advantage is that a multitude of sensors (possibly hundreds) can be placed along a single fiber, which reduces complexity in wiring significantly. Because of working on an optical basis the system is immune to any electromagnetic interference. It has shown robustness with regard to in-service application (BOLLER; MEYENDORF, 2008).

2.4.5 Acoustic Emission

When mechanically loaded, a structure can give warnings of its integrity by emitting a sound; a tree branch emits a crack sound before actually breaking, for instance. In this method, transducers listen for acoustic signals generated by cracks, delamination or fiber breakage (KHAN et al., 2014). Acoustic emission is generated by stress waves produced by movement (growth) of defects in solids. A necessary requirement is that the structure is stressed during the inspection and noisy environments could be a problem (DIAMANTI; SOUTIS, 2010).

Acoustic emission differs from other NDT techniques in that its inspection is done in a passive way. Other NDT techniques use an active way to detect damage, *i.e.* gives energy to a

system and record the response of that actuation. The energy measured by transducers in acoustic emission is the one released by the damage itself when it occurs.

2.5 CONSIDERATIONS FOR THIS RESEARCH

The present work is a Master's degree dissertation done in the Laboratory of Composite Materials with the "Grupo de Estruturas Aeronáuticas", or GEA, of the São Carlos School of Engineering of the University of São Paulo. This work is focused on expanding the current know-how of the group in the area of Structural Health Monitoring, concentrating, particularly, on aeronautical-grade structures.

2.5.1 Technology selection

Of all the explained technologies, **Active Acoustic Emission is the one chosen to be the focus of this study**. The compliment "Active" means that, instead of the passive approach already explained, energy will be given to the system and its response to this input will be used to do the integrity monitoring. This approach is one of the most studied lines in SHM due to its advantages, being some of them:

- **Historical loading monitoring:** While in the passive scheme sensors would only listen when damage or significant events occur, in active continuous monitoring exists the possibility to create a historical tracking of the component load spectra, allowing to relate it with its degradation.

- **More freedom in detection approaches and strategies:** The necessity of knowing the medium acoustic characteristics in order to understand a determined "noise" heard by a passive transducer can be diminished by using active strategies to test the medium and characterize it to information more useful to determined task (detect damage, localize it, etc.).

- **Increased range of applications:** Many researchers have reported how hard the passive approach when tracking damages in composite materials. Again, this is due to the complexity in predicting acoustic characteristics when high anisotropy is introduced.

2.5.2 Application technique

For this technology there are also two possible approaches:

- **Pulse-Echo:** In this approach, the acoustic emission transducers produces a user-defined signal and waits for the response —or echo— of that signal. The same transducer is used as an actuator and later as a sensor.

- **Pitch-Catch:** In this approach, a transducer produces a user-defined signal that interacts with the features of the traveling medium and is "caught" later by other transducers.

The one to be studied in this work is Pitch-Catch because it can allow more flexibility in the study of detection strategies based on the location of transducers and so on. Also, allows the use of simpler time-domain calculations for speed, time of flight, etc.

2.5.3 Application means

For generating and sensing the acoustic waves, piezoelectric transducers will be used due to their low invasiveness of the plate specimen. These transducers are commercially available and are also cheap. However, a practical limitation, especially important when experimentally modeling, is the lack of engineering information about these transducer.

A wider explanation of the means by which these transducers actuate and sense is given in an independent chapter.

Part II

Theoretical Frame

3 LAMB WAVES

3.1 ELASTIC WAVES AND THEIR MOTION

A Mechanical wave consists of the oscillatory propagation of energy through some medium; liquid, gaseous or solid. If the propagation medium is an elastic solid, the wave is said to be elastic and its propagation characteristics depend on the elastic and inertial properties of the material in which it travels (BEDFORD; DRUMHELLER, 1994).

According to the particle motion with respect to the propagation direction, there are three basic types of waves patterns for elastic waves:

- **Longitudinal waves:** Known also as compressional waves or P-waves, the particle motion is parallel to the propagation direction (BEDFORD; DRUMHELLER, 1994), as shown in Fig. 4.

Figure 4 – Longitudinal wave motion.

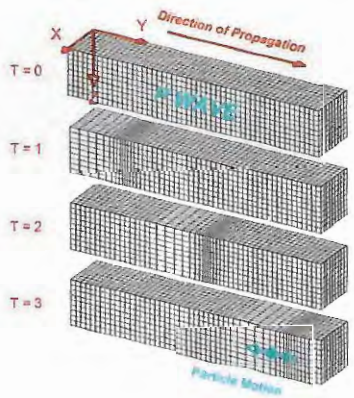

Source: Braile (2017).

- **Transverse waves:** Known also as shear waves or S-waves, the particle motion is perpendicular to the propagation direction. If the motion is outside the material's plane, the wave is called Shear Vertical, or SV-wave. Likewise, if in the material's plane, the wave is called Shear Horizontal, or SH-wave (BEDFORD; DRUMHELLER, 1994). Figure 5 shows a SV-wave.

- **Surface waves:** In general, surface waves are those in which its propagation occurs in the interface between two mediums. This category can be subdivided into many others according to the particular motion shape of the particles. For instance, Rayleigh waves are characterized for an elliptical motion; Love waves, for their in-plane oscillation, as in a

Figure 5 – Transverse wave motion.

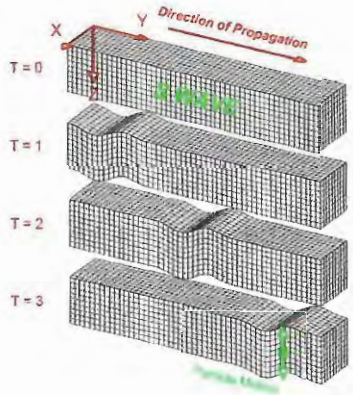

Source: Braile (2017).

SH-wave, but with decreasing amplitude as it distances away from the surface (BRAILE, 2017). These two surface waves are presented in Fig. 6.

Figure 6 – Surface wave motion.

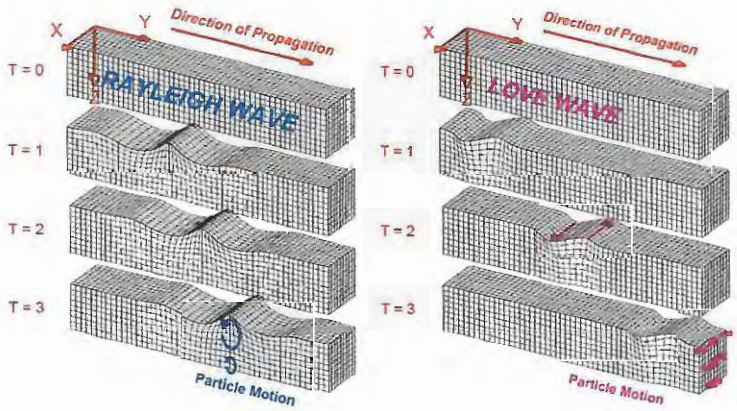

Source: Braile (2017).

The type of wave encountered will depend on the excitation and in the medium. Surface waves are studied mostly in geological science, specifically their behavior in layered elastic media (BRAILE, 2017). However, many parts of the theory developed for geology is applicable to other elastic materials.

3.2 GUIDED WAVES

Elastic waves propagating in a plate are called Guided waves (GW). The research on guided waves is vast and dates back to 1885, with the work of Lord Rayleigh (AAIJ, 2016). Rayleigh analyzed the propagation of elastic waves on the free surface of a semi-infinite solid.

Later, the shear horizontal waves were described by Love in 1911, also for one free surface. In 1917, the motion of waves propagating in an elastic, thin, infinite and isotropic medium with two free surfaces were first described by Horace Lamb (SU; YE; LU, 2006).

In practice, the main difference between Lamb waves and the original Rayleigh waves is their penetration through the thickness. As Rayleigh waves can be encountered in mediums with a great thickness in which not necessarily all the particles oscillate, in Lamb waves the full thickness oscillates. However, it is common in the literature to find references using the term Rayleigh-Lamb waves for describing the same type of GW.

3.3 LAMB WAVE PROPAGATION

On his 1917 study, Horace Lamb obtained results for the displacement field and dispersion relations of Lamb waves in a 2D isotropic medium. In this section, those results are introduced together with other propagation relations regarding phase velocity.

3.3.1 Phase Velocity

Phase Velocity is the linear speed with which the wave propagates, and it depends on the material's constitutive matrix (Hooke's law) and density, the type of wave excitation, vibration mode and the frequency of propagation.

The generalized phase velocity relation, *i.e.* for any direction, for an elastic, anisotropic material was determined by German mathematician Elwin Bruno Christoffel in the late 19^{th} century, and this result is mostly used in seismology study for the propagation of waves in elastic layered media (TSVANKIN, 1997). The equation is:

$$[C_{ijkl}n_j n_l - \rho v_p^2 \delta_{ik}]U_k = 0 \tag{3.1}$$

Where C_{ijkl} is the material's stiffness —or Hooke's— tensor, n_j is the unit vector of the desired propagation direction, v_p is the phase velocity in the desired propagation direction, ρ is the material density (assumed to be uniform), δ_{ij} is the Kronecker's delta, and U_k is the displacement vector. Clearly, Eq. 3.1 is an eigenvalue problem, and it is derived from Newton's second law in the form usually used in the elasticity field.

The complete Hooke's law is:

$$\sigma_{ij} = C_{ijkl}\epsilon_{kl} \tag{3.2}$$

Where σ_{ij} is the stress tensor, and ϵ_{kl} is the strain tensor.

$$\begin{bmatrix} \sigma_{11} \\ \sigma_{22} \\ \sigma_{33} \\ \sigma_{12} \\ \sigma_{13} \\ \sigma_{23} \end{bmatrix} = \begin{bmatrix} C_{1111} & C_{1122} & C_{1133} & C_{1112} & C_{1113} & C_{1123} \\ C_{2211} & C_{2222} & C_{2233} & C_{2212} & C_{2213} & C_{2223} \\ C_{3311} & C_{3322} & C_{3333} & C_{3312} & C_{3313} & C_{3323} \\ C_{1211} & C_{1222} & C_{1233} & C_{1212} & C_{1213} & C_{1223} \\ C_{1311} & C_{1322} & C_{1333} & C_{1312} & C_{1313} & C_{1323} \\ C_{2311} & C_{2322} & C_{2333} & C_{2312} & C_{2313} & C_{2323} \end{bmatrix} \begin{bmatrix} \epsilon_{11} \\ \epsilon_{22} \\ \epsilon_{33} \\ 2\epsilon_{12} \\ 2\epsilon_{13} \\ 2\epsilon_{23} \end{bmatrix} \tag{3.3}$$

For which 21 material constants are required for the most anisotropic case, due to the symmetry of C_{ijkl}. However, only two cases are of interest in the study of SHM of aeronautical-grade structures: Isotropic and Orthotropic materials.

3.3.1.1 Isotropic Case

In the case of an isotropic travel medium, the simplest case, the tensor is considerably simplified, and the needed constants are reduced to only two; the stiffness, Y, and the Poisson's ratio, ν, resulting in:

$$C = \frac{Y}{(1+\nu)(1-2\nu)} \begin{bmatrix} 1-\nu & \nu & \nu & 0 & 0 & 0 \\ \nu & 1-\nu & \nu & 0 & 0 & 0 \\ \nu & \nu & 1-\nu & 0 & 0 & 0 \\ 0 & 0 & 0 & \frac{1-2\nu}{2} & 0 & 0 \\ 0 & 0 & 0 & 0 & \frac{1-2\nu}{2} & 0 \\ 0 & 0 & 0 & 0 & 0 & \frac{1-2\nu}{2} \end{bmatrix} \tag{3.4}$$

So, the constitutive equation for isotropic solids, in term of Lamé parameters is:

$$\begin{bmatrix} \sigma_{11} \\ \sigma_{22} \\ \sigma_{33} \\ \sigma_{12} \\ \sigma_{13} \\ \sigma_{23} \end{bmatrix} = \begin{bmatrix} 2\mu+\lambda & \lambda & \lambda & 0 & 0 & 0 \\ \lambda & 2\mu+\lambda & \lambda & 0 & 0 & 0 \\ \lambda & \lambda & 2\mu+\lambda & 0 & 0 & 0 \\ 0 & 0 & 0 & \mu & 0 & 0 \\ 0 & 0 & 0 & 0 & \mu & 0 \\ 0 & 0 & 0 & 0 & 0 & \mu \end{bmatrix} \begin{bmatrix} \epsilon_{11} \\ \epsilon_{22} \\ \epsilon_{33} \\ 2\epsilon_{12} \\ 2\epsilon_{13} \\ 2\epsilon_{23} \end{bmatrix} \tag{3.5}$$

Where λ and μ, the Lamé parameters, are defined as:

$$\lambda = \frac{Y\nu}{(1+\nu)(1-2\nu)} \tag{3.6}$$

and

$$\mu = \frac{Y}{2(1+\nu)} \tag{3.7}$$

By resolving Eq. 3.1 using the stiffness tensor in Eq. 3.5 the following relations can be obtained (TSVANKIN, 1997):

$$\begin{bmatrix} \Gamma_{11} - \rho v_p^2 & \Gamma_{12} & \Gamma_{13} \\ \Gamma_{21} & \Gamma_{22} - \rho v_p^2 & \Gamma_{23} \\ \Gamma_{31} & \Gamma_{32} & \Gamma_{33} - \rho v_p^2 \end{bmatrix} \begin{bmatrix} U_1 \\ U_2 \\ U_3 \end{bmatrix} = \begin{bmatrix} 0 \\ 0 \\ 0 \end{bmatrix} \tag{3.8}$$

With:

$$\Gamma_{11} = (2\mu + \lambda)n_1^2 + \mu n_2^2 + \mu n_3^2 \tag{3.9}$$

$$\Gamma_{22} = \mu n_1^2 + (2\mu + \lambda)n_2^2 + \mu n_3^2 \tag{3.10}$$

$$\Gamma_{33} = \mu n_1^2 + \mu n_2^2 + (2\mu + \lambda)n_3^2 \tag{3.11}$$

$$\Gamma_{12} = (\lambda + \mu)n_1 n_2 \tag{3.12}$$

$$\Gamma_{23} = (\lambda + \mu)n_2 n_3 \tag{3.13}$$

$$\Gamma_{13} = (\lambda + \mu)n_3 n_1 \tag{3.14}$$

Now, if solving for a principal direction, *i.e.* for the X_1 direction, that is $n = (n_1, n_2, n_3) = (1, 0, 0)$, gives:

$$\begin{bmatrix} (2\mu + \lambda) - \rho v_p^2 & 0 & 0 \\ 0 & \mu - \rho v_p^2 & 0 \\ 0 & 0 & \mu - \rho v_p^2 \end{bmatrix} \begin{bmatrix} U_1 \\ U_2 \\ U_3 \end{bmatrix} = \begin{bmatrix} 0 \\ 0 \\ 0 \end{bmatrix} \tag{3.15}$$

So the eigenvalues, or phase velocities, for Lamb waves propagating through an isotropic material are:

$$v_{p,11} = v_{p,P} = \sqrt{\frac{2\mu + \lambda}{\rho}} \tag{3.16}$$

$$v_{p,12} = v_{p,S} = \sqrt{\frac{\mu}{\rho}} \tag{3.17}$$

$$v_{p,13} = v_{p,S} = \sqrt{\frac{\mu}{\rho}} \tag{3.18}$$

The subscripts in Eq. 3.16, Eq. 3.17, and Eq. 3.18 mean wave propagation in the X_1 direction, particle motion in the X_1, X_2, and X_3 directions. The latter is equivalent to the phase velocities of the P ($v_{p,P}$), SH and SV ($v_{p,S}$) waves.

3.3.1.2 Orthotropic Case

Next, is the Orthotropic case, which models composite laminates. For a composite lamina, the X_1 axis is chosen to be aligned with the fibers, and the X_3 to be perpendicular with the lamina's plane. Isotropic properties lie in the X_2X_3 plane.

Carbon Fiber laminate show isotropy in the local 2-3 plane, making $Y_2 = Y_3$, $G_{12} = G_{13}$, and $\nu_{ij}/Y_i = \nu_{ji}/Y_j$. Then, the stiffness tensor requires six elastic constants,

$$C = \begin{bmatrix} Y_1\frac{1-\nu_{23}\nu_{32}}{\Lambda} & Y_1\frac{\nu_{21}+\nu_{31}\nu_{23}}{\Lambda} & Y_1\frac{\nu_{31}+\nu_{21}\nu_{32}}{\Lambda} & 0 & 0 & 0 \\ Y_1\frac{\nu_{21}+\nu_{31}\nu_{23}}{\Lambda} & Y_2\frac{1-\nu_{13}\nu_{31}}{\Lambda} & Y_2\frac{\nu_{32}+\nu_{12}\nu_{31}}{\Lambda} & 0 & 0 & 0 \\ Y_1\frac{\nu_{31}+\nu_{21}\nu_{32}}{\Lambda} & Y_2\frac{\nu_{32}-\nu_{12}\nu_{31}}{\Lambda} & Y_2\frac{1-\nu_{12}\nu_{21}}{\Lambda} & 0 & 0 & 0 \\ 0 & 0 & 0 & G_{12} & 0 & 0 \\ 0 & 0 & 0 & 0 & G_{13} & 0 \\ 0 & 0 & 0 & 0 & 0 & G_{23} \end{bmatrix} \tag{3.19}$$

With,

$$\Lambda = 1 - \nu_{12}\nu_{21} - \nu_{23}\nu_{32} - \nu_{31}\nu_{13} - 2\nu_{21}\nu_{32}\nu_{13} \tag{3.20}$$

In the same way as the isotropic case, by solving Eq. 3.1 the Christoffel's coefficients for an orthotropic material.

$$\Gamma_{11} = C_{11}n_1^2 + C_{66}n_2^2 + C_{55}n_3^2 \tag{3.21}$$

$$\Gamma_{22} = C_{66}n_1^2 + C_{22}n_2^2 + C_{44}n_3^2 \tag{3.22}$$

$$\Gamma_{33} = C_{55}n_1^2 + C_{44}n_2^2 + C_{33}n_3^2 \tag{3.23}$$

$$\Gamma_{12} = 2(C_{12} + C_{66})n_2n_1 \tag{3.24}$$

$$\Gamma_{23} = 2(C_{13} + C_{55})n_3 n_1 \tag{3.25}$$

$$\Gamma_{13} = 2(C_{44} + C_{23})n_2 n_3 \tag{3.26}$$

Then, if solving again for the X_1 direction, that is $n = (n_1, n_2, n_3) = (1, 0, 0)$, gives

$$v_{p,P} = \sqrt{\frac{C_{11}}{\rho}}, \tag{3.27}$$

$$v_{p,SV} = \sqrt{\frac{C_{55}}{\rho}}, \tag{3.28}$$

$$v_{p,SH} = \sqrt{\frac{C_{66}}{\rho}}. \tag{3.29}$$

3.3.2 Dispersiveness

Dispersiveness is said to occur when wave characteristics, like phase velocity, vibration modes, wavelength or wavenumber, are dependent on the oscillation frequency. The mathematical functions stating these relations are called dispersion relations. It is important to note that, the phase velocities found for P, SH and SV waves (Eq. 3.16, Eq. 3.17, and Eq. 3.18) do not account for dispersiveness, so they, in practice, will be valid for low values of frequency. When higher frequencies and other vibration modes start to act, phase velocities vary greatly.

Horace Lamb obtained dispersion relations for isotropic plates and demonstrated the existence of two types of vibration modes in plates: Symmetrical and Anti-symmetrical modes (LAMB, 1917). He reached the following dispersion relations:

$$\frac{\tan(wh)}{\tan(lh)} = -\left[\frac{(w^2 - k^2)^2}{4k^2 lw}\right]^{\pm 1} \tag{3.30}$$

With $+1$ for the Symmetric modes and -1 for the Anti-symmetric modes. Also,

$$l^2 = \frac{\omega^2}{v_{p,P}^2} - k^2 \tag{3.31}$$

$$w^2 = \frac{\omega^2}{v_{p,S}^2} - k^2 \tag{3.32}$$

where ω is the angular frequency, h is half the plate's thickness and $k = \omega / v_p$ is the wavenumber. Dispersiveness depends, then, on mechanical properties and plate thickness.

Dispersion relations have also been developed for anisotropic materials, with the aim to apply them to the achievement of dispersion relations for the modeling of Lamb wave propagation on composites, and have been found to be very similar, however more complex in their computing. For reference on the development of the equation for both isotropic and anisotropic materials, reference Giurgiutiu (2007) is suggested.

Equation 3.30 relates all the wave characteristics and can be used to determine magnitudes ranging from the displacement field, up to frequency dependent phase velocities (ROYER; DIEULESAINT, 2000). However, Lamb waves exhibit an infinite number of modes associated with their propagation, that is, Eq. 3.30 has infinite solutions (STASZEWSKI; MAHZAN; TRAYNOR, 2009).

The first solutions for the Symmetric and Anti-symmetric modes are called S_0 and A_0, respectively. The shapes across the thickness of these two modes are shown in Fig. 7.

Figure 7 – Lamb wave fundamental modes: S_0 (left) and A_0 (right).

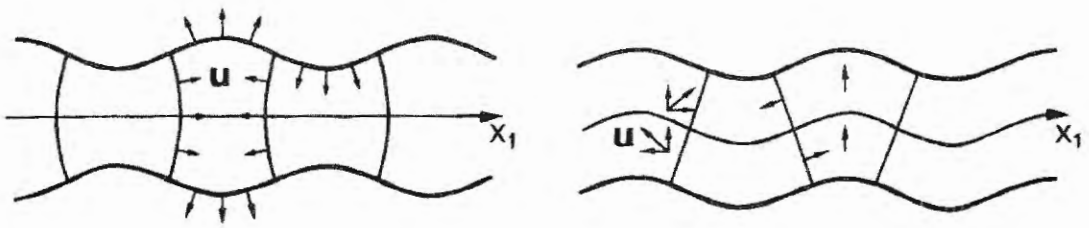

Source: Royer and Dieulesaint (2000).

It is common to show the solutions for the phase velocity, obtained from the dispersion relations, like curves in function of the product of frequency and thickness. For a given thickness $2h$ and frequency $F_c = \omega/2\pi$, the dispersion curves can be obtained for different materials. Figure 8 shows a dispersion curve for a steel plate.

The line shapes of Fig. 8 are mostly the same for any other isotropic material. It can be seen how the firsts, or fundamental, modes start from the low-frequency times thickness range (<1.5 MHz x mm); however, the next modes (A_1, S_1, etc.) start far from the origin. The latter is also described as, the first modes have no cutoff frequency, as the other ones do.

The knowing of this dispersive behavior is key for any numerical modeling attempt of Lamb waves because it will define the geometrical and temporal refinement required for the meshes involved in the study.

3.3.3 Group Velocity

Dispersive waves commonly occur in problems involving boundaries and interfaces. If dispersion (dependence to frequency) exists, a wave tends to spread as it propagates (BEDFORD;

Figure 8 – Phase velocities (solid line) and Group velocities (broken lines) curves for a Steel with $v_{p,P}$= 5900 m/s and $v_{p,S}$= 3100 m/s.

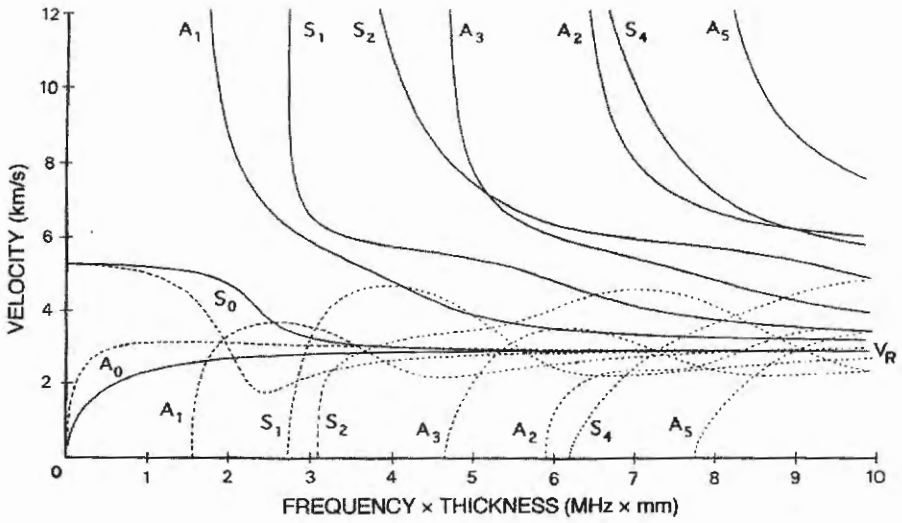

Source: Royer and Dieulesaint (2000).

DRUMHELLER, 1994). The spreading occurs by the wave separating in many components with different frequencies, depending on the grade of dispersiveness of the medium. This spreading is measured by comparing the velocity of the group or wave package (external envelope) with the phase velocity, as shown in Fig. 9.

In a non-dispersive medium, a steady state Lamb wave propagating at a natural frequency, ω_0, will have constant phase velocity, $v_p = \omega_0/k$, as already explained. However, due to the dispersive properties of the medium:

$$v_p(\omega) = \frac{\omega}{k(\omega)} \tag{3.33}$$

If the wavenumber function is expressed as a Taylor expansion and considering the error term very small:

$$k(\omega) = k(\omega_0) + (\omega - \omega_0)\frac{dk}{d\omega}\bigg|_{\omega_0} = k(\omega_0) + \frac{\omega - \omega_0}{v_g(\omega)} \tag{3.34}$$

Where:

$$v_g(\omega) = \frac{d\omega}{dk} \tag{3.35}$$

Is the group velocity.

The group velocity is another characteristic determined from the dispersion relation (Eq. 3.30). Once obtained, there are three possible scenarios:

Figure 9 – Group Velocity (broken line) and Phase Velocity (solid line).

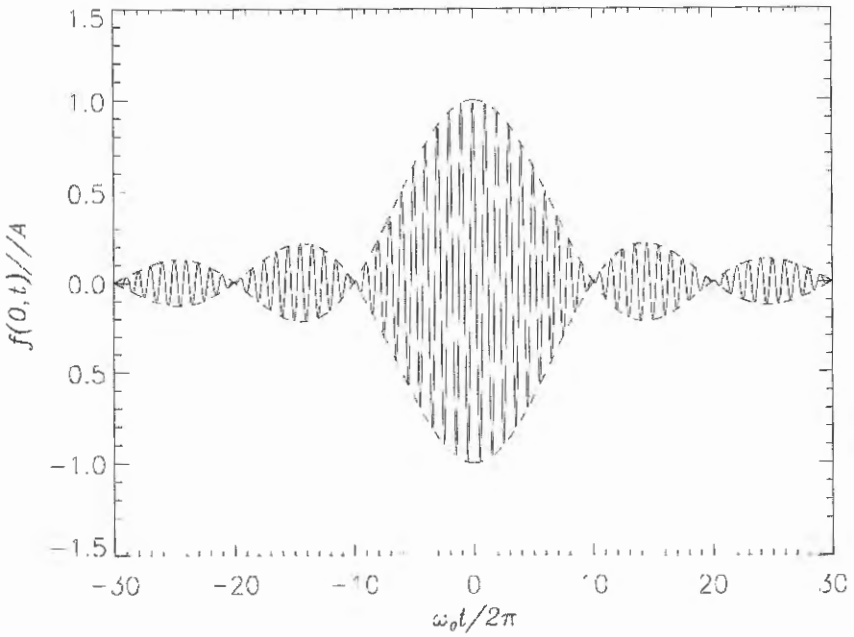

Source: Bedford and Drumheller (1994).

- $v_g > v_p$: When the phase wave propagates more slowly than the group wave, an observer stationary with respect to the package envelope (broken line in Fig. 9) sees waves being "created" at the front of the group, traveling backward, and disappearing at the back (BEDFORD; DRUMHELLER, 1994).

- $v_g = v_p$: In this case, both waves move together, and the wave appears with a "static" shape that propagates forward.

- $v_g < v_p$: When the phase velocity is greater, the observer in the envelope sees waves being created at the back of the group, moving forward, and disappearing at the front (BEDFORD; DRUMHELLER, 1994).

3.4 LAMB WAVE ATTENUATION

Theoretically, if the medium is non-dissipative, the standing straight waves described by the dispersion relation of Eq. 3.30 will propagate indefinitely without loss of amplitude. However, this assumption will not hold true when the transducer, or the wave source in general, it is in a localized point of the plate, and not along one of its axis; in such cases, the propagation will have a geometric spreading that does exhibit an amplitude loss, or attenuation, while it travels due to energy conservation. The latter means **the Lamb wave propagation, in the way in which it is understood in SHM, can be modeled as a perturbation on a system, originated in a**

punctual location on it. Greater attenuation can be observed if the damping properties of the medium are considered. To understand attenuation can provide insight on the extents of Lamb wave detection range, and also provide tools for damage detection, as done in this work and explained in a later chapter.

Works done by Gresil and Giurgiutiu (2015) studied the effects of Lamb wave attenuation for the purpose of SHM, and they described the phenomenological origins of attenuation in CFRP materials, contrasting them to the origins in metals, as the Viscoelastic nature of the matrix and/or fiber materials; Damping due to interphase; Damping due to damage; Viscoplastic damping at large amplitudes of vibration/high stress levels; and Thermo-elastic damping (GRESIL; GIURGIUTIU, 2015).

Now, from the global perspective, the Lamb wave attenuation can be attributed to:

- **Geometric spreading:** This component describes the loss of amplitude due to the growing length of a wavefront departing into all directions from the source.
- **Material damping:** Describes how much energy stored in the wave dissipates due to non-perfect elastic material behavior.
- **Wave dispersion:** this component is attributed to the existence of many wave modes propagating at different velocities.
- **Dissipation into adjacent media:** Describes the dissipation due to the surrounding medium, which is almost non-existent in the general case, which is air.

If the dissipation into adjacent media is neglected and the wave dispersion is controlled through adequate signal windowing (this will be explained in the signal processing chapter), the wave propagation signal measured from a circular wavefront through a damped plate can be established as (GRESIL; GIURGIUTIU, 2015):

$$\phi(r,t) = A\frac{1}{\sqrt{r}}e^{-\eta r}e^{i(\omega t - kr)} \tag{3.36}$$

Where r is the distance between the source and the sensor, A is the magnitude, or amplitude, of the signal, ϕ is a generic disturbance, taken here as the voltage signal, that propagates in space as a wave, and η is the medium's structural damping.

Equation 3.36 shows clearly the interaction of three components. The factor $1/\sqrt{r}$ is associated with the geometrical spreading of the wave. The factor $e^{-\eta r}$ represents the material damping and the factor $e^{i(\omega t - kr)}$ represent the temporal and spatial harmonics. The structural damping coefficient η relates to the Rayleigh damping factors α and β as:

$$\frac{(\alpha + \beta\omega^2)}{2v_g} = \eta \tag{3.37}$$

However, if those constants are unknown, **the amplitude and damping parameters can be obtained through curve fitting Eq. 3.36 with measuring at two different locations.** Also, it is better suited to work with the peak-to-peak maximum magnitude of the wave packet.

Figure 10 shows the transducer response for various values of r to show the amplitude attenuation. Figure 11 shows the fitting of the geometric spreading and material damping of Eq. 3.36 and comparing it by the geometric-only and damping-only curves to reveal how the geometric spreading is predominant over short distances from the source and how the material damping becomes predominant over large distances. Gresil and Giurgiutiu (2015) demonstrated how this formulation fits behaves well with experimental data, especially when r increases.

Figure 10 – Signal received at various distances (damped medium).

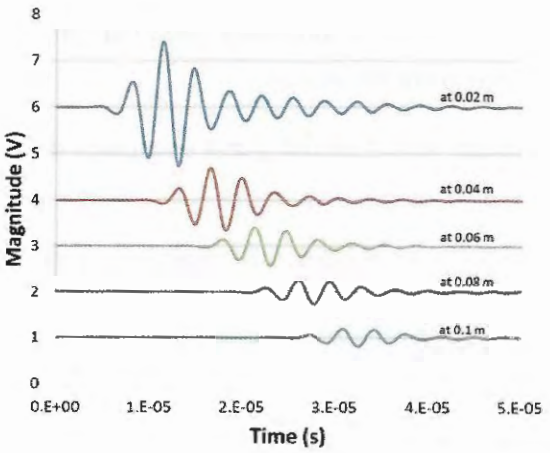

Source: Gresil and Giurgiutiu (2015).

Figure 11 – Maximum peak-to-peak magnitude of ϕ at various distances.

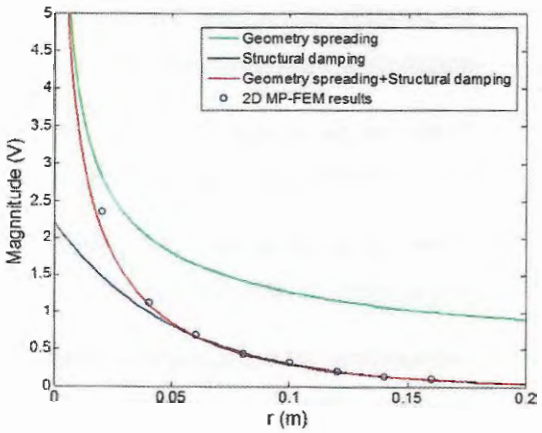

Source: Gresil and Giurgiutiu (2015).

In practice, **it is more convenient to work with the maximum peak-to-peak magnitudes, rather than arbitrarily chosen values of instant peak-to-peak amplitude at a given time**. The reason is that this quantity is directly comparable between transducers and measures, *i.e.* the time of flight of a wave can be determined by comparing the times of appearance of the maximum peak-to-peak amplitude at the transducer and sensor. In the other hand, the values of different peak-to-peak magnitudes will depend on wave dispersion also, complicating its comparison.

This maximum peak value, V_p, of the envelope of the wave response function, $V(r,t)$, can be established as the infinity norm evaluated over the Hilbert Transform (HT) of the Lamb wave voltage response, as:

$$V_p = \|H\{V\}(r,t)\|_\infty \tag{3.38}$$

For propagation with multiple modes, the norm should be taken locally.

3.5 LAMB MODES INFLUENCE ON SHM

Researchers such as Alleyne and Cawley (1992), and Ihn and Chang (2008) have shown the mode-sensitivity of Lamb waves. For example, the S_0 mode is sensible to cracks, and the A_0 mode is sensitive to failures such as delamination or debonding, which happen in composites. All these possibilities make the use of Lamb waves to be very attractive to the aerospace industry, ground transportation and civil engineering where composite material plates are becoming increasingly common (BALAGEAS; FRITZEN; GÜEMES, 2010).

In the case of composites, the main problem is that depending on the stacking sequence of a given laminate, the dispersiveness behavior is even more complex, direction-dependent and harder to predict. Also, composite materials are used to create complex geometry parts that can difficult the dispersiveness prediction. For instance, the dispersion curves for the phase velocity obtained for a composite plate can be different for the ones obtained for a curved fuselage section; even with the same layup sequence.

Figure 12 – Dispersion curves for a composite lamina in the 0deg (left) and 90deg (right) directions.

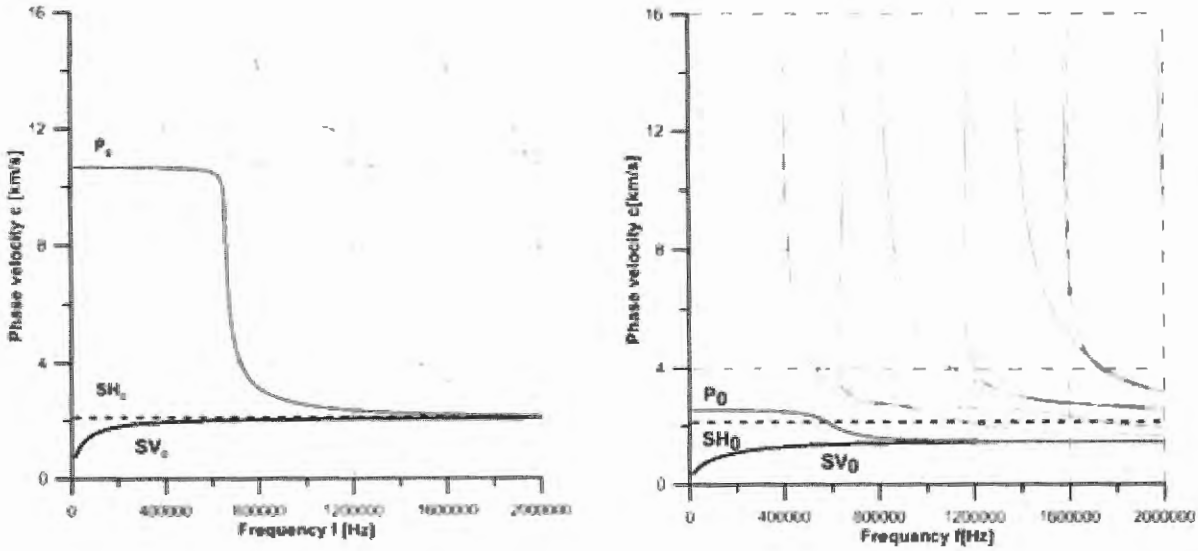

Source: Barski and Pająk (2016).

Figure 12 (left) shows the dispersion curves for phase velocity in the directions parallel to the fiber. P_0, SH_0, and SV_0 mean fundamental compressional, shear horizontal and shear vertical wave modes. It is notable how these modes coexist in the low-frequency range (< 700 kHz), but, when the product frequency times thickness increases, other modes (P_1, SH_1, SV_1, P_2, etc.) start to coexist. Until now, the same behavior as in isotropic plates.

In contrast, in the right graph of Fig. 12, the same dispersion curve is shown, but for

propagation perpendicular to the fiber direction. The behavior changed completely and can be seen how a range of less than 700 kHz does not guarantee low dispersiveness in this direction, as it did along the fiber. Instead, the existence of only the fundamental modes is bounded by 400 kHz now. This situation proves to be more difficult to predict once the laminae are stacked up. Methods as the Global Transfer Matrix are used to calculate dispersion for laminate materials.

This challenge can also be expected on assemblies of isotropic material, in which features like holes, rivets, welds, and fasteners can change the dynamics of the system, derailing the Lamb wave inspection performance from its designed effectiveness.

4 PIEZOELECTRICITY

Piezoelectricity is the property by which certain materials become electrically polarized when they are strained, referred to as the direct piezoelectric effect, and by which also become strained when exposed to an electric field, referred to as the converse piezoelectric effect. This property was discovered in 1880 by Pierre and Jacques Curie during their study of the effects of pressure on the generation of electrical charge by crystals such as Quartz (JORDAN; OUNAIES, 2001).

This material gained visibility in the industry in the 19^{th} century when they opened up opportunities for underwater applications as ultrasonic transducers, or microphones, accelerometers, etc. (JORDAN; OUNAIES, 2001). Today they are found in a wide range of applications, and they are mostly made by synthetic production.

The interest in the use of piezoelectric materials in this work is due to their capacity as transducers. Transducers made of piezoelectric ceramics are relatively cheap, easy to attach to a given structure, and come in a wide range of forms; even allowing for custom dimensions. Examples of these transducers are shown in Fig. 13.

Figure 13 – Piezo transducers of various forms: Disk (left) and Strip (right).

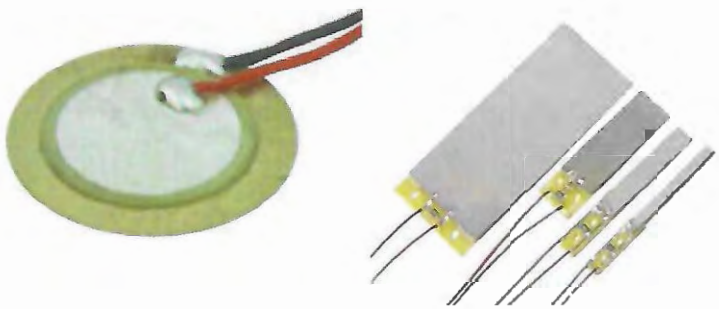

Source: Balageas, Fritzen and Güemes (2010).

In this chapter, the constitutive relations regarding piezoelectricity are presented. Also, considerations of their modeling for simulation purposes are introduced.

4.1 CONSTITUTIVE EQUATIONS

According to the 1987 IEEE standard on Piezoelectricity, in linear piezoelectricity, the equations of linear elasticity are coupled to the charge equation of electrostatics by means of the piezoelectric constants. These constants are usually expressed in many forms, depending on

what is intended to model, or what information is available, or even in which conditions were taken the experimental data regarding the material.

In general, piezoelectric materials are described with the same stress/strain relations for elastic solids and electrical displacement relations of continuous media. Additional to them, an "electro-mechanical", or piezo, coupling is added to the equations. If these materials are usually in the small strains regime, with thermal-related and electrical hysteresis effects neglected, then the linear piezoelectric behavior is valid. In total, linear piezoelectricity has three equivalent equation forms. These are described next with the notation used in ABAQUS literature (CORP, 2014).

- **e-form:** In this form, σ_{ij} is the stress tensor, C^E_{ijkl} is the Material Stiffness matrix measured with zero electrical gradient present in the specimen, ϵ_{kl} is the strain tensor, e^{ϕ}_{mij} is the piezoelectric coupling, E^p_m is the electric field, q_i is the electric flux vector or displacement, and D^{ϕ}_{ij} are the dielectric constants. Superscripts E, ϕ, and q are constant electrical field, strain and electrical displacement, respectively.

$$\sigma_{ij} = C^E_{ijkl}\epsilon_{kl} - e^{\phi}_{mij}E^p_m \tag{4.1}$$

$$q_i = e^{\phi}_{ijk}\epsilon_{jk} + D^{\phi}_{ij}E^p_j \tag{4.2}$$

- **d-form:** In this form, S^{E}_{ijkl} is the Material Compliance matrix measured with zero electrical gradient present in the specimen, and d^{ϕ}_{mij} is the piezoelectric coupling.

$$\epsilon_{ij} = S^E_{ijkl}\sigma_{kl} - d^{\phi}_{mij}E^p_m \tag{4.3}$$

$$q_i = d^{\phi}_{ijk}\sigma_{jk} + D^{\phi}_{ij}E^p_j \tag{4.4}$$

- **g-form:** In this form, S^q_{ijkl} is the Material Compliance matrix measured with zero electrical displacement present in the specimen, and g^{ϕ}_{mij} is the piezoelectric coupling.

$$\epsilon_{ij} = S^q_{ijkl}\sigma_{kl} - g^{\phi}_{mij}q_m \tag{4.5}$$

$$E^p_i = -g^{\phi}_{ijk}\sigma_{jk} + (D^{\phi})^{-1}_{ij}q_j \tag{4.6}$$

In ABAQUS, the e-form is default, but d-form is also available. To implement g-form, is necessary to calculate the equivalent of its constants in the e-form or d-form (CORP, 2014). Hereafter, when commenting the constitutive relations for piezoelectricity, the d-form will be assumed.

4.2 POLED PIEZOELECTRIC CERAMICS

When polarized, a piezoelectric ceramic becomes transversely isotropic in the plane perpendicular to the polarization direction. The local coordinates are arranged with the X_3 axis along the Polarization direction, leaving the plane X_1X_2 as the plane of isotropy. The latter is traduced in a local coordinate system as shown in Fig. 14.

Figure 14 – Local coordinate system on a polarized piezo disk.

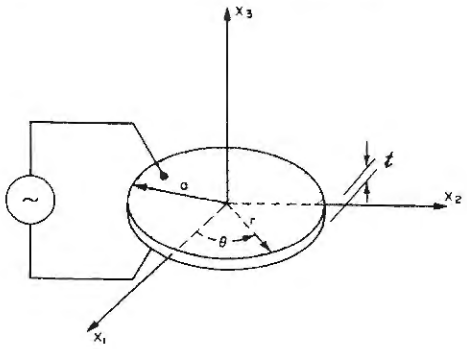

Source: Meeker (1996).

Do to this transversal isotropy, the shapes of the elastic, dielectric and piezoelectric properties can be established, and are shown in Eq. 4.7. Note the compliance matrix corresponds to the orthotropic stiffness tensor of the type described in Eq. 3.19.

$$\begin{bmatrix} \epsilon_{11} \\ \epsilon_{22} \\ \epsilon_{33} \\ \epsilon_{12} \\ \epsilon_{13} \\ \epsilon_{23} \\ q_1 \\ q_2 \\ q_3 \end{bmatrix} = \begin{bmatrix} S^E_{1111} & S^E_{1122} & S^E_{1133} & 0 & 0 & 0 & 0 & 0 & d_{311} \\ S^E_{1122} & S^E_{2222} & S^E_{2233} & 0 & 0 & 0 & 0 & 0 & d_{311} \\ S^E_{1133} & S^E_{2233} & S^E_{3333} & 0 & 0 & 0 & 0 & 0 & d_{333} \\ 0 & 0 & 0 & S^E_{1122} & 0 & 0 & 0 & d_{113} & 0 \\ 0 & 0 & 0 & 0 & S^E_{1133} & 0 & d_{113} & 0 & 0 \\ 0 & 0 & 0 & 0 & 0 & S^E_{2233} & 0 & 0 & 0 \\ 0 & 0 & 0 & 0 & d_{113} & 0 & D_{11} & 0 & 0 \\ 0 & 0 & 0 & d_{113} & 0 & 0 & 0 & D_{11} & 0 \\ d_{311} & d_{311} & d_{333} & 0 & 0 & 0 & 0 & 0 & D_{33} \end{bmatrix} \begin{bmatrix} \sigma_{11} \\ \sigma_{22} \\ \sigma_{33} \\ \sigma_{12} \\ \sigma_{13} \\ \sigma_{23} \\ E^p_1 \\ E^p_2 \\ E^p_3 \end{bmatrix} \tag{4.7}$$

Hence, to fully model the Piezoelectric electro-mechanical behavior of a piezoelectric ceramic, the following set of constants are required to be known, additional to density ρ :

- **Six Elastic constants:** Y_1, Y_3, ν_{12}, ν_{31}, G_{12}, and G_{13}.
- **Two Dielectric constants:** D_{11}, and D_{33}.
- **Three Piezoelectric constants:** d_{113}, d_{333}, and d_{311}.

4.3 PIEZO INTERACTION WITH HOST STRUCTURE

Figure 15 shows a piezo transducer attached at the top of a composite laminate. This way, the harmonic electrical excitation in a piezo translates, due to the piezo coupling, into a harmonic deformation of it, transmitting these into the plate's surface, then generating the propagating Lamb waves.

Figure 15 – Polarized piezo disk on composite plate.

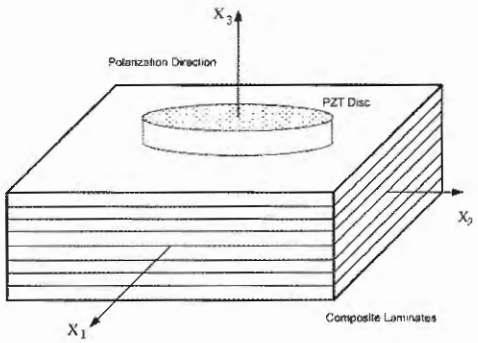

Source: Yang et al. (2006).

The modeling of the latter described interaction is done by determining the actuating tractions on both sides of the coupling between the piezo and the laminate. The following discussion is based on the work of Yang et al. (2006) titled "Some aspect of numerical simulation for Lamb wave propagation in composite laminates", which addresses the modeling of the piezo-structure interaction, which is also used for damage detection in a later study. **This work is highly recommended for any introductory revision on numerical Lamb wave modeling.**

In a case as shown in Fig. 15, plane stress state can be assumed in the piezo. Also, if in addition, polarization is considered only in the X_3 direction, then Eq. 4.7 is reduced to:

$$\sigma_{11} = \frac{Y}{1-\nu^2}\left((\epsilon_{11} + \nu\epsilon_{22}) - (1+\nu)d_{311}E_3^p\right) \tag{4.8}$$

$$\sigma_{22} = \frac{Y}{1-\nu^2}\left((\epsilon_{22} + \nu\epsilon_{11}) - (1+\nu)d_{311}E_3^p\right) \tag{4.9}$$

$$q_3 = D_3E_3^p + d_{311}(\sigma_{11} + \sigma_{22}) \tag{4.10}$$

Where Y and ν, are Young's module and Poisson's ratio in the plane of isotropy (plane parallel to X_1X_2 in Fig. 15). **These harmonic stresses can be solved and used as boundary condition input if desired.**

There are two possible configurations when attaching transducers to a plate: to use them one-sided or two-sided. These configurations can be seen in Fig. 16 and Fig. 17, respectively. The motivation to use one or another is the type of Lamb modes desired to be excited. The one-side option will generate both anti-symmetrical and symmetrical modes simultaneously. In the two-side approach, single modes can be achieved by choosing the harmonic voltage input to be in phase for both transducers, Anti-symmetric, or phase-shifted 180 degrees, symmetric (YANG et al., 2006).

Figure 16 – Composite plate with single actuator: both modes.

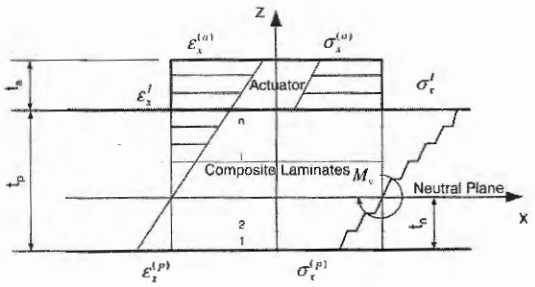

Source: Yang et al. (2006).

Figure 17 – Composite plate with double actuator: Antisymmetric mode (left), Symmetric mode (right).

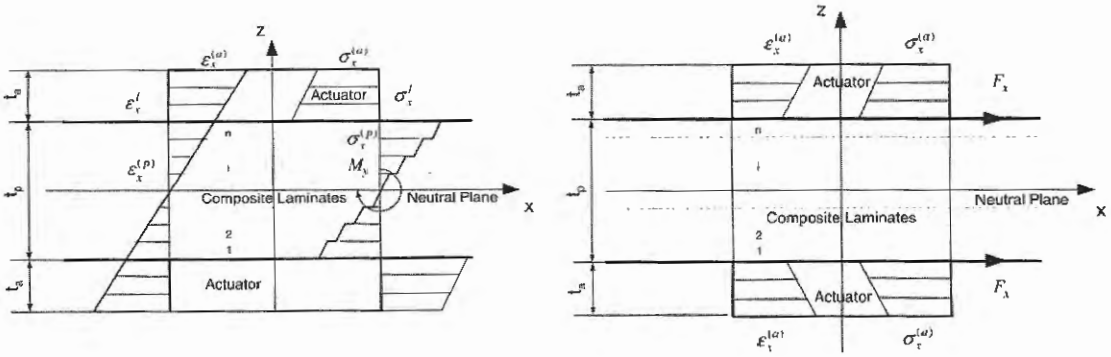

Source: Yang et al. (2006).

The reason for both modes appearing in the single transducer case is the unsymmetrical actuation. As can be seen in Fig. 16, the transducer stresses communicated to the plate through their contact area, generate stress and strain distributions that will not necessarily coincide with the geometric middle plane of the plate, thus generating an "irregular" wave pattern that can be decomposed into the two modes. In the other hand, the plate two-sided with transducers in the correct phase can make the neutral axis with the geometric center. However, this will not be

always the case, depends on the laminate stacking to be symmetrical; nevertheless, the individual mode excitation can still be achieved.

4.4 LAMB WAVE TUNING WITH PIEZOELECTRIC TRANSDUCERS

As already explained, the interaction of a piezoelectric transducer with a host structure through an adhesive layer induces a series of surface strains that generate the Lamb waves. The nature of the strain pattern, the kind of adhesive transducer-structure contact, and the physical shape and dimension of the transducer can have a distinctive effect on the different propagation modes. The application of these different properties to affect the Lamb modes is what it is called Lamb wave mode tuning (GIURGIUTIU, 2007).

Giurgiutiu (2005) demonstrated how the Lamb wave response amplitude of each one of the two fundamental modes, S_0 and A_0, in aluminum, are dependent on the excitation frequency and the transducer's length (he used strip transducers in this first study). He experimentally demonstrated the existence of "sweet spots" or combinations of frequency times thickness values that, for a given transducer with a fixed length, amplify certain mode while diminishing the other, so in practice a (quasi) single mode is excited.

Figure 18 – Lamb wave response on 1 mm thick aluminum plate under a 7 mm strip piezoelectric transducer: Predicted (left), Experimental (right).

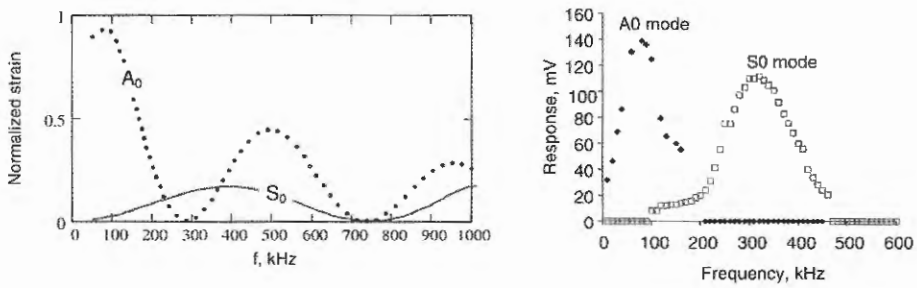

Source: Giurgiutiu (2005).

Figure 18 shows the predicted and experimentally measured tuning curves obtained by Giurgiutiu (2005). It can be seen how in the low-frequency range, the A_0 mode is dominant, while in the high range, the S_0 is dominant. In particular, the frequency around 100 kHz is of interest because it maximizes A_0 while S_0 is minimal in comparison. The contrary case occurs around 300 kHz, where the S_0 mode propagates alone. Some authors have exploited this feature for damage detection.

5 DATA FUSION AND SIGNAL PROCESSING

Another important branch of SHM is the processing and data fusion of signals. This branch of study consists, basically, in receiving all the information obtained by the sensors and to process it in a way that is manageable and it gives relevant information to use it as input to the diagnosis tool or algorithm (WORDEN; STASZEWSKI, 2003).

Data Fusion is itself a wide and interdisciplinary area. Its beginnings lie in the military framework, were many information sources (or sensors) have to be quickly assessed and processed to give real and, very often, vital information about the state of any given situation (WORDEN; STASZEWSKI, 2003). This interpretation can be easily extended to many other applications, including SHM.

In the other hand, Signal Processing involves the techniques of extracting useful information and features from signal data history, given in the adequate shape (*i.e.* treated with Data Fusion techniques), and feeding them into a diagnosis or damage detection tool.

In that order, many common signal processing techniques involve features as transforming time-domain information into frequency-domain or finding patterns in the shape, or envelope, of data on both domains. However, certain kinds of data still offer a challenge to some of the classic techniques. The Hilbert-Huang Transform (HHT) is a recent signal processing tool designed to solve some of these practical problems (HUANG et al., 1998). The use of this tool for damage detection in composites is just recent and, due to this, its application is also explored in this work.

In this chapter, a general review on data fusion and traditional signal processing tools, with their advantages and limitations, are presented in order to introduce the HHT. First, a review on the field of data fusion is introduced. Then, the Fourier, Short-Time Fourier, Wavelet and Hilbert transforms, common tools in signal processing, are described to give insight of their practical limitations regarding nonlinear and non-stationary signals. Finally, the Hilbert-Huang transform and its empirical mode decomposition are explained in detail and how it can be used to analyze signals. Also, the current limitations of the method are mentioned.

5.1 REVIEW ON DATA FUSION FOR SHM

A short review of basic data fusion concepts will be presented in this section. Is worth noting that, since this work is oriented on numerical simulations of a short number of transducers, the application of data fusion is quite simplistic and it is not one of its main focus. However, when applications call for a greater number of transducers, or situations with nonlinear damages and more, the fusion of received data will shape in a significant manner the correct assessment and diagnosis of the health integrity of a given structure. Also, most of the information shown in

this review is taken from the work on the matter done by Worden and Staszewski (2003).

Figure 19 – information treatment process for a single sensor.

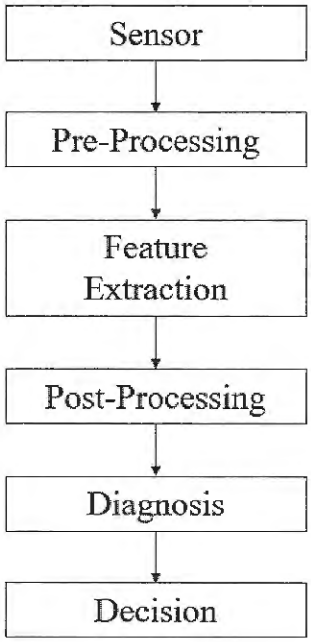

Source: Worden and Staszewski (2003).

The basic structure of information processing for a single sensor will be a chain of acts, as shown in Fig. 19.

- **Sensor:** Provides an electrical signal proportional to the structural variable of interest, *i.e.* Lamb wave response of the medium.

- **Pre-Processing:** This step aims to reduce the dimension of the data vector and eliminate as much redundancy as possible, *i.e.* shrinking the portion of data history to analyze by excluding sections of no interest.

- **Feature Extraction:** Signal processing techniques enter in this stage. The objective is to extract all the information-rich content of the signals, *i.e.* modal resonances, peak times, maximum amplitudes, etc.

- **Post-Processing:** This step consists of taking the features extracted in the latter step and to turn them treatable by the damage detection algorithm, *i.e.* normalizing amplitudes, calculating wave energy, etc.

- **Diagnosis:** In this step the system is classified and quantified in basis of a diagnostic or pattern recognition algorithm, *i.e.* "damaged plate with a delamination 20 mm wide, approximately".

- **Decision:** The final stage in which, after the diagnosis assessment, a decision and action are taken by the computer or a human operator.

It is evident that, in such a scheme, the use of a single sensor will yield into rather fragile monitoring, where if one part of the information processing chain fails, the rest will give no useful or, even worse, false information. The use of many sensors, even redundant ones, can solve this issue. However, the integration, or fusion, of all the data requires a different approximation. This is when data fusion models start to appear.

In their review, Worden and Staszewski (2003) introduce many data fusion models with their application, advantages, and disadvantages. Basically, the use of one or other type of model will depend exclusively on the nature of the phenomenon and the level of reliability of the sensing and processing tools available for that phenomenon.

The model most suited for the current work, on the scale that is currently involved, is the denominated "Diagnosis-level fusion model", and it is shown on Fig. 20.

Figure 20 – Information treatment process for multiple sensor according to a diagnosis-level data fusion.

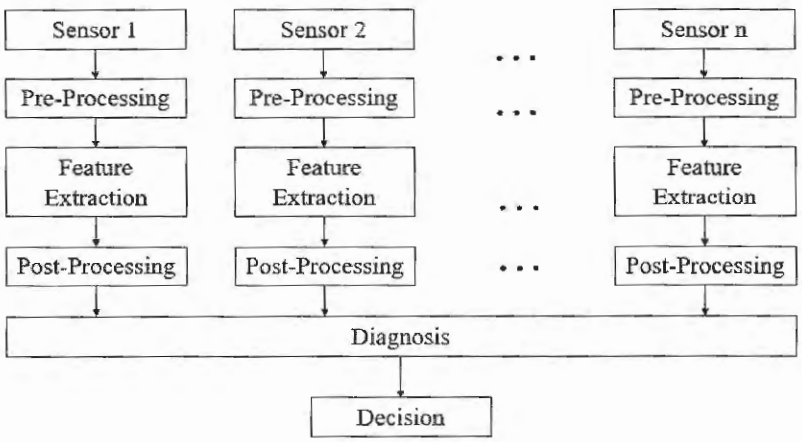

Source: Worden and Staszewski (2003).

This model states that, for each transducer in the system, the sensing, pre-processing, the extraction of features, and post-processing is done at the transducer level, *i.e.* for all individual signals. Then, the multiple features are sent to a centralized diagnosis, where they are plugged into a damage detection algorithm and the result is sent to the operator so he or she can take a decision based upon it.

5.2 REVIEW ON SIGNAL PROCESSING TOOLS

Signal processing is a vast theoretical and experimental field intending to study the connection between measurements made in the form of signals and the conclusions we draw from those measurements. Its objective is to identify or describe variability and relation between variables. However, the tools used can sometimes change the nature of signal data itself; hence their study is of great importance.

The signal processing tools try to give an insight into a system by using the information contained in a set of measured signals. These signals are usually described as a combination of basis, or shape, functions times some amplitude constants. The latter means, if $f(t)$ is a signal in the time domain, it can be described as:

$$f(t) = \sum_{i=1}^{n} a_i \Phi_i(t) \tag{5.1}$$

Where a_i and Φ_i are the i-th amplitude constant and basis function, respectively. A signal such that it can be satisfactorily described as in Eq. 5.1, **it is said to be linear**. Also, if a signal shows little or no variation of its mean and variance along the time, **it is said to be stationary**.

Some signal processing and analysis tools will be described to give insight into how many approaches can be taken from the same set of data contained in a signal described as Eq. 5.1, and all the information that can be withdrawn from it.

5.2.1 Fourier Transform (FT)

When analyzing periodic fluctuation in measured data, the most common form of data analysis is Fourier analysis, which was formulated by Joseph Fourier in the early 19^{th} century. This tool uses the postulate that any signal $f(t)$ can be constructed as a sum of sinusoidal functions with different central frequencies, ω_i; that is, sines and cosines can be used as basis functions in Eq. 5.1, thus:

$$f(t) = \sum_{i=1}^{n} a_i \sin(\omega_i t) \tag{5.2}$$

So the a_i and ω_i are yet to be found. The process to obtain them is the Fourier Transform, defined as:

$$a(\omega) = \int_{-\infty}^{\infty} f(t) e^{-i\omega t} dt \tag{5.3}$$

Because the frequency of each sinusoidal function must be time-independent, Fourier analysis is able to construct linear and stationary data only. This means that the frequency of the signal is assumed to not change with time. Also, because the sine waves used to describe a signal

are infinite in extent, Fourier analysis is considered a global analysis tool. Figure 21 shows the transformation graphically.

Figure 21 – Fourier Transform process.

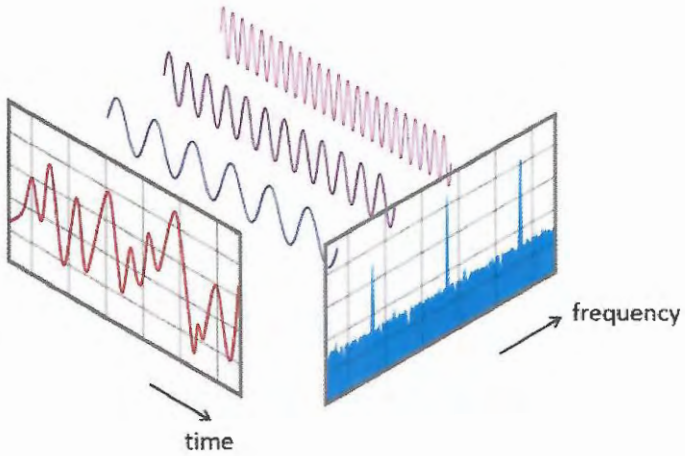

Source: NTi Audio AG (2017).

This tool clearly is not suited for nonlinear and specially non-stationary signals. Due to its global scope, and its transformation into the frequency domain, information contained in signals can be lost. For instance, the Fourier spectrum for two different square signals will be the same regardless of the order in which they appear in the time domain (POULARIKAS, 2010). To solve this, and other problems, the short-time Fourier transform was developed.

5.2.2 Short-Time Fourier Transform (STFT)

Non-stationary signals such as sporadic impulses or aperiodic signals cannot be described locally using Fourier analysis. To accommodate for non-stationary signals, the short-time Fourier transform, or STFT, was developed and it is defined as:

$$STFT(\omega, t) = \frac{1}{2\pi} \int_{-\infty}^{\infty} f(t)h(t-\tau)e^{i\omega t}d\tau \tag{5.4}$$

The idea is to break a non-stationary signal into sections, in all of which the signal is admitted. Then, regular Fourier transform can be used in each section. That is, this tool is adequate when the signal shows to be stationary within each window. The window function, $h(t-\tau)$, is chosen by the user to be of a particular size.

Caution must be taken when selecting the window size. If taken too short, only high-frequency components will be captured, and low-frequencies, with longer time periods, will not be resolved. In the other hand, longer windows have more possibility of capturing non-stationary waves, inducing to errors.

5.2.3 Wavelet Transform (WT)

The wavelet transform is a recent mathematical tool developed mainly since the middle 1980s. Its intention is efficient multiresolution local spectrum analysis of non-stationary, linear, and fast transient signals. It has been studied as a powerful tool with application in fields such as sound, radar, sonar, seismic, electrocardiograph signals, image compression, image processing, and pattern recognition (POULARIKAS, 2010).

The continuous wavelet transform of a function $f(t)$ is a decomposition of $f(t)$ into a set of basis functions, $\psi_{a,b}(t)$, called wavelets. Wavelets are generated from a single pre-defined wavelet, $\psi(t)$, as:

$$\psi_{a,b}(t) = \frac{1}{\sqrt{a}}\psi\left(\frac{t-b}{a}\right) \tag{5.5}$$

Where a and b are parameters called dyadic dilation and position, respectively. The wavelet transform of $f(t)$, F_{wt}, is defined as:

$$F_{wt}(a,b) = \frac{1}{\sqrt{a}}\int_{-\infty}^{\infty} f(t)\psi\left(\frac{t-b}{a}\right)dt \tag{5.6}$$

The wavelet transform basically represents the similarity between a signal and the predetermined wavelet, ψ, at a scale a at time b. The union of these many wavelets of different size and frequency is used to construct the original signal.

These wavelet basis functions are very flexible in their application. They allow local analysis, and low and high frequencies can be analyzed. However, as the wavelet form is chosen a priori, its precision is guaranteed only by a good selection of the basic form function. Erroneous picking could lead to misleading results with poor or no physical interpretation.

Examples of different wavelet basis functions, generated in MATLAB, are shown in Fig. 22 and Fig. 23.

Figure 22 – Mexican hat wavelet.

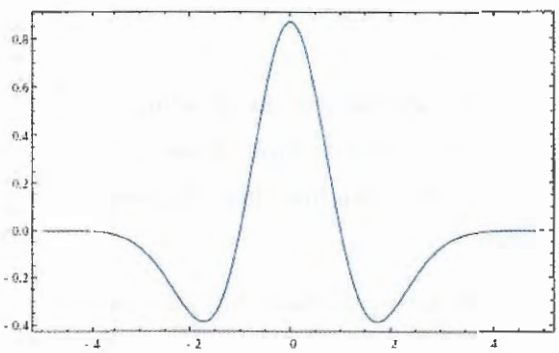

Source: The Author (2019).

Figure 23 – Meyer's wavelet.

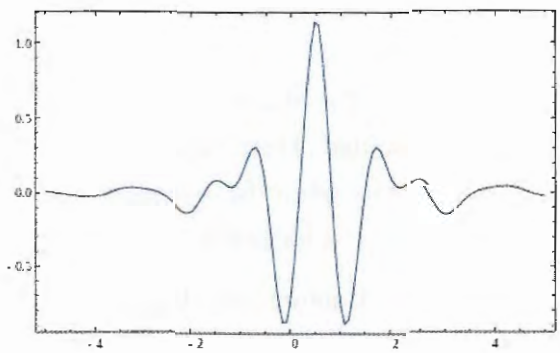

Source: The Author (2019).

5.2.4 Hilbert Transform (HT)

The Hilbert transformations are of widespread interest because they are applied in the theoretical description of many devices and systems, such as analog or digital filters (POULARIKAS, 2010). Its importance lies in the derivation of analytic representation of real-valued signals, that is, the transformation of a real-valued signal function into a complex-valued one without negative frequency components, in contrast to those obtained through the Fourier transform, for instance. A signal with non-negative frequencies allows many useful mathematical manipulations, such as easier conversion from complex to real.

The Hilbert transform, $H\{U\}(t)$, of a one-dimensional real signal, $U(t)$, is defined by the following integral transformation:

$$H\{U\}(t) = \frac{-1}{\pi} P \int_{-\infty}^{\infty} \frac{U(\tau)}{\tau - t} d\tau \tag{5.7}$$

And the inverse Hilbert transformation is:

$$U(t) = \frac{1}{\pi} P \int_{-\infty}^{\infty} \frac{H\{U\}(\tau)}{\tau - t} d\tau \tag{5.8}$$

Where P stands for Cauchy's principal value of the integral and τ is an integration variable. The pair of functions $U(t)$ and $H\{U\}(t)$ is called "Hilbert pair". It is worth noting that **the Hilbert transform does not change the domain of the function**; in contrast to the Fourier transform, which translates a time domain into a frequency domain.

The usefulness of the Hilbert transform is the construction of analytic signals, which are the real-valued parts of the complex analytic functions. An analytic function, Z, is made out of two continuously differentiable complex-valued functions, U and $H\{U\}$, defined on a domain D in the complex plane, such as any point (t, τ) on D can be described as:

$$Z(t, \tau) = U(t, \tau) + iH\{U\}(t, \tau) \tag{5.9}$$

So, an analytic signal is a complex valued function on the real variable t which takes the values of the analytic function along the real axis. That is:

$$Z(t) = U(t) + iH\{U\}(t) \tag{5.10}$$

Therefore, a analytical signal can be constructed from a Hilbert pair by using the original signal $U(t)$ in the real part and $H\{U(t)\}$, the HT, as its complex conjugate.

5.3 THE HILBERT-HUANG TRANSFORM

The Hilbert-Huang Transform (HHT) is a recent breakthrough in the analysis of nonlinear and non-stationary time series. It was published in 1998 by NASA scientist Norden E. Huang. The method consists in a sifting, or sectioning, process called the Empirical Mode Decomposition (EMD), which in combination with Hilbert spectral analysis represent "a desperate attempt to break the suffocating hold on data analysis by the twin assumptions of linearity and stationarity" (HUANG, 2014).

The HHT tries to address both nonlinear and non-stationary data, in contrast to methods, such as the Fourier or Short-Time Fourier transforms, which can only process linear and stationary data; or the Wavelet analysis or Wagner-Ville distribution, which can process non-stationary but not nonlinear data (HUANG, 2014; POULARIKAS, 2010). The biggest issue is that traditional data analysis relies on the use of pre-defined basis functions, and the data is forced to fit with these functions. The EMD process does the opposite, *i.e.* it constructs post-defined functions based on the input data. These functions are named Intrinsic Mode Functions (IMF) and exhibit interesting properties for applications ranging from denoising filters, to structural damage detection (HUANG et al., 1998).

5.3.1 Signal Analysis through the HT and its limitations

Due to Hilbert Transform's capacity of creating an analytic signal from the original time series, some modal magnitudes of interest in analysis of linear and nonlinear systems, such as instantaneous amplitude, phase angle and frequency, among others, can be obtained.

The calculation of these quantities shows how analytic signals describe a more general form of the Phasor concept, which is basically the representation of harmonic functions using the length and angle with respect a horizontal axis of a vector centered at the origin of a complex plane, formed by a Hilbert pair, as shown in Fig. 24.

- **Instantaneous Amplitude:** Also known as "envelope function", is the length of the Phasor.

$$A(t) = \sqrt{U^2(t) + H\{U\}^2(t)} \tag{5.11}$$

- **Instantaneous Phase angle:** It is obtained as the angle relative to the real axis of the Phasor.

$$\theta(t) = \arctan\left(\frac{H\{U\}(t)}{U(t)}\right) \tag{5.12}$$

- **Instantaneous frequency:** It is obtained as the time derivative of the instantaneous phase angle.

$$\omega(t) = \frac{d\theta(t)}{dt} = \frac{U(t)\dot{H\{U\}}(t) - H\{U\}(t)\dot{U}(t)}{U^2(t) + H\{U\}^2(t)} \tag{5.13}$$

Figure 24 – Phasor created by a Hilbert pair of functions.

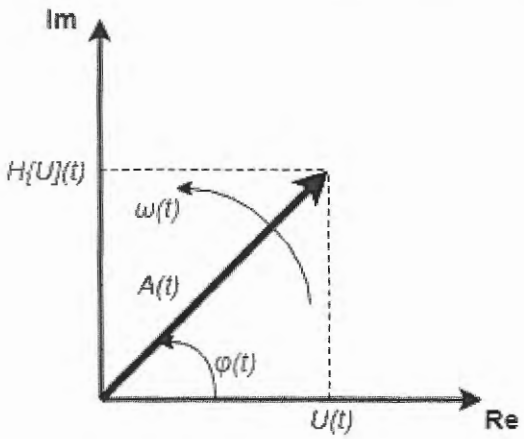

Source: The Author (2019).

Such an approach cannot be obtained by the FT or the STFT alone, because they assume, for instance, constant frequency for each sine function of the basis. With the WT instantaneous values can be obtained only locally for every wavelet used to construct the signal.

The HT allows for instantaneous values, but, to be consistent, the Hilbert pair must be continuously differentiable. In practice, this is achieved for simple harmonic signals only (HUANG et al., 1998), and real signals usually require special filtering and pre-processing before being further analyzed. Also, the simple and direct application of the HT could give analytic signals representations with negative frequencies, thus complicating physical interpretation. The empirical mode decomposition process of the Hilbert-Huang Transform (HHT) was aimed to solve these problems (SOUZA, 2008).

5.3.2 Empirical Mode Decomposition

The empirical mode decomposition, or EMD, method was introduced in 1998 by Norden Huang as a way to overpass the problems that made the HT difficult to apply to real signals with multiple frequency components(HUANG et al., 1998). In this paper, Huang exposed how the EMD could be potentially superior to the FT or the WT for processing nonlinear and non-stationary signals (SOUZA, 2008).

In contrast to traditional methods, the EMD method is intuitive, direct, and adaptive, with a post-defined basis derived entirely from the data (HUANG, 2014). The basic assumption made is that any data set consists of simple intrinsic modes of oscillations (HUANG et al., 1998). **Each intrinsic mode, linear or nonlinear, represents a simple oscillation, that has the same number of extrema and zero-crossings** (HUANG, 2014). This notion of IMF are summarized with the following two assumptions (HUANG, 2014):

i. In the whole dataset, the number of extrema and the number of zero-crossings must either equal or differ at most by one.

ii. At any point, the mean value of the envelope defined by the local maxima and the envelope defined by the local minima is zero.

The EMD is, then, the iterative process of decomposing (or sifting) functions in the time domain, $f(t)$, in a set of n number of Intrinsic Mode Functions, $c_k(t)$, and a residue, r_n, which combined return the original signal:

$$f(t) = \sum_{k=1}^{n} c_k(t) + r_n \tag{5.14}$$

To exemplify the obtaining of the different IMF, an application case shown in Huang (2014) will be presented here. The objective is to extract the first IMF of a test data, $x(t)$, shown in Fig. 25.

Figure 25 – Test data of $x(t)$.

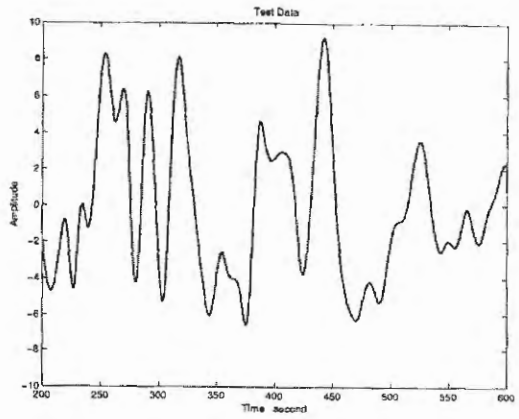

Source: Huang (2014, p.5).

Figure 26 – Envelopes and mean for $x(t)$.

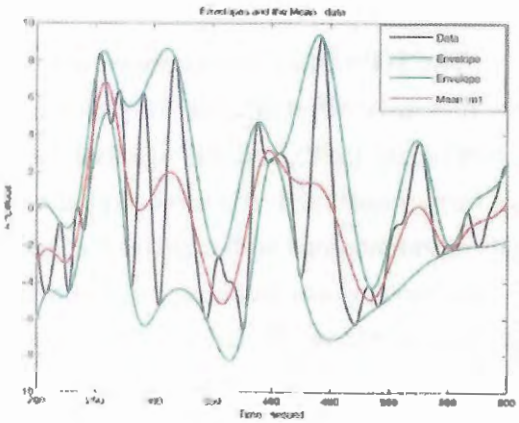

Source: Huang (2014, p.6).

First, all local maximums and minimums are identified and then interpolated to generate upper and lower envelopes. Later, the mean curve, $m_1(t)$, between the two envelopes is also taken. Figure 26 shows these two envelopes in green and $m_1(t)$ in red. A first h curve, $h_1(t)$ is then defined as:

$$h_1(t) = x(t) - m_1(t) \tag{5.15}$$

This $h_1(t)$ is shown in purple on Fig. 27 and it should be theoretically an IMF by fulfilling the two conditions mentioned before. By the construction of $h_1(t)$, the above process should

have made it symmetric with all of its maxima positive, and all its minima negative (HUANG, 2014); the result clearly does not correspond to an IMF. In that case, the process is repeated with $h_1(t)$ as shown in Fig. 28. The result is a function $h_2(t)$, which should fulfill conditions to be an IMF. If not, then the loop is repeated on $h_2(t)$, as shown in Fig. 29. The IMF conditions should be fulfilled after sifting k-times, which is a number of sufficient loops. Then, the first IMF, c_1 is:

$$c_1 = h_k \tag{5.16}$$

Figure 27 – Data for $h_1(t)$ and $x(t)$.

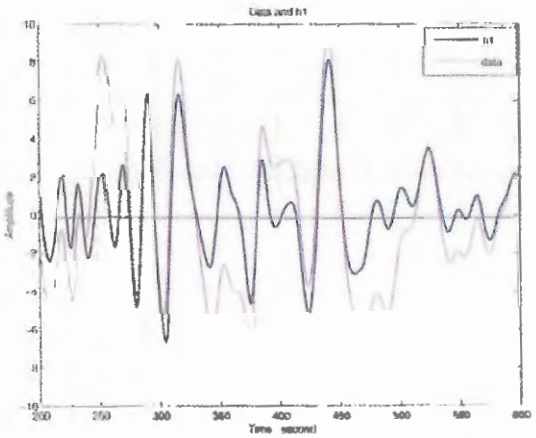

Source: Huang (2014, p.6).

Figure 28 – Envelopes and mean for $h_1(t)$.

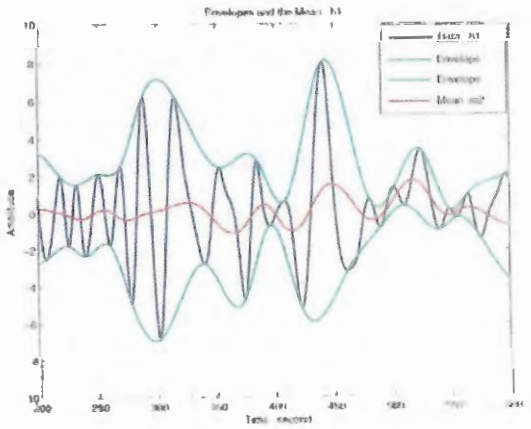

Source: Huang (2014, p.7).

Considering the present particular case, the first IMF was obtained after 12 steps, and it is shown in Fig. 30.

Figure 29 – Envelopes and mean for $h_2(t)$.

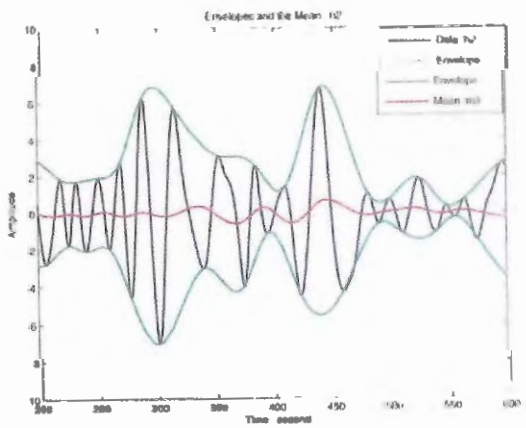

Source: Huang (2014, p.7).

Figure 30 – $h_{12}(t)$ data.

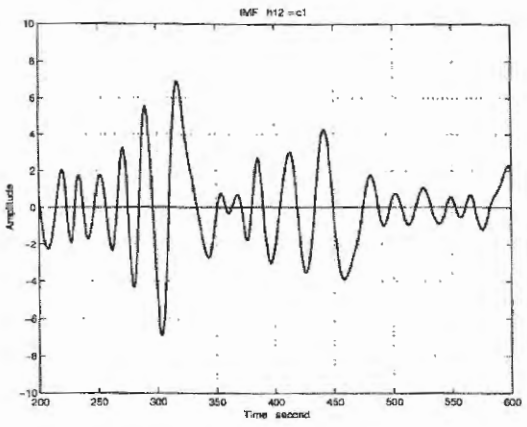

Source: Huang (2014, p.8).

At this point, a stop criteria for exiting the loops must be given to the algorithm. The one originally published by Huang in 1998 uses a Cauchy type of convergence test: repeat until the normalized squared difference between two successive sifting operations is minimized to some tolerance (HUANG, 2014). This Normalized squared difference is defined as:

$$SD_k = \frac{\sum_{t=0}^{T} |h_{k-1}(t) - h_k(t)|^2}{\sum_{t=0}^{T} h_{k-1}^2} \tag{5.17}$$

Huang recognized that such an approach is difficult to implement, due to some difficult considerations, such as how small SD_k should be (SOUZA, 2008). Today, **the stoppage criteria is an ongoing discussion**. Proposals range from comparing wave energy ratios, up to determining a "proper" number of iterations to achieve an IMF, which could be in between 4 or 8 as determined by Huang in a later work (SOUZA, 2008).

Once the first IMF, $c_1(t)$ is obtained, it is subtracted from the original signal, $x(t)$, leading to a residue $r_1(t)$, in which the sifting algorithm is repeated to extract the next IMF, $c_2(t)$, from it. That is:

$$r_i = c_{i-1} - c_i \tag{5.18}$$

Where c_0 is the original signal $x(t)$. This process repeats until the residue function turns into a monotonic function, from which no more extrema can be extracted. This last residue function after n sifting repetitions is the r_n function in Eq. 5.14.

Finally, the algorithm for the empirical mode decomposition can be summarized as follows (TOLWINSKI, 2007):

Input: Time domain signal, $x(t)$.
Output: Set of n intrinsic mode functions, $c_1(t)$, ..., $c_n(t)$, and a residue, r_n.
$r_n = x(t)$
$h_1(t) = r_n$
$i = 1$
$k = 1$
while *($r_n \neq 0$) OR (r_n not monotone)* **do**
  while *($h_i(t)$ does not fulfill stoppage criteria)* **do**
    $U(t)$ = spline through local maxima of $h_i(t)$
    $L(t)$ = spline through local minima of $h_i(t)$
    $m(t)$ = 0.5*($U(t) + L(t)$)
    $h_i(t) = h_i(t)$ - $m(t)$
    $i = i + 1$
  end
  $c_k(t) = h_i(t)$
  $r_n = r_n$ - $c_k(t)$
  $k = k + 1$
end

5.3.3 Hilbert Spectral Analysis

Once all the intrinsic mode functions have been extracted from the original signal, individual Hilbert transform can be applied to every one of them. The latter results in obtaining **a set of analytic representation of modes suited for extraction of individual instant amplitudes, frequencies, and phase angles**, which allows to better account for the nonlinearities of the signal. The combination of the EMD and Hilbert transformation of the resulting IMF is what it is called the Hilbert-Huang Transform.

A graphical method to account for these nonlinearities is the construction of the Hilbert spectrum. This spectrum arises from the generalization of the Fourier Transform resulting from the modal decomposition. Such generalization comes from the analytic signals (Hilbert pair representation) of the IMF, $c_k(t)$, obtained. The set of n analytic functions can be rewritten as a function of the instantaneous amplitude, phase, and frequency as:

$$Z_k(t) = c_k(t) + iH\{c_k\}(t) = A_k(t)e^{i\theta_k(t)} = A_k(t)e^{i\int \omega_k(t)dt} \tag{5.19}$$

Clearly, by the last equality, the restriction of constant frequency in the Fourier Transform no longer exists by means of the Hilbert transformation. Now, if all the instant modal parameters are varied, the resulting distribution is the Hilbert Spectrum.

To exemplify its usefulness, an example found in Tolwinski (2007) is used. The objective is to plot the Hilbert Spectrum of the following predefined signal:

$$f(t) = a(t) + b(t) + c(t) = \cos(t^2) + 3\cos(3t) + \cos(t) \tag{5.20}$$

This signal clearly possesses three intrinsic components with a nonlinearity on its first component, $a(t)$, due to the t^2 term inside the cosine, which implies a linear increase of frequency with time. This non linearity is the kind of features which should get into evidence by the plotting of the spectrum. Also, the EMD algorithm should give ideally three IMF of roughly the same shape and magnitude as every single term of the known signal. Now, the original signal, with its known components, and the EMD decomposition results are shown in Fig. 31.

It can be seen how the IMF obtained through the EMD match with decent accuracy. Some deviations can be found at the instantaneous amplitude at the beginning of every decomposition. These kind of deviations are usually occasioned by the cubic spline interpolation of the envelopes.

The Hilbert spectrum is obtained by computing the energy at every point of the three analytic signals formed by the IMF and their HT. These energies are usually plotted as a point in the frequency *vs.* time plane, and a with a color scale which denotes the intensity of the energy concentration at that point. The latter is useful to see which modes have more weight than others.

Figure 32 shows the Hilbert spectrum from the test data. It can be easily identified, three "trend lines", which correspond to the three IMF. Two of them are almost horizontal

Figure 31 – Original signal and its components (left) with its decomposition by the EMD (right).

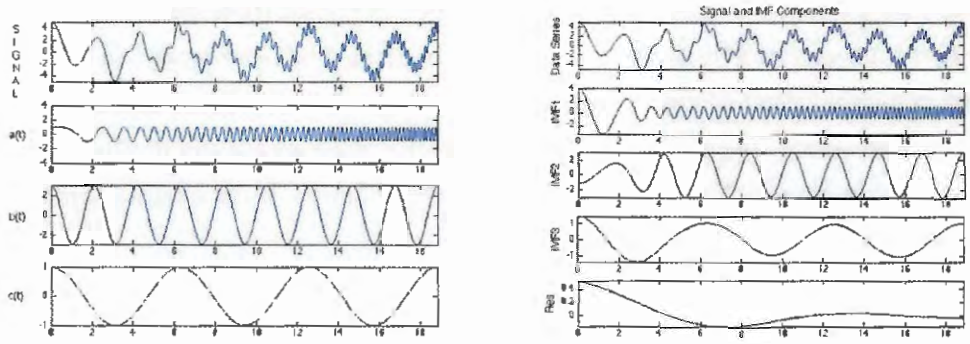

Source: Tolwinski (2007).

lines, which correspond to the cosines with constant frequency components. Other line shows a steady slope, which represents the non linear component. All the signal qualitative characteristics of importance can be appreciated graphically. **The resulting Hilbert spectrum, also called Hilbert-Huang spectrum, is, in essence, the complete Hilbert-Huang Transform.**

Figure 32 – Hilbert spectrum for the test signal.

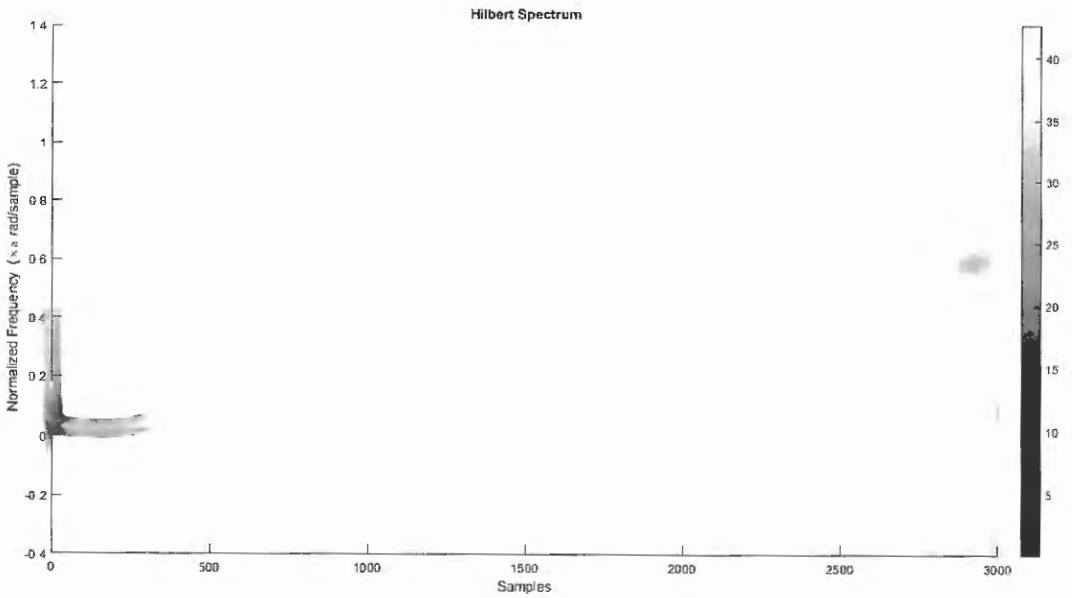

Source: Tolwinski (2007).

5.4 WAVE DISPERSION CONTROL THROUGH WINDOWED SIGNALS

As introduced in chapter 3, composite plates are dispersive mediums, *i.e.* propagation characteristics depend on the oscillation frequency and their relationship is nonlinear, especially when modes besides the fundamental ones start to appear. Understanding Lamb wave responses will depend on controlling dispersion. In general, it is considered that signals with high dispersion are far more complicated to process and to give particular physical meaning. Here, the concepts of tone bursts or windowed signals gain relevance.

In practice, it is difficult to achieve static, or standing, Lamb wave propagation. Instead, single wave packages, of a single carrier (or central) frequency, ω_c, called tone bursts are used, which are obtained through the use of windowed signals (GIURGIUTIU, 2007). Common window functions are the Hanning window, the Gaussian window, Hamming window, etc.

The windowing process can be better understood by examining the upper line of Fig. 33. The product of stationary sinusoidal signals oscillating at the carrier frequency and the window function gives the tone burst to be used. However, when windowed, the final signal is a combination of multiple frequencies, and each waveband will propagate with different velocity; thus, the control of the tone burst's frequency band is also important. Figure 33 in its lower line shows the same operation, but with the Fast Fourier Transform (FFT) of the signals. It can be seen how the thin, single frequency, initial wave, transforms into a lobe with a wider frequency band after the windowing.

Figure 33 – Tone bursts through windowing of signals, in time and spectral domains.

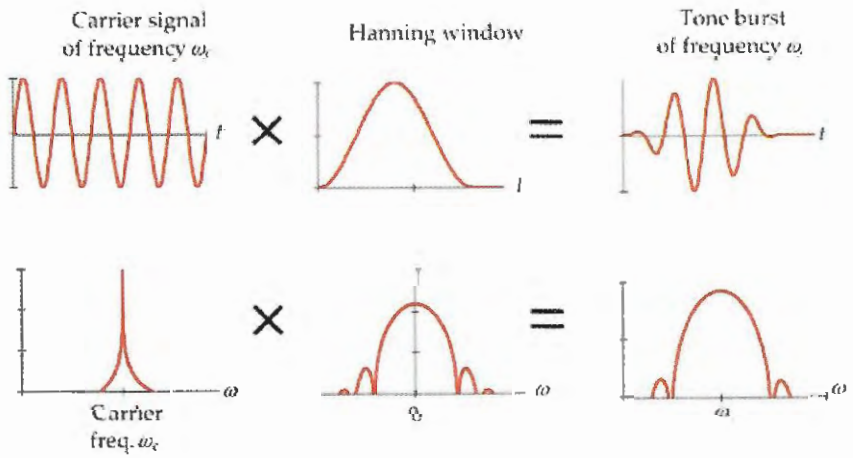

Source: Giurgiutiu (2007, p.235).

The final bandwidth of the tone burst can be controlled by modulating the signal using the total number of cycles of the tone burst, which is inversely related to the wave dispersiveness. This relation can be seen in Fig. 34, where with more cycles, the bandwidth is reduced. In

exchange to this, the number of peaks increases, and this can further complicate the analysis, especially when reflections and other features are involved. Also, in practice, a bigger sampling acquisition rate would be required when incrementing frequency or number of cycles, adding another practical limit to this modulation. The correct modulation will be case-dependent, and it is also a current branch of research to know which modulation is better for the detection of a given feature.

Figure 34 – Tone burst bandwidth modulation through cycle count.

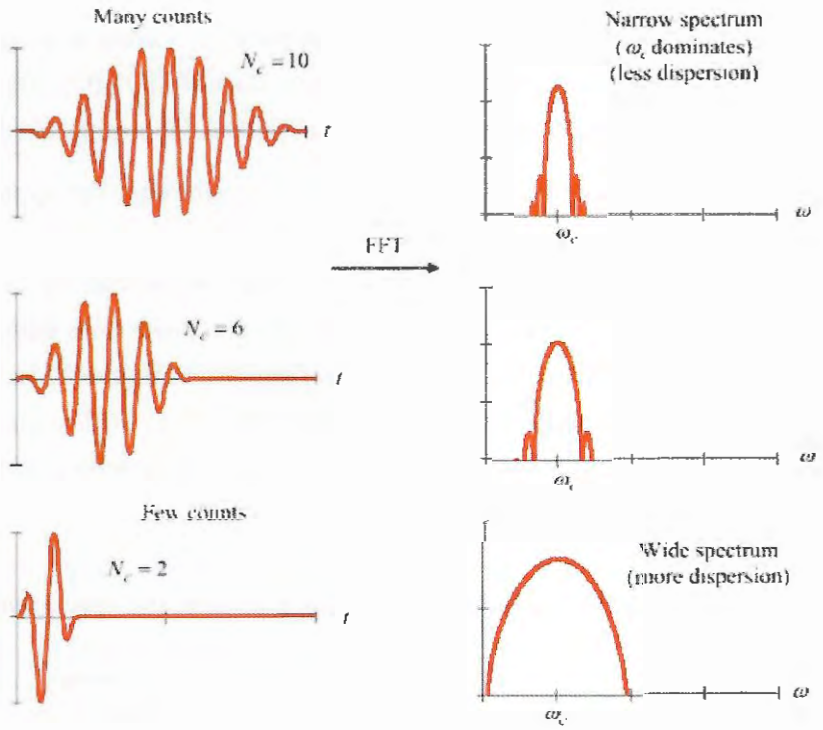

Source: Giurgiutiu (2007, p.236).

To initially asses which combination of parameters give the best modulation, the knowledge of dispersion charts for phase and group frequency is a must. For the case of interest of this work, which are composite materials, the objective was to avoid using a great number of cycles (or peaks), which require refined, and heavier to compute, FEM models.

Part III

One Dimensional Damage Detection

6 DAMAGE DETECTION WITH PIEZOELECTRIC TRANSDUCERS

The study of damage detection can be described, in general, as an interdisciplinary and multi-physics area. To properly assess damage detection, many complexities related to failure modes and material characteristics at the micro and macro levels are required to be understood. Also, the physical phenomenons involving sensors and actuators add practical and technical difficulties resulting, commonly, in a big spectrum of solutions for a reduced range of features and damages. For instance, for detecting failures in welds exists a wide range of solutions, from X-rays and Ultrasonic tests, to Dye penetrant inspection.

For composite materials, many methods are being tested to achieve SHM, as already explained. The particular focus of this work in piezoelectric sensors comes from its many economic benefits and easiness of practical application. However, the modeling of the interaction between the many systems is yet to be refined to obtain satisfactory results suitable for practical commissioning on real aerospace structures which, in a later stage, have to be also airworthiness-compliant.

In this chapter, the ways of integration of the different concepts explained with the objective of detect features or damages in a given medium are presented.

6.1 REVIEW ON THE USE OF PIEZO TRANSDUCERS FOR DAMAGE DETECTION IN AEROSPACE STRUCTURES

Osegueda et al. (2003) proposed to detect rivet hole cracks on aluminum and quantify their length by processing Lamb wave response through the use of the HHT. They showed how by comparing transmitted and reflected waves, in the pristine and damaged states, the energy wave profile is susceptible to geometric discontinuities and can be used as a measure of damage existence. Also, Osegueda et al. (2003) published a "purely geometrical" model that used the time of flight of signals received by two transducers to triangulate the source of reflected signals in a plane.

Quek, Tua and Wang (2003) also used the HHT along with the WT to detect anomalies in the forms of crack, delamination and stiffness loss in beams and plates. These authors also relied in times of flights and wave propagation characteristics in addition to frequency changes to detect the existence of delamination within a sandwiched aluminum beam; they did not quantify it, however.

Raghavan and Cesnik (2004) studied the generation and sensing of Lamb waves with piezoelectric transducers of strip and circular formats. They presented the expansion of the original Lamb wave propagation relation for straight-crested waves, originated by strip transducers, to circular-crested waves, originated by circular transducers. In general, the dispersion relation for

the symmetric and antisymmetric modes is the same for both strip and circular forms; however, for the latter transducer shape, propagation exhibits decreasing amplitude, in contrast to the straight-crested case, due to the outward distribution of wave energy. These results were obtained for Lamb waves propagating in an isotropic material.

Yang et al. (2006) presented a 2D model for the Lamb wave actuation and sensing by a piezoelectric transducer in an infinite, straight-crested, laminated composite medium. Giurgiutiu (2007) published a book with a big compendium of theoretical results for the Lamb wave generation, sensing, propagation and some damage detection cases for the SHM-oriented applications with piezoelectric transducers; for both straight-crested and circular-crested, flexural, compressional, shear vertical and horizontal. Meanwhile, Chen, Yan and Jiang (2007) applied the HHT combined with vibration response investigating the effects of damage on the modal parameters of a composite wing box.

Lu et al. (2007) studied the use of piezo transducer generated Lamb waves to determine the orientation of linear cracks in aluminum. Their study consisted of utilizing the scattered wavefield, *i.e.* the resulting field after interacting with damage, to define energy based reflection and transmission coefficients in order to characterize crack orientation. All the assessment process involved the use of the Hilbert Transform to utilize maximum peaks, wave energy, and times of flight of signals.

Gangadharan et al. (2010) used time domain methods along with the WT, HHT and the spectral finite element method to detect delamination in a composite beam of glass-epoxy with different ply up sequence and delamination sizes. **The detection was made with the plotting of the unwrapped phase** for the signal of each sensor. Differences between plots in the damaged state were used to assess delamination size.

The use of the unwrapped phase angle of signals to determine damage in structures has been also integrated with the HHT, as shown by Huang (2014). Samaratunga and Jha (2012) used this approach to detect, numerically, delaminations and to quantify them using the net phase change between cases with different delamination sizes. This same author and others, later in 2015, used again the HHT to process vibration data to detect damage from vibration response data in a Carbon/Epoxy beam when it is exposed to elevated temperatures (MICHAEL et al., 2015).

Esmaeel and Taheri (2012) proposed a damage index based on energy calculated from the first IMF of the EMD process. The indicator uses a relative one-norm error between the responses sensed along a path of transducers. The higher the index value for a determined path, the higher the probability of damage. They applied it to composite beams with positive results for a set of cases. In Huang (2014) it is also presented a definition for an unwrapped phase difference damage indicator by using a relative two-norm error for the phase change along a given path of transducers.

6.2 HIGHLIGHTS OF THE REVIEW

By considering the review made in the latter section, the following conclusions can be drawn from it:

- **There is no a unified approach to the delamination detection problem:** All the works resolve particular problems chosen by the authors, but there is no consistent characterization of the problem that allows a uniform assessment of the different detection techniques.

- **There is not a cross-study between detection indicators:** Most authors define indicators, but these are not compared with others.

- **Damage indicators are mostly probability indicators:** A damage indicator different of zero does not imply the existence of damage. The existence of damage is given by the comparison of indicators between paths.

- **Most works detect damage, but does not quantify it:** In the works that do quantify it, it is usually done by the delimitation of a delaminated area. Others only show in which transducer path exists a high probability of being the right "zone", rather than "spot".

- **The estimation of residual strength from transducer data is not yet properly studied:** The most studied part of the SHM on composites is, by far, the detection of delamination only.

- **The Hilbert-Huang Transform is a promising tool:** The use of the HHT for SHM of aerospace material, especially regarding delamination detection, is yet to be fully explored. The number of papers found that explore the use of the HHT in proportion to the WT or other signal processing tools is extremely low.

- **The use of time-domain techniques is almost ubiquitous:** The usage of times of flight of signals, maximum peaks of waves and other measures taken in the time domain are the principal source of information for detection models.

The present work will focus on some of these aspects that present opportunities of novel works, considering this the first Lamb wave related work of the laboratory in which was developed. Then, in order to be a first attempt at approaching and modeling the detection problem, an initial characterization of a "one-dimensional problem" is proposed here and explained next.

6.3 ONE-DIMENSIONAL DETECTION SCHEME

Figure 35 – one-dimensional delamination detection model.

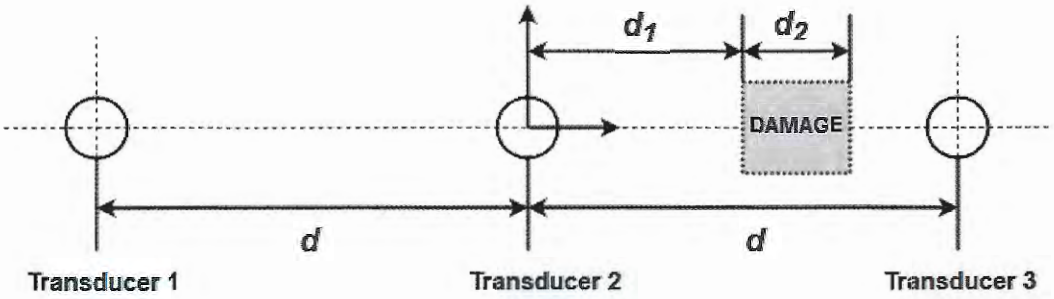

Source: The Author (2019).

The one-dimension detection case has the form shown in Fig. 35. The context is defined as a set of piezoelectric transducers along a single line and a single damage defined between any pair of transducers. The full detection problem consists of determining, from the transducers signals, the following information:

- **Detect Damage:** To determine the existence of damage and in which transducer path is located. "A damage is present in between transducers 2 and 3" on Fig 35, for instance.
- **Localize Damage:** To determine the linear distance, measured from the closest transducer, to the damage boundary. This is, distance d_1 in Fig. 35.
- **Quantify Damage:** To determine the linear extent of the damaged region. This is, distance d_2 in Fig. 35.
- **Assess Severity:** To determine the proportion of stiffness lost due to the defect. This is the percent of change in the rigidity of the damaged region compared to the undamaged region.

Two clear examples of one-dimension detection cases are shown in Fig. 36 and Fig. 37. In Fig. 36, piezoelectric strips are adhered to a very large composite beam of the same width and a delamination is defined between any of them. This model accounts for straight-crested Lamb waves that, unless propagating in a damping medium, will propagate infinitely on it with constant energy and amplitude (GIURGIUTIU, 2007), changes in that pattern can only be accounted to energy loss when passing through a damaged zone.

In Fig. 37, piezoelectric disks are adhered to a composite plate of very large dimensions and a delamination, of finite width, but also very large length, is defined between any of them. This model accounts for circular-crested Lamb waves that, regardless of propagating in a damped

medium, they will decay in amplitude due to the outward propagation of energy (GIURGIUTIU, 2007). Again, changes are attributed to the damaged zone.

Figure 36 – one-dimensional detection model for a composite beam.

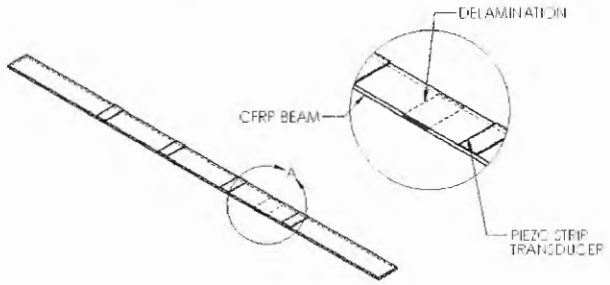

Source: The Author (2019).

Figure 37 – one-dimensional detection model for a composite plate.

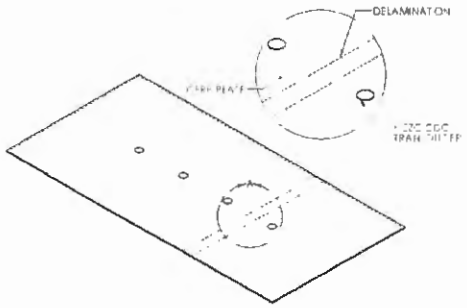

Source: The Author (2019).

This is the kind of detection problem that is of interest of this work and it is proposed here an assessment of it, including the detection, localization, quantification, and stiffness loss estimation (which is the first step to determine residual strength of the component).

6.4 DAMAGE DETECTION

In this study, a benchmarking of two damage detection methods will be done to assess their effectiveness for the same case. Both are based in the use of signals processed through the EMD part of the HHT.

6.4.1 Damage Detection using a Energy Damage Index

The empirical mode decomposition, shown in the Signal Processing chapter, can be used to calculate the energy carried by a wavefront, passing through a transducer, at any given time. Once the original signal is decomposed, the Hilbert Transform can be used on every IMF to obtain their analytical signal representations. Then, the energy of the $k-$th IMF, E_k, will be:

$$E_k(t) = \frac{1}{2}A_k^2(t) \tag{6.1}$$

Where $A_k(t)$ is the instantaneous amplitude of the $k-$th IMF, obtained through Eq. 5.11. Then, the total energy will be the superposition of the energies for each IMF:

$$E(t) = \sum_{k=1}^{n} E_k(t) \tag{6.2}$$

Authors, such as Osegueda et al. (2003) have successfully used energy-based Lamb wave scanning, obtained through the EMD formulation, for the detection of notches and cracks on

aluminum plates. The study consisted of a qualitative assessment of the formation of lobes due to the reception of a reflected wave, which was originated from a crack around a rivet hole in an aluminum plate. Esmaeel and Taheri (2012) applied an energy-based damage index, developed by Cheraghi, Riley and Taheri (2005), based on the EMD for the detection of delamination on composite beams. The index is built by taking the first IMF and calculating energy from it as:

$$E = \int_0^{t_0} (IMF_1)^2 dt \tag{6.3}$$

Where E is the total energy of the first IMF, from time zero, up to t_0. The use of only the first IMF comes with the assumption that high-frequency modes are more susceptible to damage, and the first IMF always has the highest frequencies and amplitudes (energy).

This calculation is done for all transducer paths implemented on the structure, so it monitors the variation of the index between different geometrical positions on the specimen. Finally, when the structure is in service, and it could be potentially damaged, the Empirical Mode Decomposition Energy Damage Index, or EMD-EDI, will be calculated as:

$$EMD - EDI = \left| \frac{E_{Healthy} - E_{Damaged}}{E_{Healthy}} \right| \tag{6.4}$$

Once the EMD-EDI of each path is calculated, the existence and severity of damage may be determined by associating the high index values with the existence of damage; the higher the value of the path, the more likely is this path to be the damaged region (ESMAEEL; TAHERI, 2012).

6.4.2 Damage Detection using the Phase Angle Difference

Another damage detection method in which the HHT has shown promising application is the use of the phase angle difference, obtained from the phase angle of the constructed analytic signals. This method relies on the dependency of the phase angle with the modal rigidity of traveling medium.

As in the case of energy, the total phase angle of a transducer's signal, $\theta(t)$, decomposed through the EMD will be the sum of the phase angle of every IMF.

$$\theta(t) = \sum_{k=1}^{N} \theta_k(t) \tag{6.5}$$

Where θ_k is the phase angle of the $k-$th IMF, from a total of N IMF product of the EMD. This phase angle is obtained from the HT of every IMF and using Eq. 5.12. The phase angle is usually treated unwrapped with radian phases in time, so it assigns the total number of rotations in the complex plane (formed by the real and imaginary parts of the analytic function) for a

unique time value t (HUANG, 2014). The unwrapped phase obtained from the EMD is usually smoother than the phase obtained directly with HT, especially when treating non-stationary data.

The use of the $\theta(t)$ as a damage indicator is done by assigning to a point p on the structure, *i.e.* a transducer p attached to the structure in a predefined location, a phase value $\theta_p(t)$, and defining the relative phase with respect to a reference point of the structure, $\theta_0(t)$, as:

$$\Delta\theta_s(t) = \mid \theta_p(t) - \theta_0(t) \mid \tag{6.6}$$

The variable $\theta_s(t)$ describes the relative phase relationship of a traveling structural wave for a given state of a structure s. The idea is that damages will alter the speed at which energy traverses the medium, hence occasioning a change in the phase difference between a pristine and damaged state (HUANG, 2014). This change is also perceptible in the phase angle alone; however, measuring the relative difference allow to estimate the path between sensors in which the damage is most probable of being located. The quantitative detection is done by defining an EMD Phase Damage Index, EMD-PDI, as:

$$EMD - PDI = \sqrt{\frac{\sum_{t=0}^{N_t} \mid \Delta\theta_1(t) - \Delta\theta_0(t) \mid^2}{\sum_{t=0}^{N_t} \Delta\theta_0^2(t)}} \tag{6.7}$$

Where, $\theta_1(t)$ and $\theta_0(t)$ are the phase angle differences, for a fixed path, in the damaged and pristine states, respectively; N_t is the number of time divisions, dependent of the acquisition frequency. Huang (2014) presented the application of this method theoretically for a one-dimensional system and experimentally for an scaled three-stories building model. Samaratunga, Wang and Jha (2012) used the phase difference obtained through the EMD to detect delamination in a numerical study and used a curve fitting of the total phase difference for different delamination sizes to quantify the damage. Kim and Jha (2011) also used the phase difference through EMD to detect delamination, but also compared it with the phase difference obtained through the Continuous Wavelet Transform and shown how the former exhibits a smoother and easier to inspect shape.

6.5 DAMAGE LOCALIZATION

The model assumes that the delamination can be modeled as a layer portion with reduced stiffness coefficients, and such delamination generates a complete thickness section with degraded properties. Thus, damage localization consists of estimating the distance between the beginning of the fault zone and the closest transducer; that is, to find the distance d_1 in Fig. 35. In such conditions, the whole delaminated section behaves like a second traveling medium, that is assumed also to be uniform, and an interface is defined between them.

In such condition, according to the theory of elastic wave propagation in a 1D medium, when interacting with an interface, it is assumed that three types of waves will exist (BEDFORD; DRUMHELLER, 1994):

- Incident wavefield, $u_I(x,t)$.
- Reflected wavefield, $u_R(x,t)$.
- Transmitted wavefield, $u_T(x,t)$.

When the incident wavefield reaches the interface (Fig. 38), it splits into reflected (u_{r1}) and transmitted (u_{t1}). The reflection will propagate in the opposite direction of the incident wave, and the transmitted will keep propagating in the same direction. The latter wave will keep splitting, into u_{r2} and u_{t2}, when transitioning from the damaged zone up to healthy before reaching sensor 2 in Fig. 38.

Figure 38 – Wave propagation patterns for the 1D Model.

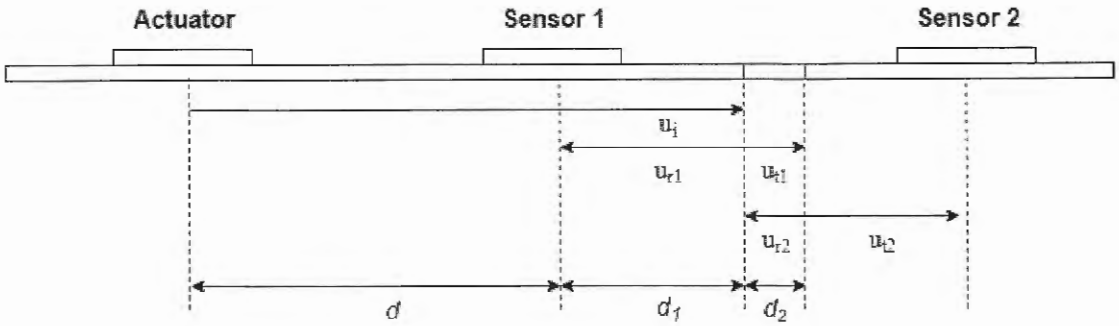

Source: The Author (2019).

The reflected wavefield can be used to estimate the location of the damage if it can be measured and extracted from the transducer right before it (Sensor 1). The reflected wavefield's voltage response, V_r^R, can be "constructed" from the responses in damaged, V_r^D, and pristine, V_r^P, states in Sensor 1 (propagated distance of $r = d + 2d_1$) as:

$$V^R_{r=d+2d_1}(t) = V^D_{d+2d_1}(t) - V^P_{d+2d_1}(t) \tag{6.8}$$

One should expect to see a zero signal, up to the apparition of a clear wave package consisting of the reflection. However, this constructed signal can exhibit hard-to-predict shapes, dependent of many factors such as the size or depth of the delamination, or just "false waves" created from the phase change between the damaged and pristine signals.

To solve the latter issue, an extraction window is defined using the expected maximums and minimums times of flight of wave packages. If it is assumed that the damage is next to

the transducer, *i.e.* $d_1 \approx 0$, then this transducer will receive the fastest wave package after one pristine time of flight, or TOF_P. In the extreme case of the delamination being next to the farthest transducer, *i.e.* $d_1 \approx d$, then the reflection of the fastest propagating mode will reach the same transducer in $3TOF_P$, as much. Finally, adding the actuator peak time occurrence, t_p, the reflection of interest will be the highest-energy wave package contained in $V_d^R(t)$ in the interval $[TOF_P + t_p, 3TOF_P + t_p]$.

IF TOF_R is the time of flight from the extracted reflected wave in Sensor 1, then, by inspecting the complete wave path from the actuating transducer (see Fig. 38), passing through Sensor 1 and then reflecting back to the same sensor, with $v_{g,P} = d/TOF_P$ being the pristine state group velocity, this time is:

$$TOF_R = \frac{2d_1 + d}{v_P} = TOF_P\left(1 + 2\frac{d_1}{d}\right) \tag{6.9}$$

Hence d_1 can be estimated as:

$$d_1 = \frac{1}{2}\left(\frac{TOF_R}{TOF_P} - 1\right)d \tag{6.10}$$

6.6 DAMAGE QUANTIFICATION

To quantify the extent of the damage, the parameter to find is d_2 in Fig. 35. For this purpose, the reflected and transmitted waves are both used. But, first, other acoustic properties must be introduced.

The acoustic impedance of a medium, Z, is a quantity representing how much stress is needed to impart a prescribed velocity to the medium particles (GIURGIUTIU, 2007; BEDFORD; DRUMHELLER, 1994). It is defined as:

$$Z_0 = \rho_0 v_{g,0} \tag{6.11}$$

Where Z_0, ρ_0 and $v_{g,0}$ are the medium's acoustic impedance, density, and group (wave package) velocity, respectively. This parameter is defined for every propagating mode since each one propagates with different velocity.

When analyzing interfaces in 1D mediums, the reflected and transmitted wavefields are usually expressed as a function of the acoustic impedance of the incident and transmitted mediums. These relations are more conveniently presented defining an acoustic impedance ratio, K, defined as the ratio of the transmitted acoustic impedance over the incident acoustic impedance:

$$K = \frac{Z_T}{Z_I} = \frac{\rho_T v_{g.T}}{\rho_I v_{g.I}} \tag{6.12}$$

Then, in terms of the impedance ratio and the incident wavefield, the reflected wavefield is:

$$u_R(x,t) = \frac{1-K}{1+K} u_I(x,t) \tag{6.13}$$

And the transmitted field is:

$$u_T(x,t) = \frac{2}{1+K} u_I(x,t) \tag{6.14}$$

For this particular case, the delamination does not significantly affect the density of the material, hence the following simplification can be made:

$$K = \frac{v_{g,T}}{v_{g,I}} \tag{6.15}$$

Hence, by estimating K from transducer response the propagation velocity in the damaged zone can be obtained, and **this velocity is directly related to the extension of the delaminated zone and the time of travel through** as explained next.

It is important to say that the above relations **were developed for axial waves propagating in 1D medium** (BEDFORD; DRUMHELLER, 1994); in contrast to the current case which account, rigorously speaking, for plate waves, which are a kind of **flexural waves**, *i.e.* with displacement that resembles beam bending along the plate length dimension (1D reduction). However, Giurgiutiu (2007) presented the interface analysis of flexural waves, and he showed how flexural waves end not only in reflected and transmitting standing propagating waves, but also a portion of the energy goes to transient reflected and transmitted waves that decay after some traveled distance. Using this approach would yield no direct solution at first, because **the matrix solution developed by Giurgiutiu (2007) requires the knowledge of the acoustic properties of the other medium, *i.e.* the damaged zone in the present case, and that is not available**. In conclusion, the use of K in the method proposed in this work **does not account for these transient waves** as it assumes that they decay before reaching any transducer and that their energy share can be neglected, hence neglecting their existence in the estimation of K.

Due to the damaged zone, with reduced overall stiffness, the propagation front will slow down, to a damaged velocity, $v_{g,D}$, and will recover the pristine velocity, $v_{g,P}$, when it enters again into the remaining healthy zone before the last transducer in Fig. 35.

As already mentioned, this wavefront will present an amplitude attenuation due to geometrical spreading (more perceptible when using circular transducers) and to damping properties of the propagating medium. When damaged, the delamination extension will define two interface, *i.e.* at the starting and ending of the delamination, and for each interface, it will exist refraction and transmission.

When the wave originated at Transducer 1 in Fig. 35 reaches the damaged zone at d_1 (total propagated distance of $r = d + d_1$), the "voltage response" amplitude (Hilbert Transform magnitude), read by a theoretical piezoelectric transducer placed immediately before the damage (incident medium of Eq. 6.12), or to the left of d_1, will be (recalling Eq. 3.36):

$$V^I_{d+d_1}(t) = \frac{A_1}{\sqrt{d+d_1}} e^{-\eta_P(d+d_1)} e^{i(\omega t - k_P(d+d_1))} \tag{6.16}$$

Where A_1 is the amplitude determined from the pristine state, η_P is the material damping in pristine state, and k_P is the wavenumber of the pristine medium. However, it is more useful to work with the maximum amplitude because these maximum peaks can be related directly to others. To obtain this value, the infinity norm (supreme value of the magnitude of a function) of the signal's Hilbert Transform is taken:

$$\|V^I_{d+d_1}\|_\infty = \left| \frac{A_1}{\sqrt{d+d_1}} e^{-\eta_1(d+d_1)} \right| \tag{6.17}$$

Where the last exponential disappears as it is harmonic with unitary magnitude. This form can also be applied to obtain A_1 from the pristine measure at transducer 2 ($r = d$):

$$A_1 = \|V_d\|_\infty \sqrt{d} e^{\eta_P(d)} \tag{6.18}$$

When interacting with the damage interface at $r = d + d_1$, the infinity norm of the reflected wave at this location is obtained by applying Eq. 6.13:

$$\|V^R_{d+d_1}\|_\infty = \frac{1-K}{1+K} \|V^I_{d+d_1}\|_\infty \tag{6.19}$$

From this point, the attenuation is assumed to keep the same function and damping for the pristine zone, since the reflection still travels pristine medium. Then, using the infinity norm of the reflected wave in transducer 2, which has been already obtained from Eq. 6.8 and noting that this value is attained after **propagating** a distance of $r = d + 2d_1$, the amplitude constant for the reflected wave's attenuation, A_r, can be estimated as:

$$A_r = \|V^R_{d+2d_1}\|_\infty \sqrt{d+2d_1} e^{\eta_P(d+2d_1)} \tag{6.20}$$

Then, by calculating "backwards", the reflected wave infinity norm value after the interaction with the interface can be estimated as:

$$\|V^R_{d+d_1}\|_\infty = \frac{A_r}{\sqrt{d+d_1}} e^{-\eta_P(d+d_1)} \tag{6.21}$$

With the latter equation, K can be obtained through Eq. 6.19, and, with it, the propagation velocity in the damaged zone, $v_{g,D}$, can be found with the definition of K (Eq. 6.15).

Finally, by inspecting the **propagation path of the transmitted wave**, the time of flight of this wave, measured at the transducer 3, is:

$$TOF_D = \frac{d_1}{v_{g,P}} + \frac{d_2}{v_{g,D}} + \frac{d - d_1 - d_2}{v_{g,P}} = TOF_P + d_2\left(\frac{v_{g,P} - v_{g,D}}{v_{g,P}v_{g,D}}\right) \tag{6.22}$$

Where TOF_D is the wave time of flight in the damaged state, that is the time that takes to the incident, and then transmitted, wave to pass through the pristine zone and the damaged zone up to transducer 3. From the latter relation, the value of d_2 can be obtained as:

$$d_2 = \frac{(TOF_D - TOF_P)v_{g,P}v_{g,D}}{v_{g,P} - v_{g,D}} \tag{6.23}$$

Where the factor in parentheses is the time delay due to damage. It is worth to note that this model assumes that the interaction with damage, implicate a positive time delay, *i.e.* $TOF_D > TOF_P$ is necessary, to yield physically valid results. However, due to dispersion and modal conversion during the interaction with damage, exists the possibility that a particular wave package converts into a faster mode in which case could complicate the analysis, in addition of turning the present method unreliable.

Figure 39 – Maximum Peak-to-Peak *vs.* propagated distance from source for the reflected wave measured at transducer 2 (graph is not to scale).

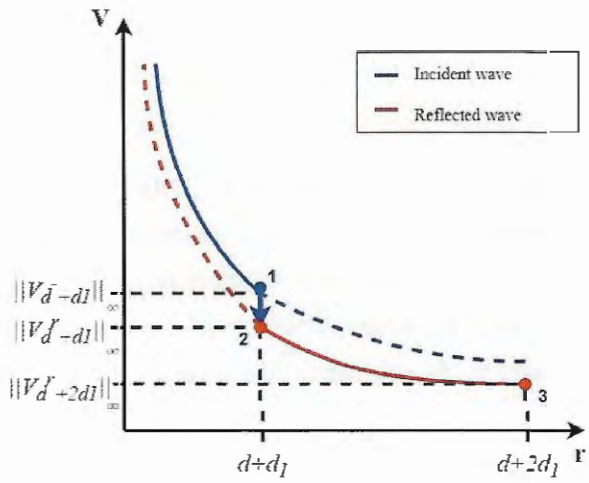

Source: The Author (2019).

The quantification deduction can also be explained graphically using a plot of maximum peak response against propagated distance, shown in Fig. 39 (not drawn to scale). When a damage exists, the incident wave (blue solid line) is attenuated at a rate as it would be normally in pristine state, A_1, until it reaches the damage at $r = d + d_1$ (point 1). Then, the reflected wave

acquires the amplitude $\|V^R_{d+d_1}\|_\infty$ (point 2), due to Eq. 6.13, and it then propagates back through a new curve with the same propagation law, but different amplitude, A_r, until it reaches back transducer 2 after traveling $r = d + 2d_1$ and having the amplitude $\|V^r_{d+2d_1}\|_\infty$ (point 3). Hence, the amplitude proportion lost due to the reflection (solid blue arrow between 1 and 2) can be determined and K with it.

6.7 STIFFNESS LOSS ESTIMATION

The stiffness loss in the damaged zone, that can be used to do the Residual Life Estimation (RLE), is estimated using the basic relation for propagation velocity for elastic waves in composite materials, as:

$$v_{g,D} = \sqrt{\frac{f(C_D)}{\rho}} \tag{6.24}$$

Where $f(C_D)$ is a function that depends on the "damaged" stiffness matrix of the damaged zone, associated with the correspondent propagation mode (usually a linear combination of stiffness components). If the fastest propagation mode is used, it can be deduced without loss of generality that this velocity is a function of the highest (or stiffest) value of the f function. This function can be directly compared to the same function in a pristine state. The direct correlation will vary from case to case, for instance, a 90% decrease in the C_{11} component of a lamina, will not necessarily represent that same reduction at the laminate level.

The way in which damage is assessed at the laminate level (the work of Talreja (1986) is highly recommended to introduce the reader in these aspects) and the failure criteria used will affect the consideration of the Residual Life. However, a basic estimation can be done for the change in the proportion of the pristine and damaged f functions as:

$$\Delta f = 1 - \frac{f(C_D)}{f(C_P)} = 1 - \left(\frac{v_{g,D}}{v_{g,P}}\right)^2 = 1 - K^2 \tag{6.25}$$

It will finally depend on a specific model for the Lamb wave propagation to know which stiffness components are involved in the particular f function, and will also depend on a particular damage model, at the lamina level, to know how each stiffness component is penalized. Both tasks are out of the scope of this work.

7 METHODOLOGY

7.1 MULTIPHYSICS FEM APPLICATION MODEL

To test the algorithm, an ABAQUS model of a bidirectional, quasi-isotropic, 2 mm thick, 8-plies, composite plate was used. The plate in-plane dimensions and transducer location are shown in Fig. 40. Three transducers are disposed in line every 100 mm, and a strip (shadowed area in Fig. 40) is used to model the delaminated area for a variety of cases shown in Tab. 1. These cases intend to study the effect of the position and extent of the damage on the reliability and sensitivity of the proposed method.

First, the strip is modeled with undamaged properties to simulate the pristine state. Then, a delamination is introduced between the 4^{th} and 5^{th} plies of the strip zone. Boundary conditions are defined as fixed in both of the 300 mm edges. The geometry of the transducer used is 8,7 mm round disks. Also, the voltage on the lower face of transducers, *i.e.* the face in contact with the plate, was fixed at 0 V. By this way, all the voltage inputs and outputs are received and sent at the top of the transducers.

Figure 40 – ABAQUS model (in millimeters) of a composite plate with three piezo transducers in line.

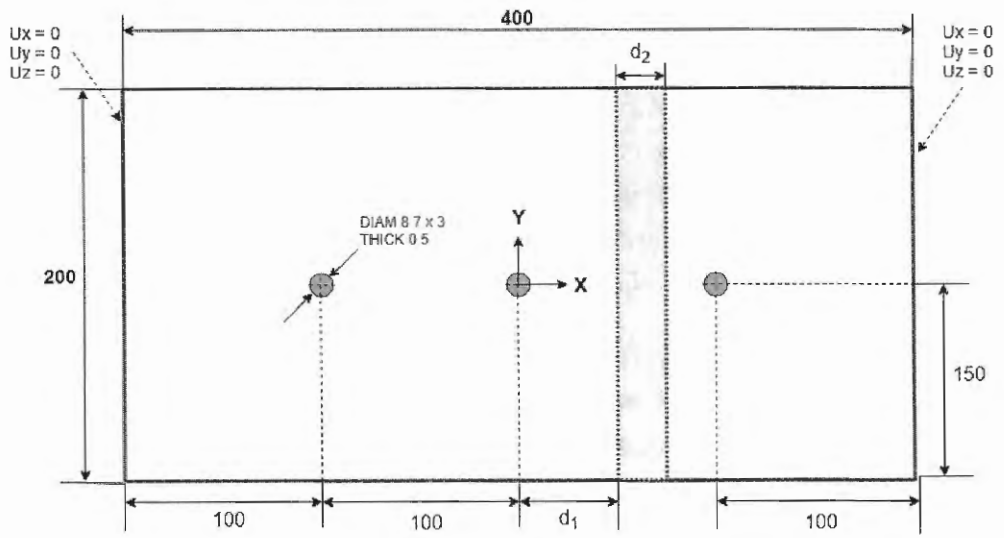

Source: The Author (2019).

All the modeling, which will be described in detail next, was based on experimental properties used by Gresil and Giurgiutiu (2015) in studies done in the Laboratory for Active Materials and Smart Structures (LAMSS) of the University of South Carolina, which were experimentally validated. That is, since no experimentation, *i.e.* strong validation, was performed during the project, the usage of this data allows to assess results under a coherent validated base.

Table 1: Delamination cases to be studied.

	Case					
Parameter	1	2	3	4	5	6
d_1	50	25	70	50	50	50
d_2	15	15	15	10	20	25

Source: The Author (2019).

7.2 NUMERICAL MODELING FOR LAMB WAVE PROPAGATION

In this section, all the steps, formulas and considerations for the definition of the numeric parameters involving the study are introduced. The final parameters used, along with a summary of the model, will be presented in a later section after the particular properties employed for the different materials are introduced, so the equations hereby to be described can be applied.

7.2.1 Analysis type selection

The present study is a multi-physics time-dependent study, hence it is a Dynamic Analysis. There are two types of dynamic analysis in ABAQUS depending on the type of time integration used:

- **Explicit:** An Explicit analysis does the incremental procedure and at the end of each increment updates the stiffness matrix based on geometry changes and material changes. Then a new stiffness matrix is constructed and the next increment of load (or displacement) is applied to the system. The problem with the method is the need of many small, time-consuming, increments for good accuracy. If the number of increments are not sufficient, the solution tends to drift from the correct one. This method does not enforce the equilibrium of the internal structure forces with the externally applied loads.

- **Implicit:** An Implicit analysis is the same as Explicit with the addition that after each increment the analysis does Newton-Raphson iterations to enforce equilibrium of the internal structure forces with the externally applied loads. This analysis is usually more accurate and can stand for bigger increment steps. In the other hand, during the Newton-Raphson iterations one must update and reconstruct the stiffness matrix for each iteration, this is computationally costly.

However, regarding dynamic studies with piezoelectric materials, the ABAQUS element library exhibits a limitation in which their piezoelectric elements can only be used with the implicit scheme. Hence, for the characteristic of the implicit dynamic analysis, one can expect high computation times. In contrast, the memory consumption is not expected to be excessively high.

This study will require only two dynamical steps. An initial one in which restrictions and boundary conditions are applied and a second in which the harmonic electric potential is applied to the actuator and Lamb waves propagate through the plate.

7.2.2 Plate modeling for wave propagation

- **Element Type and Form:** Conventional Shell elements, as known in ABAQUS literature were selected to model the CFRP plate. Conventional Shell elements, in contrast to Solid elements, exhibit more accurate responses in bending problems with low thickness (CORP, 2014), which is desirable since Lamb waves can be seen as a kind of flexural waves. Also, having less degrees-of-freedom per element, analysis and post-processing is usually faster and require less hard drive space when compared to solid elements.

  To give an insight of the magnitude of this difference, Tab. 2 compares the required number of elements, nodes, and the degrees-of-freedom (DOF) to mesh solid and shell plate models, using the same criteria for element sizing for an isotropic material (aluminum). It can be seen how the employment of solid elements almost tripled the number of elements and increased the number of equations to solve in about a half.

Table 2: Examples of an Aluminum plate ABAQUS model specs.

FE models	Nodes	Elements	DOF	Average element size in mm
3D linear Shell with reduced integration (S4R)	163,288	162,481	979,728	0.75 x 0.75 x 1.275
3D linear Solid with reduced integration (C3D8R)	320,128	482,595	1,447,785	0.75 x 0.75 x 0.6375

Source: Yang et al. (2006).

The form chosen is the general-purpose linear 4-node shell element with reduced integration, S4R as called in ABAQUS literature (CORP, 2014). This element is selected also for reasons of context. The GEA research group is simultaneously working in **Unified Formulations (UF)** for Finite Elements, starting to implementing algorithms for these 4-node shell elements. A validated model constructed with these elements will allow future computational research on this area.

Reduced Integration means that the ABAQUS solver is using less Gaussian points to solve integration through the Gaussian Quadrature. This allows faster computation with a possible accuracy reduction that has to be assessed case by case.

- **Mesh dimensioning:** Wave propagation is a dynamical problem, which has special considerations when defining the size of the elements on the mesh and the time discretization. The meshing needs to have adequate refinement in order to have, first, convergent and, then, coherent results.

  For the mesh to capture the phenomenon, it has to be smaller than the shortest wavelength expected to be present in the study (HAN, 2007). If the distance between nodes is larger, then the displacement field could be either estimated as non-existent or false. Many authors in their own study, such as Han (2007) or Giurgiutiu (2003), recommend a minimum edge length, L_e, from 10 to 20 elements per wavelength.

  To calculate L_e, first, the full tensor of Eq. 3.19 must be available, *i.e.* the material must be fully characterized. This step should be enough for a common isotropic, or even a common orthotropic, material. However, laminates are formed by laying up individual lamina in different directions, for which the final tensor can be somewhat different and, in consequence, the elements of the tensor for which the phase and group velocities are solved can be different of those shown for a single lamina. The laminate stiffness tensor can be obtained through the classical theory of laminates. **Plotting dispersion curves for the complete laminate can make this step easier.**

  In any case, the objective is to find the slowest speed for a given maximum frequency, F_{max}, of simulation. This is a practical limitation, because larger frequencies will require smaller elements, giving in exchange a larger and heavier to solve the FEM model. So a given numerical model, with a fixed plate thickness, will always have reliability up to a certain range of frequency.

  Once the slowest phase speed, V_{slow}, is obtained the minimum wavelength, Λ_{min}, to expect in the system will be:

$$\Lambda_{min} = \frac{v_{slow}}{F_{max}} \tag{7.1}$$

  Then, one should select, according to literature, the minimum edge length, L_e, as:

$$L_e < \frac{\Lambda_{min}}{10} \tag{7.2}$$

- **Integration time step:** The main criteria in selecting the maximum allowable time step is the one given by the Courant-Friedrichs-Lewy —or CFL— criterion. The time step should be small enough to prevent the fastest traveling wave to pass through an entire element in less than one time step. The latter is:

$$\Delta t^1_{max} = \frac{L_e}{v_g} \tag{7.3}$$

Also, in literature the following thumb rule is also found:

$$\Delta l_{max}^2 = \frac{1}{20 F_{max}} \tag{7.4}$$

So in order to choose the most reliable step time:

$$\Delta t < min(\Delta t_{max}^1, \Delta t_{max}^2) \tag{7.5}$$

7.2.3 Piezoelectric transducer modeling

- **Element type and form:** Piezoelectric elements in ABAQUS are only available as solid 3D or 2D bricks. The only parameter to configure is the linear or quadratic approximation. Linear is selected to reduce the size of the problem without general lose of accuracy due to the intention to acquire global results and no localized effects. Then, **the element C3D8E, an 8-node linear piezoelectric brick** is used, as defined in ABAQUS literature (CORP, 2014). This element possesses all the mechanical degrees of freedom, with the addition of the electric potential one.

- **Mesh dimensioning:** The dimensioning of the transducer mesh obeys to same criteria for the plate mesh. The only caution taken was to achieve the best aspect ratio possible (DOWLING, 2012), so safer numerical stability is achieved. The aspect ratio in ABAQUS is defined as the ratio between the longest edge of an element to the shortest (CORP, 2014). The ideal aspect ratio is 1.0, and elements too away (usually above 5.0 or 8.0) are considered too distorted to be computationally stable. This is worst if reduced integration is considered. **The objective was to keep it below 3.0**.

- **Voltage boundary condition:** The application of electrical voltage to both sides of the transducers is made through an equation restriction. The degree of freedom 9, corresponding to electric potential, of the nodes in one face (top or bottom), except one, are bonded to a master node in which the voltage is applied. The restriction equation is then: $DOF_9^{(nodes)} - DOF_9^{(master)} = 0$, for all transducers.

7.2.4 Contacts and Restrictions

The contact to be modeled is the one existing between the plate and the two transducers. In an experimental model, the bond is usually through an adhesive layer of epoxy glue which is commonly modeled in literature as a shear layer in which the mechanical effects are transmitted through shear (BOTTAI; GIURGIUTIU, 2005).

However, currently there is no available engineering data to properly model this adhesive layer (and is one proposed future work for the research group) so it will be no initially considered in the model, and **the contact between the plate and the transducers will be modeled as a**

Tie contact, as known in ABAQUS literature. This contact is equivalent to perfect bond; that is, the displacement degrees of freedom in the nodes located in the contacting surfaces have the same magnitude.

Also, for numerical stability and post-processing sake, a restriction is implemented regarding the nodes in the transducers for which the voltage is applied. The idea behind the restriction is to be able to apply or measure the electric potential on the transducers through a single node, or probe node. To do this and keep coherence, **the restriction will force all the nodes in the same face as the probe node to have the same electrical potential.**

7.2.5 Loads and Boundary Conditions

The plate boundary conditions are fixed constrains at the plate extremes. Since the plate has adequate dimensions, the effect on the use of these boundary conditions is not significant. For the electrical inputs, ABAQUS does not allow to give input electric potential profile as a Load; instead, this inputs should be given as boundary conditions in the probe node of the transducer's upper face. The restriction applied in the latter section will assure uniform potential distribution. The electric potential input was the exact experimental input, given as a point by point tabular data.

7.3 PROPERTIES AND PARAMETERS

In this section, all the independent parameters required for the complete definition of the different numerical models involved are introduced. As already stated, the parameters used were selected from sources in which they were experimentally validated in order to give real physical ground.

7.3.1 Composite Plate

For the plate, eight Hexply M18/1/939 bidirectional CFRP plies, with stacking $[0/45/45/0]_S$, and 0.125 mm of thickness each is used. The properties used are the ones used in the different works of the LAMSS and are shown in the "Pristine" column of Tab. 3. The degraded properties used to model de delamination were the pristine ones reduced to a 1% ("Damaged" column of Tab. 3) to recreate the delamination, and it was defined using two additional layers of 0.03 mm each at the center of the plate thickness (oriented to 0 deg).

Also, the experimental dispersion curves, required for the laminate to be correctly modeled, are available from Gresil and Giurgiutiu (2015). The curves for the 0deg and 90deg propagation directions can be assumed equal, due to the fact that the ply up gives a quasi-isotropic laminate, and are shown in Fig 41.

In Fig. 41, the red and blue lines, which correspond to the experimental fundamental symmetric, S_0, and anti-symmetric modes, A_0, respectively, are the ones of interest. The cutoff

Table 3: Hexply M18/1/939 properties in Pristine and Damaged state.

Property	Pristine	Damaged
Y_1 (GPa)	37	0.37
Y_2 (GPa)	39	0.39
Y_3 (GPa)	10	0.1
ν_{12} (GPa)	0.1	0.001
ν_{13} (GPa)	0.1	0.001
ν_{23} (GPa)	0.3	0.003
G_{12} (GPa)	5	0.05
G_{13} (GPa)	5	0.05
G_{23} (GPa)	5	0.05
ρ (kg/m^3)	1605	1605
α (damping)	0	0
β (damping)	7.7e-7	7.7e-7

Source: Gresil and Giurgiutiu (2015).

Figure 41 – Group Velocity curves for propagation at $\theta = 0\,\text{deg}$.

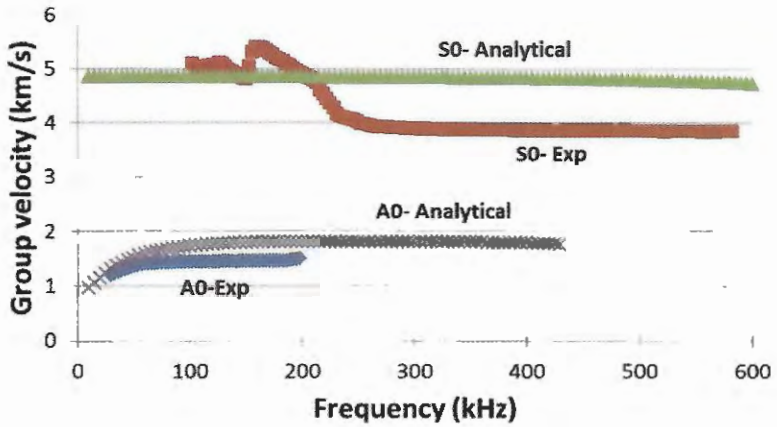

Source: Gresil and Giurgiutiu (2015).

frequency, *i.e.* the frequency in which other modes start to appear, was reported to be 400 kHz, so the numerical model should simulate in a lower frequency range.

7.3.2 Piezoelectric Transducer

The piezoelectric material used was the PZT-5H, which has good characteristics for both acting and sensing. It is also one of the most used material on the consulted references for this work. Its properties are shown on Tab. 4.

Table 4: PZT-5H mechanical and electrical properties.

Mech. Property	Value	Elec. Property	Value
$C_{11} = C_{22}$ (GPa)	97	$D_{11} = D_{33}$ (F/m)	947 E-08
C_{33} (GPa)	84	D_{22} (F/m)	605 E-08
$C_{12} = C_{13}$ (GPa)	49	e_{113} (C/m^2)	12.84
C_{23} (GPa)	44	e_{333} (C/m^2)	18.31
C_{44} (GPa)	24	e_{311} (C/m^2)	-8.022
$C_{55} = C_{66}$ (GPa)	22		
ρ (kg/m^3)	7600		

Source: Gresil and Giurgiutiu (2015).

7.3.3 Signal Properties

The input voltage profile applied on the transducer's top face was a Modulated Hann window:

$$H(t) = -\frac{A}{2}\sin(2\pi F_c t)(1 - \cos\left(\frac{2\pi F_c t}{N}\right)), \quad 0 \leq t \leq T \tag{7.6}$$

Where A is the window's amplitude, F_c is the central frequency, N is the number of cycles, and T is the time period. The signal parameters to use in Eq. 7.6 are shown in Tab. 5 and the signal's shape is shown in Fig. 42. This signal was chosen because is in the frequency range in which the antisymmetric mode is dominant (i.e bigger amplitude compare to other modes) and its shape is the same used in the works from which the properties were drawn, so it would allow for comparison. The input profile is elaborated for a temporal sampling rate of 0.1 μs (10 MHz).

Table 5: Hann's window parameters for the present study.

Parameter	Value
A (V)	20
F_c (kHz)	90
N (cycles)	3
T (μs)	33,3
δt (μs)	0.1

Source: The Author (2019).

Figure 42 – Modulated Hann Window with the parameters of Tab.5.

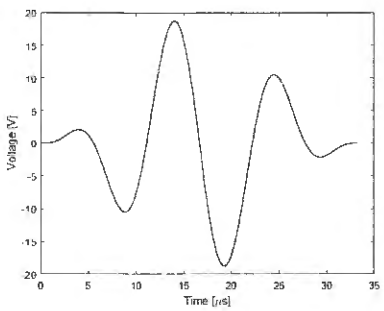

Source: The Author (2019).

7.4 NUMERICAL MODEL DIMENSION AND SETUP

With all the information of dimensions and properties available, the equations introduced in section 7.2 can be solved.

7.4.1 Composite plate

- **Mesh dimensions:** The maximum frequency of simulation is set below 50% of the cutoff frequency obtained through the dispersion curves for phase velocity: 150 kHz, was deemed as adequate. At this frequency, the slowest mode will propagate around 1500 m/s, so the minimum element edge, L_e, should be of 1 mm.

- **Time step:** In the same order, the time step for the two criteria presented are 0.2 μs for the formula using the fastest propagating mode and 0.33 μs for the rule of thumb introduced. The former is selected as maximum and, for convenience, a step time of 0.1 μs was finally used, which is conservative.

7.4.2 Piezoelectric transducer

- **Mesh dimensions:** The minimum edge length was set to be equal to that of the plate, in order to have matching meshes which will ease the application of perfect bond (Tie) constraints between the transducers and the plate.

- **Electrical boundary conditions:** All the voltage on the upper and lower faces of the transducers is acted and sensed through a single node which was defined, by convenience, at the center of the transducer.

7.4.3 Model resume

Table 6: Global model resume.

	Plate		Piezo	
Parameter	Value	Units	Value	Units
Element type	S4R	-	C3D8R	-
Element number	80384	-	133	-
Edge Length	1	mm	1	mm
Time Step	0.1	μs		
Maximum frequency	150	kHz		

Source: The Author (2019).

7.5 DETECTION METHOD APPLICATION

The detection method described in chapter 6 will be applied by implementing a data fusion methodology. The fusion model selected as appropriate for this work is one centralized at the Diagnostic level. Such a model was presented in Fig. 20, in chapter 5. Figure 43 shows the complete damage detection methodology for the two sensors used in the model (assuming transducer one is always fixed as an actuator and not sensor). The steps in Fig. 43 were the ones programmed in a MATLAB script (Annex A).

Figure 43 – Damage detection methodology constructed as a Data Fusion scheme centralized at the diagnosis level.

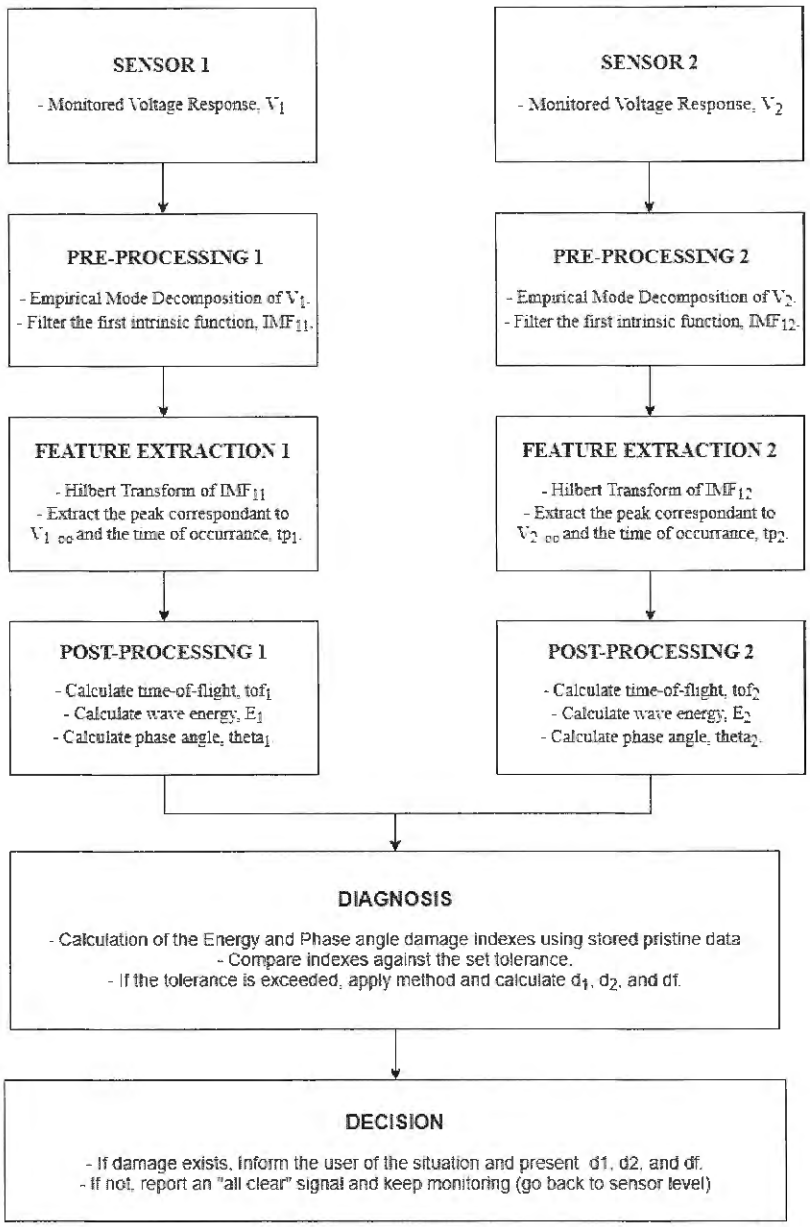

Source: The Author (2019).

8 RESULTS

In this chapter, the results of implementing the damage detection strategy for the assessment of delamination in a CFRP model are presented. The simulations, as already stated, were carried on the FEM software ABAQUS; but, the detection method introduced in this work was implemented on a MATLAB script (Annex A). The method will be assessed in the same order as the Data Fusion Model defined in Fig. 43.

The presentation of results will be focused first into the pristine propagation analysis. Then, the analysis is done for the piezoelectric responses of the first delamination case (parameters of the first row of Tab. 1) in order to explain in detail the way on how the data treatment works. Later, the results for all the delamination cases are introduced and a final consolidation of results will be presented to show general trends; especially on the sensitivity of the method.

8.1 MODEL RESPONSE

The ABAQUS model achieved propagation with the numerical setup described in the past chapter. Figure 44 shows a snapshot of the actuator sensor generating the Lamb waves on the plate by transferring strains. Again, perfect bonding was assumed. It is worth noting that, due to the woven or bidirectional fiber used, the propagation front resembles a circle, showing that the plate is quasi-isotropic for the given ply sequence.

Figure 44 – Actuator transducer responding to electrical input in ABAQUS.

Source: The Author (2019).

The voltage peak-to-peak magnitude decay with respect the propagated distance matched with the results obtained by the experimentally validated work of Gresil and Giurgiutiu (2015).

8.2 PRISTINE STATE

Sensing: Figure 45 shows the pristine responses in transducer 2 (Sensor 1) and 3 (Sensor 2) when transducer 1 (Actuator) is actuated. Due to transducer tuning, a single, very clear, wave package gets to every transducer which corresponds to the anti-symmetric fundamental mode of propagation, A_0.

Figure 45 – Voltage response in Pristine state for $F = 90$ kHz.

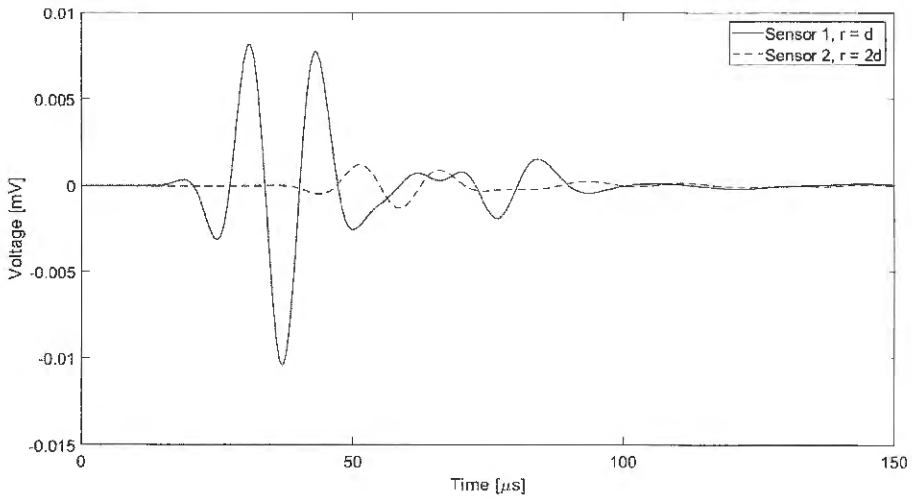

Source: The Author (2019).

It can be affirmed, without loss of generality, that the response obtained in Fig. 45 has a considerably less degree of complexity than a response in any other, more dispersive, frequency.

Pre-Processing: The objective of the Pre-processing is to filter and/or better prepare the data for the Feature Extraction process. First, it can be noticed that the data can be cropped up to 100 μs without losing important information. This will result in a smaller quantity of data to handle, thus speeding up the integrity assessment.

Other main concern is to better condition the sensed response for the use of the Hilbert Transform, which relies on smoothness for the analytic function to give accurate results. Now, the sensed data in Fig. 45 is clearly well conditioned, and this is the result of being obtained through numerical simulation. An experimental measure is expected to be accompanied by white noise, which is common in measures involving piezoelectricity.

The EMD of the HHT was used, and the IMFs obtained for sensor 1 and 2 are shown in Fig. 46. These plots were obtained through the intrinsic EMD function of MATLAB (available since the R2018 version).

By examining the magnitude of the IMF, it can be seen that only the two first functions, in both transducers, contain all the feature information and the most energetic wave modes,

Figure 46 – Intrinsic Mode Functions and residues, through the EMD, for the pristine responses in sensor 1 (left) and sensor 2 (right).

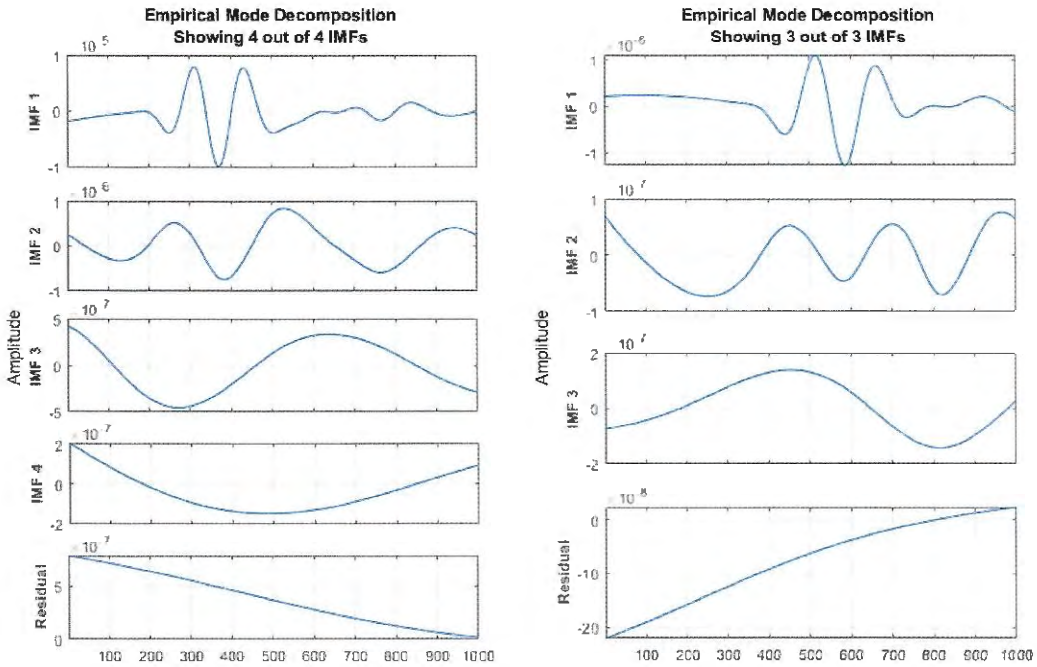

Source: The Author (2019).

especially the first IMF. As already said, the response signal itself is well conditioned for applying HT directly; however, the IMF are still calculated due to their use in the damage detection indexes.

Feature Extraction: The features required are the maximum amplitudes of the propagating wave packets and the times on which those maximums happen. This can be obtained with the infinity norm (maximum value of the magnitude) of the Hilbert Transform, of the IMF to which the measure was reduced into. Figure 47 shows the pristine response in Sensor 1 along with its envelope function and a marker showing the localization of the infinity norm, its value and time of occurrence.

The latter process must be done for all the signals, including the Actuation, so these values can be used to calculate important information such as times of flight, group velocity, and amplitude attenuation parameters. Values for the pristine state are shown in Tab. 7.

Post-Processing: With the features extracted, parameters such as the pristine accumulated energy, unwrapped phases, times of flight between transducers and more can be calculated and sent into the algorithm —Diagnosis level— for their storage and use when the structure enter service.

As already explained, all the relevant data was treated individually for every sensor, and it

Figure 47 – Feature extraction over the pristine response in Sensor 1.

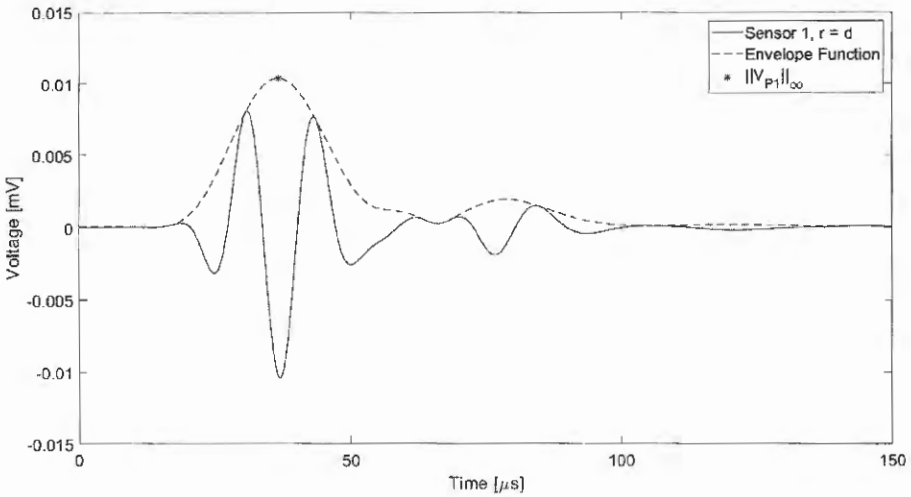

Source: The Author (2019).

Table 7: Values of maximum amplitudes and times of occurrence for the pristine state.

Transducer	Max. Amplitude	Time of Occurrence
Actuator	19,9265 V	16,7 μs
Sensor 1	10,3951 μV	36,7 μs
Sensor 2	1,34070 μV	55,8 μs

Source: The Author (2019).

was centralized in the database, which will be used for monitoring the structure during operation. The scheme in which this monitoring is planned to occur is out of the scope of this work.

8.3 DAMAGED STATE

At this point, the different delamination cases of Tab. 1 are introduced on the laminate and, with it, the proposed method in this work is assessed. First, the results for case 1 ($d_1 = 50$ mm and $d_2 = 15$ mm).

Figure 48 shows a comparison of the wavefront when propagating between Sensor 1 and Sensor 2, which is the zone where the delamination exists. It can be seen how the propagation is clear in the pristine case, and how in the damaged case, due to the delamination reflections, the propagation looks more "turbulent" with many waves superimposing others.

Sensing: Figure 49 compares the pristine and damaged responses for Sensor 2, the one after the damage, for the first delamination case, that is, delamination starting halfway between Sensor 1 and 2 with a damage of 15 mm (15% of the separation distance).

Figure 48 – Wavefront of the fundamental A_0 mode passing through sensor 1 and 2 in pristine (left) and damaged (right) states.

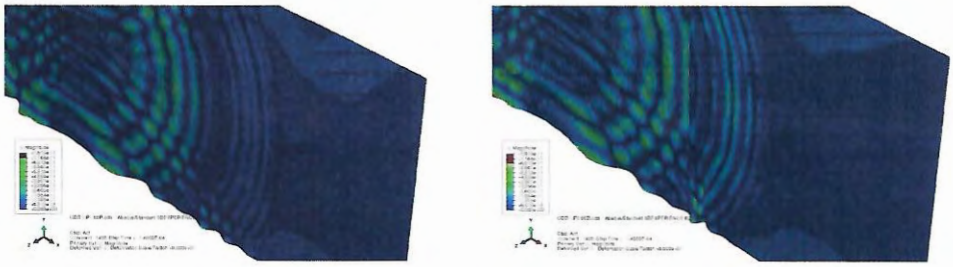

Source: The Author (2019).

Figure 49 – Pristine and Damaged responses for Sensor 2, delamination case 1

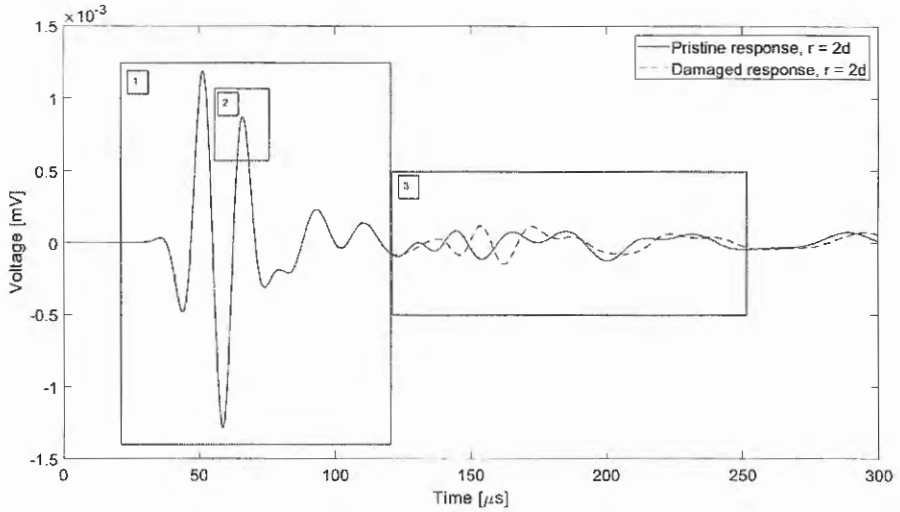

Source: The Author (2019).

The difference in responses can be observed in three main sections, which correspond to the three marked boxes in Fig. 49. In box 1, the wave packet, that is the A_0 mode, exhibit the same shape that the pristine state, this is due to the "linear" modeling of damage. This is important because it shows that this kind of damage modeling does not generate the phenomenon known as **mode conversion** in which the shape of the wave packet disperses heavily after the interaction with a feature, complicating further signal analysis. If more complicated damage is modeled, such as fiber and matrix cracking combined, is expected to see this mode conversion, as reported by authors such as Giurgiutiu (2005).

However, the "damaged" wave packet shown in box 1 is not in phase with the pristine wave package, neither their amplitudes match. The latter can be better seen by zooming at any region, for convenience, the peak in box 2 was selected to show this and is presented in Fig. 50. These differences are exploited to obtain information about structural integrity.

Figure 50 – Pristine and Damaged responses for Sensor 2, zoomed at box 2.

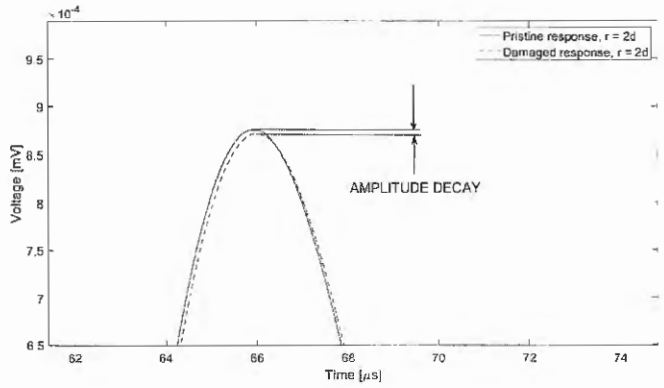

Source: The Author (2019).

In box 3 of Fig. 49, the amplitude and phase difference is a lot more accentuated. Nonetheless, these differences are harder to be exploited for damage detection; because, much of them can be attributed to border reflections or even damage reflections, but with many other waves superimposed, *i.e.* these are not pure propagation modes for which a basic predictability is associated.

The pristine and damaged responses for Sensor 1 (before the damage) are shown in Fig. 51. As the latter case, the responses look very alike, but are not the same. To show this, Fig. 52 shows the difference between the two response. The resulting pattern can be attributed directly to reflections from the damage and boundaries. To correctly see the wave corresponding to the reflection alone, the inspection window (explained in chapter 6) is drawn and the signal in between its limits is considered to be pure reflection by the algorithm.

Figure 51 – Pristine and Damaged responses for Sensor 1, delamination case 1.

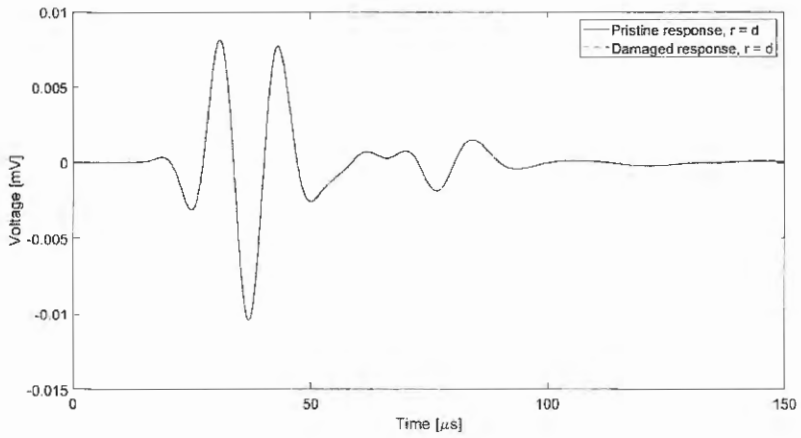

Source: The Author (2019).

The reason for which the changes between pristine and damaged signals are, however, too small, giving an unchanged appearance impression, is that the reflected wave amplitude is very small in comparison to the signal in Sensor 1. This is an indication of low damage severity because, in the case of extreme damage (rigidity zero), the reflected wave will be, theoretically, of the same order of magnitude of the incident, because acts as a free boundary which totally reflects the wave.

Pre-Processing: Again, the original signal can be directly transformed through the HT and the IMF are obtained in order to use the data for the calculation of the damage indexes. Due to the reasons already discussed, the IMF does not differ significantly from those obtained in Fig. 46 and won't be repeated here.

Figure 52 – Reflection signal obtained by subtracting Pristine and Damaged responses for Sensor 1, delamination case 1.

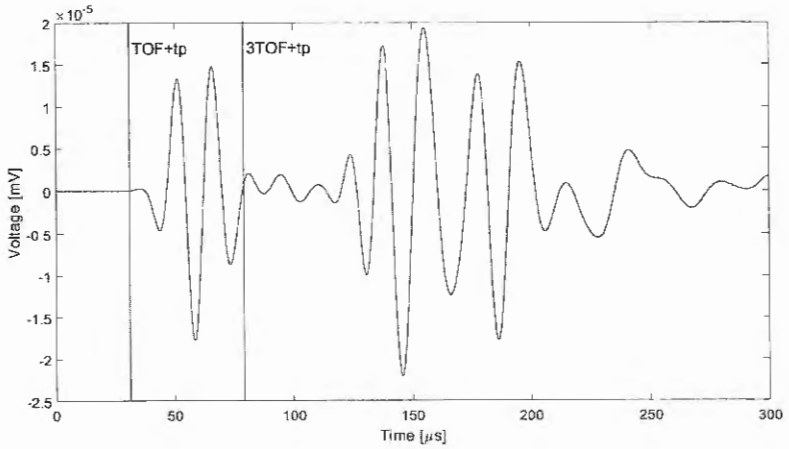

Source: The Author (2019).

Feature Extraction: The process is repeated and its results shown in Tab. 8. It can be seen that only the maximum amplitude and the time of occurrence in Sensor 2 changed due to the damage. This change is small, though, showing that in a real practical setting, equipment sensitivity, and filtering play a crucial role in a scheme like the one proposed in this work.

Table 8: Values of maximum amplitudes and times of occurrence for delamination case 1.

Transducer	Max. Amplitude	Time of Occurrence
Actuator	19,9265 V	16,7 μs
Sensor 1	10,3950 μV	36,7 μs
Sensor 2	1,33377 μV	55,9 μs

Source: The Author (2019).

8.4 DETECTION INDEX BENCHMARKING

8.4.1 Energy Index

Using the IMF obtained through the EMD for the pristine and damaged signals, the Empirical Mode Decomposition Energy Damage Index (EMD-EDI) can be constructed for all the delamination cases. This Index is constructed as a function of paths, from Actuator to Sensor 1 (path 1) and from Sensor 1 to Sensor 2 (path 2), rather than constructed for individual transducers. The results are consolidated in Tab. 9.

Table 9: Empirical Mode Decomposition Energy Damage Index for all the delamination cases.

	Case					
Path	1	2	3	4	5	6
1	0.0293	0.0756	0.0238	0.0242	0.0294	0.0435
2	0.5672	0.5900	0.5106	0.4437	1.3307	1.7152
Prop:	19.3406	7.8078	21.4576	18.3672	45.2213	39.4317

Source: The Author (2019).

The larger the damage index, the more probable the path to having some kind of damage. It is worth noticing, though, that **the index can be non zero even in pristine zones**, as it is evident for Path 1 in Tab. 9. However, by examining the proportion ("Prop." row of Tab. 9) in which the index in the second path is significantly greater, the real damaged path can be better observed. In the end, the index should be taken as a probability estimator.

Figure 53 – Energy Damage Index as function of delamination size

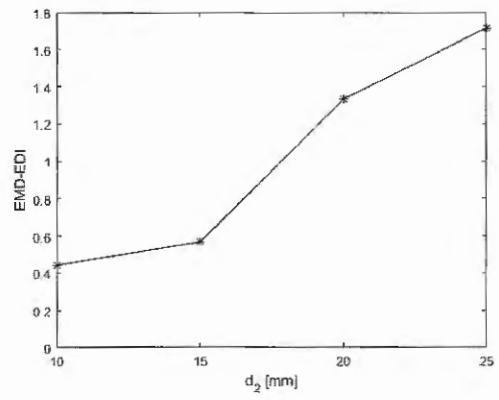

Source: The Author (2019).

Figure 54 – Energy Damage Index as function of delamination localization

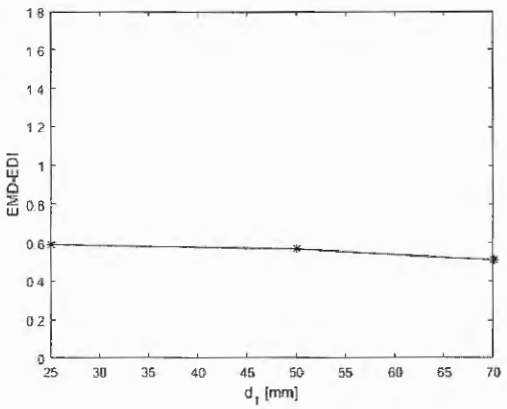

Source: The Author (2019).

Figure 53 shows the index as a function of delamination size (with constant localization $d_1 = d/2$) and a clear trend can be appreciated: the bigger the delamination, the bigger the index. This feature can be used to do quick estimation of severity of damage. In the other hand, Fig.

54 shows the index as a function of delamination localization for the same delamination size. It can be seen how the index is virtually unaffected by the localization of the damage, and on how close or away it is from the transducers.

8.4.2 Phase Difference Index

In this case, the Phase Difference Index is also capable of detecting the damaged zone with confidence. Again, care must be taken, because the index is also non zero in areas where the damage does not exist. The evidence of damage existence, again, is given by the considerably higher value of the index in a certain path in contrast to others.

However, it was expected to receive relative "low" values of the index, given that, as already shown, the responses are quite the same in shape, thus having the same value of phase for most of the spectrum, in contrast to the energy index in which the accumulated integral over the squared amplitude gives more noticeable contrasts. The index for all the delamination cases is shown in Tab. 10.

Table 10: Mean Phase Difference Damage Index for all the delamination cases.

	Case					
Path	1	2	3	4	5	6
1	0.0074	0.0435	0.0008	0.0073	0.0072	0.0071
2	0.0327	0.0326	0.0328	0.0381	0.0272	0.0267
Prop:	4.3860	0.7496	42.973	5.2598	3.7494	3.7537

Source: The Author (2019).

The examination of the index sensitivity with respect to delamination size (Fig. 55) and localization (Fig. 56), drew the same trends than in the energy index case. The phase index tends to reduce with delamination size; but, is monotone, which is the important feature for quantification.

However, it can be seen from Tab. 10 that the detection failed for the delamination case 2 because the greatest index was in path 1, where no delamination exists. The reason of this failure is attributed to the damage being "excessively" close to the reflect-picking transducer, and the use of only one IMF of the EMD could not give an appropriate smoothness to the phase angle function.

8.5 LOCALIZATION AND QUANTIFICATION DISCUSSION

After the damage is located, the method is applied using the transducers around the damaged zone. The results are shown in Tab. 11. In general, the results are encouraging, especially by the fact that the localization and quantification are of the same order of magnitude than the

Figure 55 – Phase Damage Index as function of delamination size

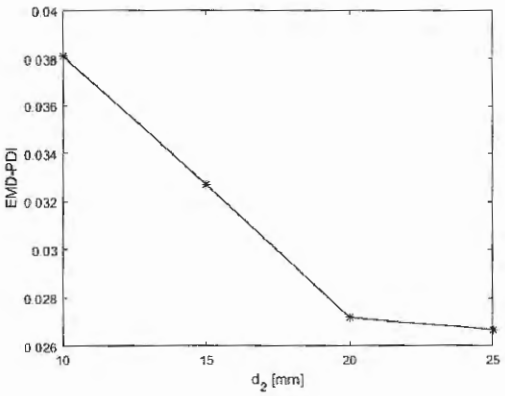

Source: The Author (2019).

Figure 56 – Phase Damage Index as function of delamination localization

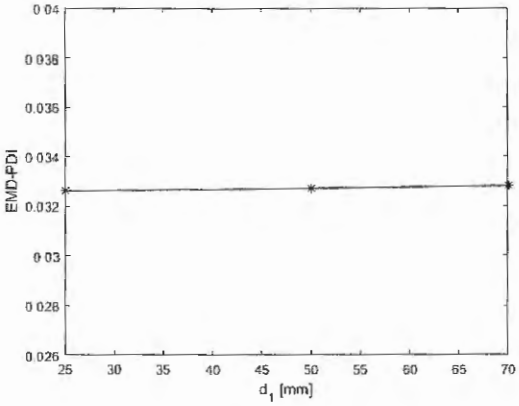

Source: The Author (2019).

actual damages. However, the error trend is not steady, showing an apparent trend to increase the closer the damage is to the reflection-receiving transducer.

Table 11: Results for the various delamination cases. A = Actual, M = Model, E = Absolute Error, T = True, F = False, EDI = Energy Damage Index, PDI = Phase Damage Index

	Detection		d_1 [mm]			d_2 [mm]			df
Case	EDI	PDI	A	M	E	A	M	E	M
1	T	T	50.00	56.00	12.0%	15.00	14.69	2.1%	6.5
2	T	F	25.00	32.00	28.0%	15.00	15.02	0.1%	6.3
3	T	T	70.00	73.50	5.0%	15.00	14.36	4.3%	6.6
4	T	T	50.00	55.50	11.0%	10.00	17.01	70.0%	5.6
5	T	T	50.00	55.00	10.0%	20.00	16.35	18.3%	5.8
6	T	T	50.00	50.25	0.5%	25.00	23.47	6.1%	3.8

Source: The Author (2019).

Regarding the localization error, Fig. 57 shows the absolute percentage error as a function of the delamination localization, d_1, with fixed delamination size d_2. The error curve is monotonically decreasing with increasing values of d_1, indicating that the method shows better precision the larger the distance between the reflection-catching transducer and the damage. Nonetheless, exists a restriction to how far can be a transducer from a possible damaged zone: if the damage is too far away it, can be expected the wave, or the reflected wave, to attenuate too much for the transducer to catch it.

Regarding the quantification error, Fig. 58 shows the absolute percentage error as a function of the delamination size, d_2, with a fixed distance from the transducer d_1. In contrast to Fig. 57, the error curve is not close to monotone, but it also shows a decreasing trend with the

size of the delamination, which is a bit intuitive since the effects of bigger damages leave more trace and, hence, are easier to catch.

Figure 57 – Absolute relative error for delamination localization

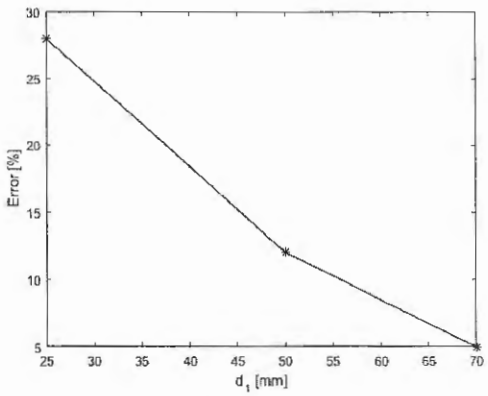

Source: The Author (2019).

Figure 58 – Absolute relative error for delamination size

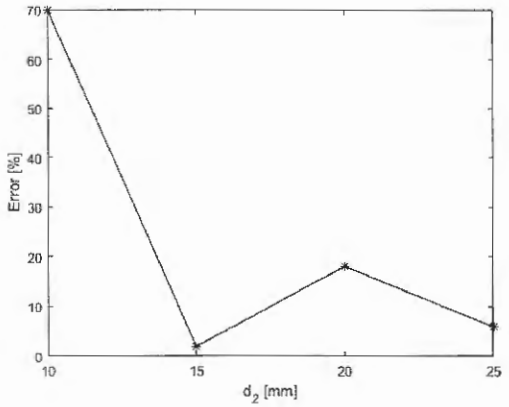

Source: The Author (2019).

These trends give suggestion on how a sensor placement optimization problem would look like. The wave attenuation gives a maximum distance restriction because if the electric response is below the limit of some high-pass filter used to pre-process the signal the response measured could be zero, incomplete, or without the most important features. The minimum separation can be approached by knowing the loss of precision in the case damage covers most of the area between transducers. This problem can also be partially solved with the use of redundancy, *i.e.* the use of more sensors in order to "confirm" the damage parameters. However, how the data fusion at the centralized diagnostic level interact, or in which situation is decided that one measure is more "credible" than other, are open questions out of the current scope.

The last column of Tab. 11 shows the estimated global stiffness loss. However, was left without comparison with an "actual" value, because it was not clear which stiffness component have to be combined in such a way so it gives a theoretical "actual" stiffness loss. However, the stability of this parameter is evidently not very good when the delamination is varied. It can be noted how, when the delamination was constant, its value remained relatively constant, but when the biggest delamination was assessed (case 6), it shows almost half the value "suggesting" a not so severe condition, which is counter-intuitive. This estimation requires further revision.

Part IV

Final Remarks

9 CONCLUSIONS

This work proposed a damage detection methodology for elastic materials based on the use of time domain Lamb wave response, actuated and measured through piezoelectric transducers. The model aims to detect, localize and quantify a single, well defined, discontinuity of material properties within an elastic medium. It was numerically applied to a composite plate made up of by stacking bidirectional carbon fiber lamina with single delamination. And, in this first study, the results encourage its experimental validation in order to gain information that could robust it or give a new insight into approaches.

The problem solved was a proposed standardized problem, **originally defined for the first time in this work**, in order to compare the results of future methods under the same frame. Such a problem was called "one-dimensional" because it quantifies the damage with only one parameter, its width along the line of propagation. A "two-dimensional" problem would consist in quantifying the width and length along, parallel and perpendicular to, the line of propagation. The complete "three-dimensional" problem would consist of also estimating the damage position across the material's thickness. Such an approach would facilitate benchmarking between already published methods, in where every author solves a unique and different problem every time with only few ones trying to get the most global results possible.

This method was elaborated during the Master's degree work of the author in the GEA group of the São Carlos School of Engineering, University of São Paulo. It started trying to solve this same one-dimensional problem but actuating through the out-of-plane displacement punctual boundary condition, instead of piezoelectric transducers. In this first approximation, published in the Meeting of Aeronautical Materials and Composites of 2017, the attenuation law was assumed quasi-linear for most of the travel path, and, even with this hard assumption, the method yielded relatively good results for a variety of simple cases.

Later, a second version was developed, now using piezoelectric transducers for which the first approximation yielded results with big errors due to the assumed attenuation law and the difference between the way on how strains are induced on the plate with circular transducers, rather than punctual displacements. This time an exponential rule was assumed for the attenuation law, and results of localization improved, but with relatively high error margins for quantification, though. This version was submitted to the Brazilian Congress of Solid Mechanics of 2019.

In this document, the last version was presented, yielding the best error margins achieved so far (see Chapter 8). **The work, on its present version, has not yet been published**.

This work also realized a theoretical revision, considering, especially, to leave it well documented so future GEA members could be used as a first lecture or introduction into the topic. It was distinctive of this work, also, the integration of many concepts ranging from pure

and classic elastic wave propagation theory (acoustic impedance, flexural wave behavior, etc.) up to the most recent concepts and notions (transducer tuning, Hilbert-Huang Transform, Data Fusion, etc.). This revision can be better described by resuming the main assumptions of the model, and their effects, next:

- **Infinite or semi-infinite boundaries:** This allows to obtain clear wave packages to process. The method counts on signal differences to compute damage which theoretically could suppress reflections from boundaries; however, this can be a hard-to-predict feature when no uniform damage appears due to be a superposition of reflections from boundaries and damages.

- **Uniform and well-defined damage region:** The notion of "well defined" acoustic impedance ratio between reflected and incident waves depend heavily in this assumption drawn from classic elastic wave propagation theory. This kind of boundary can be approximated, if controlled, in a laboratory with inserts that do not adhere when curing the plate during fabrication, *i.e.* Teflon strips. However, in real impact or fatigue damage, this assumption is hard to hold totally true.

- **Adequate tuning in the low-frequency range:** The Antisymmetric mode was verified of being a sensitive mode to delamination. However, to excite this mode, in the low thickness-frequency range, allows assuming quasi-flexural waves, which is the main assumption that allows an acoustic impedance definition to be coherent. In a more dispersive situation, this parameter is not clearly defined, at least, in theory.

Other of the main contributions of this work is the **use Hilbert-Huang Transform, a novel signal processing tool, in order to pre-process the data regarding nonlinear and dispersive acoustic signals traveling in thin solids**. The Hilbert-Huang Transform was developed as an expansion of Hilbert spectral analysis by Norden E. Huang in 1998 during his work in NASA. This tool is recently increasing its range of applications, also starting in the area of SHM of civil and aeronautical structures. **By the data on which this dissertation was written, there were less than 20 works on scientific databases applying the HHT for the detection of delamination on composites**.

Also, **a benchmarking of two damage detection methods, published by two different authors, was done; one based on energy and other in phase difference**. The use of the same problem to contrast the two methods allowed to account for some features that were not assessed in the original papers on they were published. Basically, it could be concluded that for the type of damage modeled, which is of low severity, the energy (amplitude) based index is more adequate to detect, because the damaged and pristine measures are very alike in shape, and thus in almost the same phase. The practical problem with the energy index is that, due to the integration of the signal, it is computationally more expensive to use than the phase difference

index. In the other hand, the limitations of the phase difference index can be helped to apply redundancy to confirm the existence of damage with the use of another nearby sensor. Also, the sensitivity of the indexes to the delamination size and localization was studied, and **it can be concluded that both indexes can be used for damage quantification, but not for clear localization**.

The need for redundancy and the linear arrangement of transducers allow to imagine a grid detection scheme that will allow for detection over complete areas. That is, **2D detection is done by horizontal 1D detection combined with vertical 1D detection integrated as a sensor grid**. It is worth noticing that, at first, the method here presented could also be used in this circumstance, remaining only the means of integration of inter-actuating signals.

10 FUTURE WORKS

10.1 EXPERIMENTAL VALIDATION

This project counts with a technological partnership with the Campinas State University (UniCamp). Ph.D. candidate Nilson Inocente Jr. from UniCamp developed an **electronic hardware for experimental acquisition of Lamb wave response data**, and it was recently constructed for in-house use in the GEA laboratory.

This hardware works by applying a user-defined voltage difference profile, or window, between two terminals connected to the piezo transducer, and it records the response from other piezo plugged in another terminal. This process is done 20 times in order to filter white noise. Then, the averaged signal of these 20 measurements is displayed to the user. All of the above is done in a LABVIEW interface also developed by Nilson Inocente Jr.

Traditionally, experimental Lamb wave with piezo transducer measuring requires an oscilloscope, a DC voltage source, a wave generator, and a signal amplifier; all these equipment is integrated into the acquisition hardware developed by our partners, which is energized through a USB cable from a laptop. However, some setup and calibrating is still required due to issues such as the response signal not starting at 0V, which could imply that the 20 measures are not averaged in phase. Also, there are concerns on the range of frequency in which the instrument can excite and measure, because of the shape of some responses tested in aluminum.

Other concern regarding equipment, especially for the aims of validating the method described in this work is if the hardware possesses the right sampling frequency. This is important because, as seen in the results chapter, time delays are in the order of a tenth of a microsecond, which would require at least a sampling rate of 20 MHz to be properly measured. These details are not yet resolved and are future work to be done.

Also, experimental ways of measuring dispersion curves are desirable. For this objective, additional to the acquisition equipment, a laser vibrometer would be desirable in order to study the Lamb wave response from less invasive possible measuring techniques. This requirement is due to the notion that the adhesion of an excessive number of transducers, will modify the dynamical behavior of the plate under study by increasing its modal mass.

For more information, including photos, of the experimental data acquisition developed in UniCamp by our partners, the reader is referred to Annex B.

10.2 COMPUTATIONAL TOOLS DEVELOPMENT

As presented in this work, some tools for propagation modeling, such as phase and group velocity charts and piezoelectric transducer tuning curves, and others desirable computational

tools are required if the current research wants to expand its horizon. The lack of those tools would end in always requiring, as this work essentially required, to search and deeply extracting information from papers and other published literature in order to have relevant and useful data.

Dispersion curves of isotropic solids and anisotropic laminates should be given priority. There is literature published on how these curves can be obtained numerically by the use of methods such as the Global Transfer Matrix and others. However, the actual programming has to be done in-house as there is no free source code available, only a few for-fee codes.

Also, the programming of an in-house program for the calculation of the HHT is desirable. The reason is that the application of this method for Lamb wave signals is still "experimental", hence exists the possibility of innovative research if the group has the resource to adapt it better to the particular needs of the research.

The author also recommends to work all the code concerning Lamb waves on the C++ or Fortran programming languages, due to the high volume of data that is expected to be handled by an embedded controller by the implementation of a decent number of piezoelectric transducers. These languages have proven to be the best suited for fast processing of high amounts of data.

Another area that would allow boosting simulation capacity is the development of computational code for simulating the analytical propagation of Lamb waves or the response of piezos. Such a code opens the possibility of not having to simulate the complete structure under study, because especial regions of interest could be isolated and only give the propagation input of the material at the boundary of such region, saving huge amount of computational time and by avoiding the expensive Multi-Physics Finite Element Method (MP-FEM) simulation.

10.3 CHARACTERIZATION AND MODELING OF PIEZOELECTRIC PROPERTIES

Another important issue, especially with experimental and numerical modeling, is the appropriate determination of the material properties of the piezo transducers under study. The author on his own research on the topic, in an initial stage of the work, recognized how many transducer manufacturers available in the Brazilian market offer no information of mechanical or electrical properties of the piezo transducer they produced. This is due to the fact that these elements are used as buzzers and other types of applications in where this information is not of prime concern for the mainstream consumer.

The obtaining of this information is quite complex and require special experimental equipment, such as an Impedance Analyzer, in order to obtain experimental graphs of impedance vs. frequency. Reference Perez et al. (2010) is recommended for further information on the topic.

BIBLIOGRAPHY

AAIJ, E. **Lamb Wave Propagation in Sandwich Composite Structures for the Detection of Impact Damage**. 2016. Dissertação (Mestrado) — Delft University of Technology, 2016.

ALLEYNE, D. N.; CAWLEY, P. The interaction of lamb waves with defects. **IEEE transactions on ultrasonics, ferroelectrics, and frequency control**, IEEE, v. 39, n. 3, p. 381–397, 1992.

ASSIS, B. F. d. S. P. et al. Cenários prospectivos na aviação comercial brasileira/prospective scenarios for brazilian commercial aviation. **Revista GEINTEC-Gestão, Inovação e Tecnologias**, v. 7, n. 1, p. 3686–3700, 2017.

BALAGEAS, D.; FRITZEN, C.-P.; GÜEMES, A. **Structural health monitoring**. [S.l.]: John Wiley & Sons, 2010. v. 90.

BARSKI, M.; PAJĄK, P. An application of stiffness matrix method to determining of dispersion curves for arbitrary composite materials. **Journal of KONES**, v. 23, 2016.

BEDFORD, A.; DRUMHELLER, D. Elastic wave propagation. **John Wileg g Sons**, p. 151–165, 1994.

BOLLER, C.; MEYENDORF, N. State-of-the-art in structural health monitoring for aeronautics. In: CITESEER. **Proceedings of the International Symposium on NDT in Aerospace**. [S.l.], 2008.

BOLLER, C.; STASZEWSKI, W. Aircraft structural health and usage monitoring. **Health Monitoring of Aerospace Structures**, p. 29–73, 2004.

BOTTAI, G.; GIURGIUTIU, V. Simulation of the lamb wave interaction between piezoelectric wafer active sensors and host structure. In: INTERNATIONAL SOCIETY FOR OPTICS AND PHOTONICS. **Smart Structures and Materials 2005: Sensors and Smart Structures Technologies for Civil, Mechanical, and Aerospace Systems**. [S.l.], 2005. v. 5765, p. 259–271.

BRAILE, L. W. **Seismic Waves and the Slinky: A Guide for Teachers**. Purdue University, 2017. Disponível em: <http://web.ics.purdue.edu/~braile/edumod/slinky/slinky.htm#Human_Wave>.

BRIGMAN, N. N. A. **Structural health monitoring in commercial aviation**. 2012. Tese (Doutorado) — Massachusetts Institute of Technology, 2012.

CHEN, H.; YAN, Y.; JIANG, J. Vibration-based damage detection in composite wingbox structures by hht. **Mechanical systems and signal processing**, Elsevier, v. 21, n. 1, p. 307–321, 2007.

CHERAGHI, N.; RILEY, M.; TAHERI, F. A novel approach for detection of damage in adhesively bonded joints in plastic pipes based on vibration method using piezoelectric sensors. v. 4, p. 3472–3478, 2005.

COMPANY, T. B. **Commercial Market Outlook 2018-2037**. [S.l.: s.n.], 2018.

CORP, S. **ABAQUS Analysis user's manual 6.14-2**. [S.l.], 2014.

DIAMANTI, K.; SOUTIS, C. Structural health monitoring techniques for aircraft composite structures. **Progress in Aerospace Sciences**, Elsevier, v. 46, n. 8, p. 342–352, 2010.

DOWLING, N. E. **Mechanical behavior of materials: engineering methods for deformation, fracture, and fatigue**. [S.l.]: Pearson, 2012.

ESMAEEL, R. A.; TAHERI, F. Delamination detection in laminated composite beams using the empirical mode decomposition energy damage index. **Composite Structures**, Elsevier, v. 94, n. 5, p. 1515–1523, 2012.

FARRAR, C. R.; WORDEN, K. An introduction to structural health monitoring. **Philosophical Transactions of the Royal Society of London A: Mathematical, Physical and Engineering Sciences**, The Royal Society, v. 365, n. 1851, p. 303–315, 2007.

GANGADHARAN, R. et al. Characterization of cracks and delaminations using pwas ad lamb wave based time-frequency methods. **International Journal on Smart Sensing & Intelligent Systems**, Citeseer, v. 3, n. 4, 2010.

GIURGIUTIU, V. Lamb wave generation with piezoelectric wafer active sensors for structural health monitoring, v. 5056, p. 111–123, 2003.

_____. Tuned lamb wave excitation and detection with piezoelectric wafer active sensors for structural health monitoring. **Journal of intelligent material systems and structures**, Sage Publications Sage CA: Thousand Oaks, CA, v. 16, n. 4, p. 291–305, 2005.

_____. **Structural health monitoring: with piezoelectric wafer active sensors**. [S.l.]: Elsevier, 2007.

GRESIL, M.; GIURGIUTIU, V. Prediction of attenuated guided waves propagation in carbon fiber composites using rayleigh damping model. **Journal of Intelligent Material Systems and Structures**, SAGE Publications Sage UK: London, England, v. 26, n. 16, p. 2151–2169, 2015.

HAN, S. **Finite element analysis of lamb waves acting within a thin aluminum plate**. [S.l.], 2007.

HUANG, N. E. **Hilbert-Huang transform and its applications**. [S.l.]: World Scientific, 2014. v. 16.

HUANG, N. E. et al. The empirical mode decomposition and the hilbert spectrum for nonlinear and non-stationary time series analysis. In: THE ROYAL SOCIETY. **Proceedings of the Royal Society of London A: mathematical, physical and engineering sciences**. [S.l.], 1998. v. 454, n. 1971, p. 903–995.

IHN, J.-B.; CHANG, F.-K. Pitch-catch active sensing methods in structural health monitoring for aircraft structures. **Structural Health Monitoring**, Sage Publications Sage UK: London, England, v. 7, n. 1, p. 5–19, 2008.

JAE, E. **For the first time, Army sensors can detect aircraft damage as it occurs**. The United States Army, 2017. Disponível em: <https://www.army.mil/article/196971/for_the_first_time_army_sensors_can_detect_aircraft_damage_as_it_occurs>.

JORDAN, T.; OUNAIES, Z. **Piezoelectric ceramics characterization**. [S.l.], 2001.

KHAN, A. et al. History, current status and challenges to structural health monitoring system aviation field. **Space Technol**, v. 4, p. 67–74, 2014.

KIM, I.; JHA, R. Effect of lamb wave excitation frequency on detection of delamination in composite plates. In: AMERICAN SOCIETY OF MECHANICAL ENGINEERS. **ASME 2011 Conference on Smart Materials, Adaptive Structures and Intelligent Systems**. [S.l.], 2011. p. 555–562.

LAMB, H. On waves in an elastic plate. **Proceedings of the Royal Society of London. Series A, Containing papers of a mathematical and physical character**, The Royal Society London, v. 93, n. 648, p. 114–128, 1917.

LU, Y. et al. Quantitative evaluation of crack orientation in aluminium plates based on lamb waves. **Smart Materials and Structures**, IOP Publishing, v. 16, n. 5, p. 1907, 2007.

MARAZZO, M.; SCHERRE, R.; FERNANDES, E. Air transport demand and economic growth in brazil: A time series analysis. **Transportation Research Part E: Logistics and Transportation Review**, Elsevier, v. 46, n. 2, p. 261–269, 2010.

MEEKER, T. Publication and proposed revision of ansi/ieee standard 176-1987. **IEEE Transactions on Ultrasonics Ferroelectrics and Frequency Control**, IEEE, v. 43, n. 5, p. 717–772, 1996.

MICHAEL, B. et al. **Vibration Response and Damage Detection of Carbon/Epoxy Beams at Elevated Temperatures using the Hilbert-Huang Transform**. [S.l.], 2015.

NTI AUDIO AG. **Fast Fourier Transformation FFT - Basics**. NTI Audio, 2017. Disponível em: <https://www.nti-audio.com/en/support/know-how/fast-fourier-transform-fft>.

OSEGUEDA, R. A. et al. Detection of cracks at rivet holes in thin plates using lamb-wave scanning. In: INTERNATIONAL SOCIETY FOR OPTICS AND PHOTONICS. **Smart Nondestructive Evaluation and Health Monitoring of Structural and Biological Systems II**. [S.l.], 2003. v. 5047, p. 55–67.

PEREZ, N. et al. Identification of elastic, dielectric, and piezoelectric constants in piezoceramic disks. **IEEE transactions on ultrasonics, ferroelectrics, and frequency control**, IEEE, v. 57, n. 12, p. 2772–2783, 2010.

POULARIKAS, A. D. **Transforms and applications handbook**. [S.l.]: CRC press, 2010.

QUEK, S. T.; TUA, P.; WANG, Q. Detecting anomalies in beams and plate based on the hilbert–huang transform of real signals. **Smart materials and structures**, IOP Publishing, v. 12, n. 3, p. 447, 2003.

RAGHAVAN, A.; CESNIK, C. E. Modeling of piezoelectric-based lamb wave generation and sensing for structural health monitoring. In: INTERNATIONAL SOCIETY FOR OPTICS AND PHOTONICS. **Smart Structures and Materials 2004: Sensors and Smart Structures Technologies for Civil, Mechanical, and Aerospace Systems**. [S.l.], 2004. v. 5391, p. 419–431.

ROYER, D.; DIEULESAINT, E. Elastic waves in solids, vol. 1. **Springer, Berlin**, v. 20, n. 0, p. 0, 2000.

SAMARATUNGA, D.; JHA, R. Lamb wave propagation simulation in smart composite structures. In: **SIMULIA Community Conference**. [S.l.: s.n.], 2012. p. 1–11.

SAMARATUNGA, D.; WANG, R.; JHA, R. Lamb wave instantaneous phase based method for quantitative level of delamination damage in composite structures. In: AMERICAN SOCIETY OF MECHANICAL ENGINEERS. **ASME 2012 Conference on Smart Materials, Adaptive Structures and Intelligent Systems**. [S.l.], 2012. p. 891–895.

SOUZA, M. G. d. **Identificação e caracterização de não-linearidades em dinâmica estrutural**. 2008. Tese (Doutorado) — Universidade de São Paulo, 2008.

STASZEWSKI, W.; MAHZAN, S.; TRAYNOR, R. Health monitoring of aerospace composite structures–active and passive approach. **composites Science and Technology**, Elsevier, v. 69, n. 11-12, p. 1678–1685, 2009.

SU, Z.; YE, L.; LU, Y. Guided lamb waves for identification of damage in composite structures: A review. **Journal of sound and vibration**, Elsevier, v. 295, n. 3-5, p. 753–780, 2006.

TALREJA, R. Stiffness properties of composite laminates with matrix cracking and interior delamination. **Engineering Fracture Mechanics**, Elsevier, v. 25, n. 5-6, p. 751–762, 1986.

THOMAS, G. H. Overview of nondestructive evaluation technologies. In: INTERNATIONAL SOCIETY FOR OPTICS AND PHOTONICS. **Nondestructive Evaluation of Aging Maritime Applications**. [S.l.], 1995. v. 2459, p. 5–10.

TOLWINSKI, S. The hilbert transform and empirical mode decomposition as tools for data analysis. **Tucson: University of Arizona**, Citeseer, 2007.

TSVANKIN, I. Anisotropic parameters and p-wave velocity for orthorhombic media. **Geophysics**, Society of Exploration Geophysicists, v. 62, n. 4, p. 1292–1309, 1997.

WORDEN, K.; STASZEWSKI, W. J. Data fusion—the role of signal processing for smart structures. **Smart technologies**, World Scientific, p. 71, 2003.

YANG, C. et al. Some aspects of numerical simulation for lamb wave propagation in composite laminates. **Composite structures**, Elsevier, v. 75, n. 1-4, p. 267–275, 2006.

A MATLAB CODE FOR DAMAGE DETECTION

```
%% INITIALIZATION

%   PROGRAM FOR DETECTION OF DAMAGE ON ELASTIC SOLIDS
%   DEVELOPER: LUIS EDUARDO JARAMILLO BUSTAMANTE
%   LAST VERSION: 29/03/2019

NPZT = 3;                       %NUMBER OF PIEZO TRANSDUCERS
NTD = 3001;                     %ORIGINAL NUMBER OF MEASURES
D = 0.1;                        %DISTANCE, IN METERS, BETWEEN
    PIEZOS
PVOLT = zeros(NTD,NPZT);        %PRISTINE VOLT HISTORY
MVOLT = zeros(NTD,NPZT);        %MONITORED VOLT HISTORY

%% SENSOR LEVEL

%PRISTINE VOLTAGE HISTORY
PVOLT(:,1)=ACT;
PVOLT(:,2)=P1;
PVOLT(:,3)=P2;

%MONITORED OR DAMAGED VOLTAGE HISTORY
MVOLT(:,1)=ACT;

%(UNCOMMENT FROM HERE TO USE DATA OF EACH CASE)

MVOLT(:,2)=D11;                 %CASE 1 d1 = 0.050 d2 =
    0.015
MVOLT(:,3)=D12;
%MVOLT(:,2)=D21;                %CASE 2 d1 = 0.025 d2 =
    0.015
%MVOLT(:,3)=D22;
%MVOLT(:,2)=D31;                %CASE 3 d1 = 0.070 d2 =
    0.015
%MVOLT(:,3)=D32;
%MVOLT(:,2)=[D41; zeros(1500,1)];   %CASE 4 d1 = 0.050 d2 =
    0.010
```

```
%MVOLT(:,3)=[D42; zeros(1500,1)];
%MVOLT(:,2)=[D51; zeros(1500,1)];    %CASE 5 d1 = 0.050 d2 =
    0.020
%MVOLT(:,3)=[D52; zeros(1500,1)];
%MVOLT(:,2)=[D61; zeros(1500,1)];    %CASE 6 d1 = 0.050 d2 =
    0.025
%MVOLT(:,3)=[D62; zeros(1500,1)];

%% PRE-PROCESSING LEVEL

% Redundant data exclusion
Tmax = 1500;
PVOLT = PVOLT(1:Tmax+1,:);
MVOLT = MVOLT(1:Tmax+1,:);

% Redefining vectors size
NTD = Tmax+1;
TOFP = zeros(1,NPZT);          %PRISTINE TIMES OF FLIGHT
TOFM = zeros(1,NPZT);          %MONITORED TIMES OF FLIGHT
THETAP = zeros(NTD,NPZT);      %PRISTINE PHASE ANGLE
THETAM = zeros(NTD,NPZT);      %MONITORED PHASE ANGLE
WEP = zeros(NTD,NPZT);         %PRISTINE WAVE ENERGY
WEM = zeros(NTD,NPZT);         %MONITORED WAVE ENERGY
PHIP = zeros(NTD,NPZT);        %PRISTINE PHASE DIFFERENCE
PHIM = zeros(NTD,NPZT);        %MONITORED PHASE DIFFERENCE
EP = zeros(1,NPZT);            %ACCUMULATED PRISTINE ENERGY
EM = zeros(1,NPZT);            %ACCUMULATED MONITORED ENERGY
EMD_EDI = zeros(1,NPZT);       %ENERGY DAMAGE INDEX
EMD_PDI = zeros(1,NPZT);       %PHASE DIFFERENCE INDEX

%Empirical Mode Decomposition
IMFP = PVOLT;
IMFM = MVOLT;

for i=2:NPZT
    [IMF,res] = emd(PVOLT(:,i),'Display',0);
    IMFP(:,i) = IMF(:,1);

    [IMF,res] = emd(MVOLT(:,i),'Display',0);
```

```
69      IMFM(:,i) = IMF(:,1);
70  end
71
72  clear('IMF','Tmax')
73
74  %% FEATURE EXTRACTION
75
76  % Hilbert transform on IMF
77  HP = hilbert(IMFP);
78  HM = hilbert(IMFM);
79
80  %Infinity norms and times of occurrence
81  [VP,TP] = max(abs(hilbert(PVOLT)),[],1);
82  [VM,TM] = max(abs(hilbert(MVOLT)),[],1);
83
84  %% POST-PROCESSING
85
86  % TOF
87  for i=2:NPZT
88      TOFP(i) = 0.1*(TP(i) - TP(i-1));
89      TOFM(i) = 0.1*(TM(i) - TM(i-1));
90  end
91
92  % Energy
93  for j = 1:NPZT
94      for i = 1:NTD
95          WEP(i,j) = abs(HP(i,j))^2;
96          WEM(i,j) = abs(HM(i,j))^2;
97      end
98      EP(j) = trapz(WEP(:,j));
99      EM(j) = trapz(WEM(:,j));
100 end
101
102 % Unwrapped phase angle
103 for j = 1:NPZT
104     for i = 1:NTD
105         THETAP(i,j) = atan2(imag(HP(i,j)),real(HP(i,j)));
106         THETAM(i,j) = atan2(imag(HM(i,j)),real(HM(i,j)));
107     end
```

```
108         THETAP(:,j) = unwrap(THETAP(:,j));
109         THETAM(:,j) = unwrap(THETAM(:,j));
110 end
111
112 clear('HP','HM','WEP','WEM')
113 %% DIAGNOSIS
114
115 %DAMAGE INDEXES
116
117 % Empirical Mode Decomposition Energy Index
118 for i=1:NPZT
119 EMD_EDI(i) = abs((EP(i)-EM(i)))/EP(i)*100;
120 end
121
122 % Empirical Mode Decomposition Damage Index
123 for j=2:NPZT
124 for i=1:NTD
125         PHIM(i,j)=abs(THETAM(i,j)-THETAM(i,1));
126         PHIP(i,j)=abs(THETAP(i,j)-THETAP(i,1));
127 end
128 EMD_PDI(j) = sqrt(sumsqr(PHIM(:,j)-PHIP(:,j))/sumsqr(PHIP(:,j))
        );
129 end
130
131 %% LOCALIZATION
132
133 % Reflection construction
134 RFLX = PVOLT(:,2)-MVOLT(:,2);
135
136 % Inspection window definition for reflection extraction
137 WL = round(10*TOFP(2))+TP(1);
138 WU = round(10*(TOFP(2)+2*TOFP(3)))+TP(1);
139
140 % Reflection feature extraction
141 HR = hilbert(RFLX);
142 [VR,TR] = max(abs(HR(WL:WU)));
143 TR = TR+WL-1;
144 TOFR = 0.1*(TR-TP(1));
145
```

```
146 % Damage localization
147 d1 = ((TOFR/TOFP(2))-1)*D/2;
148
149 %% QUANTIFICATION
150
151 %Group Velocity
152 Cg = D/TOFP(2)*1e6;
153
154 %Material Damping
155 eta = (1/D)*log((1/sqrt(2))*(VP(2)/VP(3)));
156
157 %Pristine Attenuation Law
158 AM = VP(2)*sqrt(D)*exp(eta*D);
159
160 %Reflected Attenuation Law
161 AR = VR*sqrt(2*d1+D)*exp(eta*(2*d1+D));
162
163 %Voltage Magnitudes at r = d+d1
164 Vd1D = (AM/sqrt(D+d1))*exp(-eta*(D+d1));
165 Vd1DR = (AR/sqrt(D+d1))*exp(-eta*(D+d1));
166
167 %Acoustic Impedance Ratio
168 a = Vd1DR/Vd1D;
169 K = (1-a)/(1+a);
170
171 %Group Velocity in the damaged zone
172 Cd = K*Cg;
173
174 %Damage Quantification
175 d2 = (TOFM(3)-TOFP(3))*Cg*Cd*1e-6/(Cg-Cd);
176
177 %% RIGIDITY LOSS
178
179 dE = (1-K^2)*100;
```

B SIGNAL GENERATION AND DATA ACQUISITION EQUIPMENT

The laboratory equipment required to generate a voltage profile for excitation and to read voltage data for sensing would be, commonly, the following:

- DC Voltage Source
- Function Generator
- Oscilloscope

However, the present project is part of a partnership between the University of São Paulo and the Campinas State University and, as part of that collaboration, a device developed by Nilson Inocente Jr., PHD student, and Prof. Euripedes De Oliveira, Nilson's promoter, was received for in house experimentation. Also, a LABVIEW interface was developed by them to post-process all de data collected. The device is shown in Fig. 59 and a screen-shot of the LABVIEW interface is shown in Fig. 60.

Figure 59 – Acquisition equipment coupled for testing aluminum.

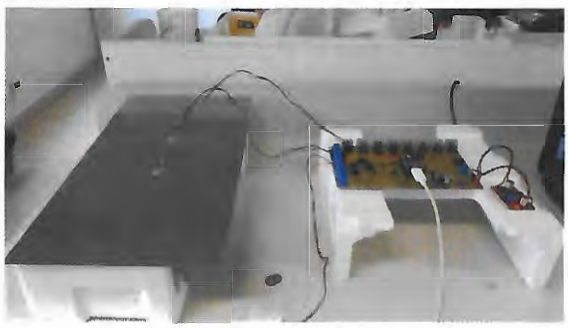

Source: The Author (2019).

Figure 60 – LABVIEW interface for data acquisition.

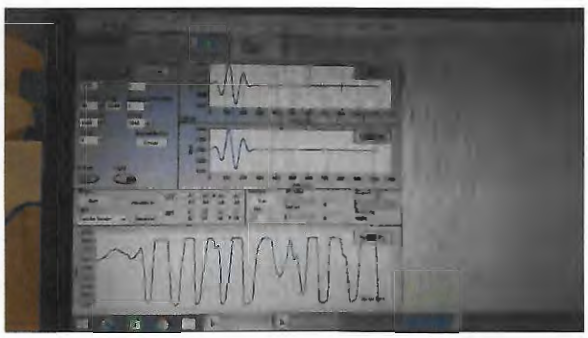

Source: The Author (2019).

The device mainly consists in a circuit specially designed to integrate the required functions of the three laboratory equipment before mentioned in a convenient and easy way. For instance, instead of supplying energy to three different equipment simultaneously, the device is capable of doing its functions by using energy supply provided by a laptop computer through a standard USB cable.

The LABVIEW interface provides the following parameters for data acquisition and excitation generation:

- **Type of signal:** There are three available types of excitation. Windowed sinusoidal, step impulse, and user inputted profile.

- **Number of points (Número de pontos):** This parameter, N_p tells the device how many time divisions, or dt to be collected. The maximum allowable is 4096.
- **Time divisions (dt):** Is the length of a individual temporal division, in μs.
- **Time period (Periodo):** Period in μs. Next, is the equivalent frequency in kHz.
- **Number of Cycles (Periodos por Janela):** Number of cycles per window. Only whole numbers allowed.
- **Amplitude:** Peak-to-peak wave amplitude in bits.
- **Offset:** Virtual ground voltage in bits.
- **Delay:** Time delay for the signal in μs, if required

Once the desired excitation profile is configured, the profile is sent to the circuit's controller. Then, the interface asks to select to which actuator send the excitation signal, and from which sensor pick up its response. The device has the possibility of attaching 8 excitation transducers and 8 sensing transducers. However, for now, it is only capable of exciting and storing one pair of transducers at a time.

For data acquisition, the user have to press the "Run" button. The controller's algorithm will then do 20 measurements, that is, 20 excitations and 20 response recording, in order to filter (post-process) the response data and reduce white noises. That filtering is done by taking the mean signal of the 20 measurements. Each measurement is done 100 ms after the time equivalent to the product $N_p dt$ which is the total recording time per sample. The total data acquisition time, T_{dq}, in seconds, per test is:

$$T_{dq} = 20 N_p dt + 2 \tag{B.1}$$

So, for instance, for a test acquiring data every 1 μs and recording the maximum 4096 points, then the total test will be due in roughly 2 seconds, and adding the time for showing the resulting post-processed signal response on screen can be all done in less than 5 seconds. Working with this device is a lot easier and time efficient than with the usual laboratory equipment listed in section signal. Is important to mention that the 100 ms gap between measures was experimentally verified that it does not interfere between responses, *i.e.* all the Lamb waves propagating have faded by the time the new excitation takes place, so there is no risk of reflections superimposing the new waves.

After the response signal is shown, the response data can be extracted as an X-Y table for its processing. This response data is also in bits, and it needs to be multiplied by a sensor gain to determine the real amplitude in Volts.